FRACTURE IN LOW CARBON STEEL

FRACTURE IN LOW CARBON STEEL

By

DONALD H. TIMBRES, B.Sc., M.Sc.

A Thesis

Submitted to the Faculty of Graduate Studies

in Partial Fulfilment of the Requirements

for the Degree

Doctor of Philosophy

McMaster University

April 1970

DOCTOR OF PHILOSOPHY (1970)
(Metallurgy and Materials Science)

McMASTER UNIVERSITY
Hamilton, Ontario

TITLE: Fracture in Low Carbon Steel

AUTHOR: Donald H. Timbres, B.Sc., M.Sc. (Alberta)

SUPERVISOR: Professor J. D. Embury

NUMBER OF PAGES: (xii) ; 178

SCOPE AND CONTENTS:

A model for slip induced cleavage fracture has been proposed to account for the influence of both grain size and grain boundary carbide size on the fracture behavior of low carbon steel.

It was shown in low carbon irons that grain boundary carbides may fracture due to inhomogeneous yielding of the ferrite matrix and provide important sources of cleavage cracks which may propagate into the ferrite matrix.

Reducing the size of the grain boundary carbide enhances the fracture resistance of the low carbon irons but continual removal has a deleterious effect.

The onset of intergranular fracture has been rationalized in terms of the stress concentrations at the head of a dislocation pile-up.

ACKNOWLEDGMENTS

It is indeed a pleasure to express my gratitude to those members of the Department of Metallurgy and Materials Science who assisted in this work. I am greatly indebted to my supervisor, Dr. J. D. Embury for his assistance in this program and in providing advice and encouragement throughout the duration of the work, and to Dr. E. Almond, who during his stay at McMaster University, contributed significantly to my understanding of fracture.

I would also like to acknowledge my appreciation of M. van Oosten for his careful work on the figures and drawings, and to R. Jarochowicz for his assistance in helping with the transmission and scanning electron microscopes.

I would also like to thank Mrs. A. Miltimore for her careful typing of this thesis and for her patience through the late stages of typing.

Thanks are also due to P. J. Worthington for his helpful discussions with regard to twinning and other matters concerned with fracture in general; and to Dominion Foundries and Steel, Limited for the use of their scanning electron microscope.

The financial support of the National Research Council was gratefully appreciated.

TABLE OF CONTENTS

LIST OF FIGURES

CHAPTER 1

INTRODUCTION

In considering the utilization of materials for many practical engineering applications it must be realized that the material must possess both strength and toughness. Specifically the processes of plastic yielding and fracture can be considered as competitive. In order to optimise the strength and toughness of materials, a detailed knowledge must be developed of the effect of variables such as temperature, rate of loading and state of stress on the processes of yield and fracture. In addition, the physical metallurgist recognizes that intrinsic properties of the materials are related to the detailed microstructural features such as grain size, the density of dislocations and the distribution of second phase particles. In the past two decades much progress has been made toward elucidating the relationship between the onset of plastic yielding and the detailed microstructure. However the competitive process of fracture is not nearly so well understood in regard to the influence of the microstructure on the fracture behavior. This in part is due to the complexity of the fracture process and the fact that variables such as temperature, environment, and strain rate may drastically modify the fracture mode. In the present work attention has been limited to the process of brittle fracture in ferrous materials. In this context the term brittle fracture is defined as the initiation and propagation of a crack with little attendant plastic deformation.

In ferrous materials brittle fracture may occur by two modes; transgranular, where separation occurs on a low index crystallographic plane known as the cleavage plane and, intergranular, where separation occurs along the grain boundaries. There have been numerous investiga-

tions on both of these types of failure and because of the obvious technological importance most of the work has been concerned with ferrous materials suitable for structural applications.

Considerable progress has been made in understanding the influence on cleavage crack formation of factors such as temperature, strain rate, grain size, the state of stress, and composition. However, the influence of the detailed microstructural features on initiation and propagation of brittle cracks remains undefined. Since variations in fracture resistance can be produced by varying the heat treatments and fabrication practices it is apparent that the microstructure exerts a marked influence on the fracture behavior. A detailed understanding of the fracture of steel therefore requires an understanding of both the physical metallurgical aspects of the material as well as an understanding of how this particular microstructure affects the fracture behavior of the material.

The purpose of the present work was to investigate the role that second-phase particles play in the initiation and propagation of cleavage cracks in low carbon iron. This type of material was chosen as a model system because variations in microstructure could be readily produced and the microstructure could be carefully characterized by a number of available experimental techniques. The initial objective of the study was to delineate the role of second-phase particles, both those at the grain boundaries and those within the grains, on the initiation and propagation of cleavage cracks. An attempt was made to describe the results by a simple quantitative model and thus relate the results of the present investigation to existing descriptions of cleavage fracture in ferrous materials. In addition to the study of transgranular cleavage fracture, consideration was given to the occurrence of intergranular fracture in low carbon irons. This aspect was concerned with rationalizing the occurrence of intergranular fracture relative to the competitive processes of plastic deformation by slip and twinning.

CHAPTER 2

LITERATURE REVIEW

2.1 Introduction

The process of fracture in crystalline materials is a complex phenomena and carries with it the potentiality of real catastrophe. Different modes of fracture can occur depending on the material, temperature, state of stress, environment and rate of loading. A number of extensive reviews (Petch 1954, Stroh 1957, Biggs 1960, Low 1963, Cottrell 1958, Tetelman and McEvily 1967) have appeared over the past two decades which document the various processes of fracture including creep, fatigue, ductile and brittle fracture. In the present work consideration has been confined to the occurrence of brittle fracture by either the transgranular or intergranular mode and thus it is appropriate to limit the review of the literature to these aspects of the fracture problem.

In the overall process of fracture there are essentially two separate stages: crack nucleation and crack growth. It is important to delineate these processes in relation to the action of the applied stress on the body and the influence of localized plastic yielding processes such as slip or twinning. In addition, it must be recognized that the processes of plastic deformation and fracture are competitive events and are both influenced by the detailed microstructure. Thus in this review it is pertinent to discuss the basic factors which influence the yielding behavior of ferrous materials prior to discussion of the mechanisms of fracture initiation and propagation.

2.2.1 Plastic Deformation in Ferrous Materials

Considerable experimental data (Hall 1951, Petch 1953, Conrad 1963) indicate in polycrystalline ferrous materials that the lower yield stress (σ_y) obeys the relation

$$\sigma_y = \sigma_o + k_y \ell^{-1/2} \qquad (1)$$

where σ_o is the friction stress opposing the motion of dislocations, which contains a thermal component and an athermal component, k_y is a measure of the difficulty of transmitting slip across the grain boundaries, and ℓ is the average grain diameter. This equation is usually referred to as the Hall-Petch relation. In all body-centered-cubic materials the lower yield stress is observed to be markedly temperature dependent, the resistance to plastic deformation increasing as the temperature is reduced. Much work (Conrad 1963, Armstrong 1968, Keh et al 1968) has been done on ferrous materials to delineate the influence on the various parameters in the Hall-Petch relation of variations in interstitial content, strain, strain rate, grain size and the presence of precipitates. The temperature dependence of the Hall-Petch equation arises through the thermal component of the friction stress parameter which also depends on strain rate and composition, while the athermal component of the friction stress is related to the dislocation substructure, the density of dislocations in the material, and the presence of precipitates. In the present work however, it is the effect of temperature and second-phase particles on the yielding process which are of greatest interest.

Let us consider the effect of second-phase particles on the yielding process. A detailed review of precipitation hardening has been given by Kelly and Nicholson (1963) in which the experimental and theoretical aspects of yielding in both ferrous and nonferrous systems was reviewed.

In general, the role of the second-phase particles can be divided into two basic types, those which deform together with the matrix (soft particles) and those which remain rigid during deformation (hard particles). In the former case, when a matrix dislocation is able to penetrate the soft particles completely they are sheared, resulting in a change in shape of the particle caused by the passage of the dislocations through the particle. This shearing process results in an increase in yield stress due to the extra energy needed either to move the dislocations through the particle due to the detailed nature of bonding in the particle or due to new interfacial area produced during the passage of the dislocations. This type of particle strengthening should result in an increase in initial yield stress but no marked change in the subsequent rate of work hardening. This behavior has been observed experimentally in a number of alloy systems (Kelly and Nicholson 1963).

In the case of hard particles, Orowan (1948) has shown that if dislocations moving on a slip plane of the matrix encounter hard particles then an additional stress will be needed to expand the dislocations between the hard particles. Provided the particles are strong enough to resist the dislocations and no particle-matrix separation occurs then the additional increment of strength should be inversely proportional to the mean separation of the particles. Although this simple prediction must be modified to account for the detailed distribution of particles (Ebeling and Ashby 1965) the Orowan model is essentially in accord with experimental observations. The major difference in the influence of hard particles on plasticity is that in order for the particles to remain rigid additional deformation must be accumulated in the matrix in the vicinity of the particles. This additional deformation or strain gradient can be described either by a simple array of shear loops (Fisher, Hart, Pry 1953) or by some more complex arrangement of prismatic dislocation

loops (Ashby (1967). The essential feature of hard particle strengthening is that the additional accumulation of dislocations in the vicinity of the particles results in an increase in work hardening rate of the two-phase alloy relative to that of the single phase matrix.

The effect of temperature on the resistance to plastic deformation of ferrous materials is well known and a detailed account of the effect of the thermal component on the yield stress has been given by Conrad (1963) and will not be reviewed here. It is important however, that in addition to temperature, composition, grain size and strain rate are important factors which also influence the yielding behavior of ferrous materials. These variables are particularly important with regard to determining whether the material will yield, twin or fracture under the action of a stress at low temperatures. In crystalline solids, plastic deformation tends to occur in specific directions on certain crystallographic planes which initially have a low resistance to shear. In body-centered-cubic materials slip may occur on $\{110\}$, $\{112\}$, and $\{123\}$ planes along $\langle 111 \rangle$ directions. When the temperature of ferrous materials is decreased an alternative mode of plastic deformation called twinning may occur. In plastic deformation by twinning the orientation of the twinned region of the crystal is changed relative to that of the matrix whereas in plastic deformation by slip, the slip process is confined to a relatively few planes and the orientation of the material is unchanged by the passage of slip dislocations. In the body-centered-cubic structure, twinning occurs on the $\{112\}$ planes in $\langle 111 \rangle$ directions. Cottrell and Bilby (1951) and more recently Sleeswyk (1968) have investigated the dislocation reactions responsible for deformation twinning in body-centered-cubic materials. Hahn et al. (1959), Rees et al.(1951), and Al et al. (1953) have throughly investigated the tensile deformation properties of polycrystalline ferrous materials over a wide range of temperatures.

These workers showed that at higher temperatures plastic deformation begins at a sufficiently low applied stress so that crack nucleation by slip or twinning does not occur and the material remains ductile. As the temperature is lowered, the resistance to deformation increases, and eventually failure may result from either a slip or twinning mechanism in combination with the action of an applied normal tensile stress.

2.2.2 Nucleation of Brittle Fracture

In body-centered-cubic ferrous materials at low temperatures fracture usually occurs by transgranular cleavage on the $\{001\}$ planes. In general these materials are not elastic brittle in nature and some plastic deformation by either slip or twinning is observed prior to the fracture event. This suggests that the processes of plastic deformation and fracture may be closely linked and that some local plastic deformation may be necessary to nucleate the fracture event.

Evidence for this interrelationship between plastic deformation and brittle fracture fall into two categories; indirect evidence that some plastic deformation always precedes fracture, and observations that the deformation process which is inhomogeneous on a microscopic scale is directly responsible for the formation of cleavage cracks.

Indirect evidence that plastic deformation precedes cleavage fracture was provided by Low's (1956) work on polycrystalline low carbon steel. Low showed that for a series of low carbon steel specimens having different grain sizes that the material cleaved with no apparent prior plastic deformation when tested in uniaxial tension at -196°C. The fracture stresses recorded in tension were coincident with the yield stresses obtained in compression at -196°C for the same series of specimens. It was concluded from this observation that some small amoun of prior plastic deformation was involved in the critical event leading to cleavage fracture nucleation.

Mild steel is not particularly suitable for direct observations

of small amounts of plastic deformation preceding fracture, although Knott and Cottrell (1963) have observed yield zones below notch bend specimens using a selected etching reagent. More direct evidence that plastic deformation precedes cleavage fracture has been provided by using 3 percent silicon iron. Silicon iron is ideal in view of its etching characteristics in the vincinity of dislocations and has been used by Griffiths and Cottrell (1965), Worthington and Smith (1966), and Hahn and Rosenfield (1965) to provide direct evidence of the occurrence of plastic deformation prior to cleavage fracture.

Additional evidence of plastic deformation preceding fracture in a number of polycrystalline metals at temperatures well below the macroscopic ductile-brittle transition temperature have also been obtained by employing sensitive strain gauge techniques (Richards et al. 1968, Low 1956, Wood and Clark 1952).

At low temperatures ferrous materials may deform initially by either slip or twinning and there has been a considerable amount of metallographic evidence reported to show that either process may be responsible for cleavage crack formation. Hull's (1962) review article shows many examples of cracks forming at the tips of twins in silicon iron single crystals when the motion of one twin is impeded by other twins. Also, cracks have been observed at the intersection of two twin bands having different glide directions in many other body-centered cubic transition metals at low temperatures (Cahn 1955, Hull 1960, Honda 1961, Sleeswyk and Helle 1963) and have led to the development of a number of mechanisms by which twinning could nucleate a crack.

Clear evidence for slip nucleated cleavage formation has been found by Honda (1961) in 3 percent silicon iron crystals. Honda in tests at -196^{o}C used single crystals having a tension axis in the [010], [110], and [111] directions. For the first case, cracks formed at specific twin intersections satisfying the criterion found by Hull.

In addition, in the case of the [110] crystals, double slip without twinning was the initial mode of deformation and in this case microcracks, parallel to the tension axis were observed to form at regions where slip bands on two different systems intersected. In the case of the [111] axis crystals, cracking was not observed until after necking had occurred and the slip had become more complex. Honda suggests that in this latter case (112) or (123) slip intersections may be responsible for crack nucleation. Also, extensive evidence of cleavage cracks in ionic crystals resulting from slip bands meeting grain boundaries or where one slip band intersects another slip band have been reported by Stokes et al (1959) and Johnston and Parker (1963).

In summary then, there is a large body of experimental evidence which indicates that some plastic deformation always precedes fracture and that crack formation is directly associated with the inhomogenous nature of plastic flow. Cracks can form at the tips of both slip and twin bands. This can be rationalized in terms of the large stress concentration present at the tips of slip bands or twins by using dislocation pile up theories.

2.2.3 Crack Propagation

From the discussion in the previous section there are a number of mechanisms by which small cracks may be introduced into a material by inhomogeneous shear. If these small cracks can grow due to the action of an applied stress acting normal to the plane of the crack then complete fracture will result. Thus it is of paramount importance to know if the controlling event is concerned with the nucleation of a crack or whether it occurs at some stage during crack growth.

The theoretical breaking strength of an ideal solid is about E/10 (Kelly 1966) where E is Young's modulus. Such values have only been approached reasonably closely in experiments on very small fibres.

Ordinary materials break at far smaller stresses. The initial attempt to bridge the gap between the theoretical and observed strengths dates from the classical work of Griffith (1920) on the fracture of glass. He postulated the presence of cracks in the material which under the action of an applied stress lead to the development of stress concentrations of sufficient magnitude that the theoretical strength can be generated locally from quite low applied stresses. He reasoned that the crack will propagate under the influence of the tensile stress only if the incremental decrease in strain energy is greater than the incremental increase in surface energy. Griffith's well known formula

$$\sigma = \left(\frac{2E\gamma}{\pi(1-\nu^2)c}\right)^{1/2} \qquad (2)$$

gives the smallest tensile stress σ able to propagate an atomically sharp crack of length c through a thick plate of elastically isotropic material, where E is Young's modulus, γ is the surface energy, and ν is Poisson's ratio.

Griffith's equation then, is concerned with propagation of an existing crack in the material. The main uncertainty in the Griffith equation lies in deciding on a value for the effective surface energy since the surface energy is equated with the total energy expended in exposing unit area of the new crack faces and this energy may be much larger than the true surface energy of the solid depending on how much plastic deformation accompanies the propagation process. Another difficulty in applying the Griffith's equation to explain the fracture stress of materials is in determining the nature of the Griffith flaws. Also the existence of the ductile-brittle transition in which the energy

for fracture changes markedly when the temperature is altered by a few degrees is not explained by the Griffith formula, since none of the factors in the equation vary strongly with temperature. Hence, the various attempts to analyze brittle crack propagation in metals fall roughly into two main categories: modification of the Griffith theory of crack propagation to take into account plastic deformation during crack propagation and examinations of the variations in the deformation processes in materials to explain why brittle crack propagation is possible in some materials and not in others.

The experimental results of Guessier and Castro (1949) on the fracture behavior of notched steel bars of various thicknesses and those of Parker (1957) on comparison of the behavior in torsion and tension showed that a superimposed hydrostatic stress component markedly increased the tendency to brittle behavior of a steel. These observations led Cottrell (1958) and Petch (1959) to independently conclude that growth was the controlling event in the fracture process, since the nucleation process depends on the shear stress and not on hydrostatic tensile stress. Knott and Cottrell (1963) have demonstrated that for specimens of mild steel tested in uniaxial tension cleavage initiation does not occur until the test temperature is below -130°C, whereas in notched specimens the corresponding temperature is -40°C. Subsequently, Knott (1966, 1967) and Oates (1968, 1969) have examined in detail the effect of superimposed hydrostatic tensile stresses on cleavage fracture by varying the included angle of notch bend specimens. Both Oates (1968) and Knott (1966) investigated cases where mechanical twinning was absent, and so presumably slip bands were responsible for the nucleation of cracks, while Knott (1967) and Oates (1969) have examined situations where mechanical twinning was occurring. The results indicated that a twin band was more effective than a slip band in nucleating a cleavage crack because of the higher effective shear stress associated

with the twin band (Worthington and Smith 1966). The salient feature of all the experimental results was in accord with the view that cleavage crack growth is the critical event in the fracture process (Griffith 1920, Stroh 1957, Smith 1966). This implies that the effective surface energy for the propagation step is higher than that for the initiation process. One obvious way in which this can arise is if growing cracks are obstructed by grain boundaries (or other similar barriers such as twin boundaries in specimens that have been subjected to prior deformation twinning); such obstruction arises as a consequence of the misorientation between adjacent regions of material (Cottrell 1958, Low 1963, Gell and Smith 1967). One consequence of the obstruction of growing cracks by grain boundaries should be the development of microcracks of length equal to grain diameters. Such grain size microcracks have been observed in uniaxial tensile testing of some mild steels by Lindley (1965) and Hahn et al (1959) although in other steels, particularly those of high manganese content obstruction at grain boundaries does not occur (Hahn et al 1962, Lindley 1966) and grain size length microcracks are not observed. Moreover, grain size length microcracks are rarely found in notch specimens of mild steel over a wide range of testing temperatures (Oates, 1966, 1967, 1968, 1969; Knott 1965, 1966, 1967; Knott and Cottrell 1963) nor have they been observed at temperatures very close to the zero measurable elongation temperature (McMahon and Cohen 1965). The latter investigators found the highest incidence of non propagating microcracks near the ductile-brittle transition temperature.

In summary then, the evidence indicates that the growth of a cleavage crack to grain size dimensions and its propagation across a grain boundary is frequently the critical event in the fracture process.

2.2.4 Ductile-Brittle Transition

Zener (1948) first recognized the importance of inhomogeneous plastic deformation with respect to the nucleation of cleavage cracks, and thereby played a major role in relating the processes of plastic deformation and fracture, which before this time had generally been regarded as independent processes. Zener suggested that slip bands acting as freely slipping shear cracks held up by some obstacle (a grain boundary for example) could give rise to the very high stresses necessary for cleavage crack nucleation. This approach does not take into account the cohesion between the faces of the slip band however, and Cottrell (1953) has modified Zener's approach by considering the slip band as a sequence of dislocations, instead of a shear crack. He considers a sequence of n dislocations of Burgers vector b gliding along a slip plane which contains some obstacle to the passage of these dislocations. Once the dislocations pile up at the obstacle they attain an equilibrium distribution against the obstacle. These dislocations are all in equilibrium under the forces on them from the applied stress (τ), the obstacle and their mutual interactions. None of the dislocations can move unless the leading one moves and if the leading dislocation moves forward by a small distance δx they all move forward by this amount Thus the work done by the applied stress in such a movement is $n\tau b\delta x$ and the work done by the leading dislocation against the internal stress τ_i is $\tau_i b\delta x$. In equilibrium then, these are equal (principle of virtual work) so that

$$n\tau = \tau_i \qquad (3)$$

The dislocation pile-up serves to amplify the applied stress and produce a stress concentration at the tip of the pile-up dependent on the pile-up length. Consequently, all modern theories of cleavage fracture (Cottrell

1958; Petch 1959; Hahn and Rosenfield 1966; Smith 1966) have employed a pile-up model to represent the inhomogeneous plastic deformation process that nucleates cleavage cracks.

The realization that the initiation of fracture was closely associated with the yielding event prompted Cottrell (1958) to examine in detail the type of slip processes which could give rise to crack nucleation and he proposed a general dislocation mechanism for nucleating cleavage cracks which is valid for both single crystals and polycrystals. If the slip system for a body-centered cubic material is considered as the motion of a/2 $\langle 111 \rangle$ glide dislocations on $\{110\}$ slip planes, then if dislocations with Burgers vectors a/2 $[\bar{1}\bar{1}1]$ glide on a (101) plane, while other dislocations with vectors a/2 $[111]$ glide on a $(10\bar{1})$ plane (Figure 1) the two slip planes meet along an $[010]$ axis (a being the lattice constant). The leading dislocations on each plane coalesce to form a new dislocation, thus

$$a/2\ [\bar{1}\bar{1}1] + a/2\ [111] \rightarrow a[001] \qquad (4)$$

and in doing so they lower their elastic energy, and are attracted together. The a$[001]$ dislocation produced by the above reaction is a pure edge dislocation which lies in the (001) cleavage plane, and Cottrell suggested that it would be cracked in view of its large Burgers vector. He also suggested that this crack could grow by other slip dislocations in the (101) and $(10\bar{1})$ planes running into it as shown in the bottom of Figure 1.

In the second part of Cottrell's work he considered the stress required to grow such a crack. Using a procedure worked out by Stroh (1957), he calculated the breaking stress (σ_F) of a perfect crystal in the presence of an isolated wedge of strength, n a, where n is the number of dislocations and a is the lattice constant. Thus, if the

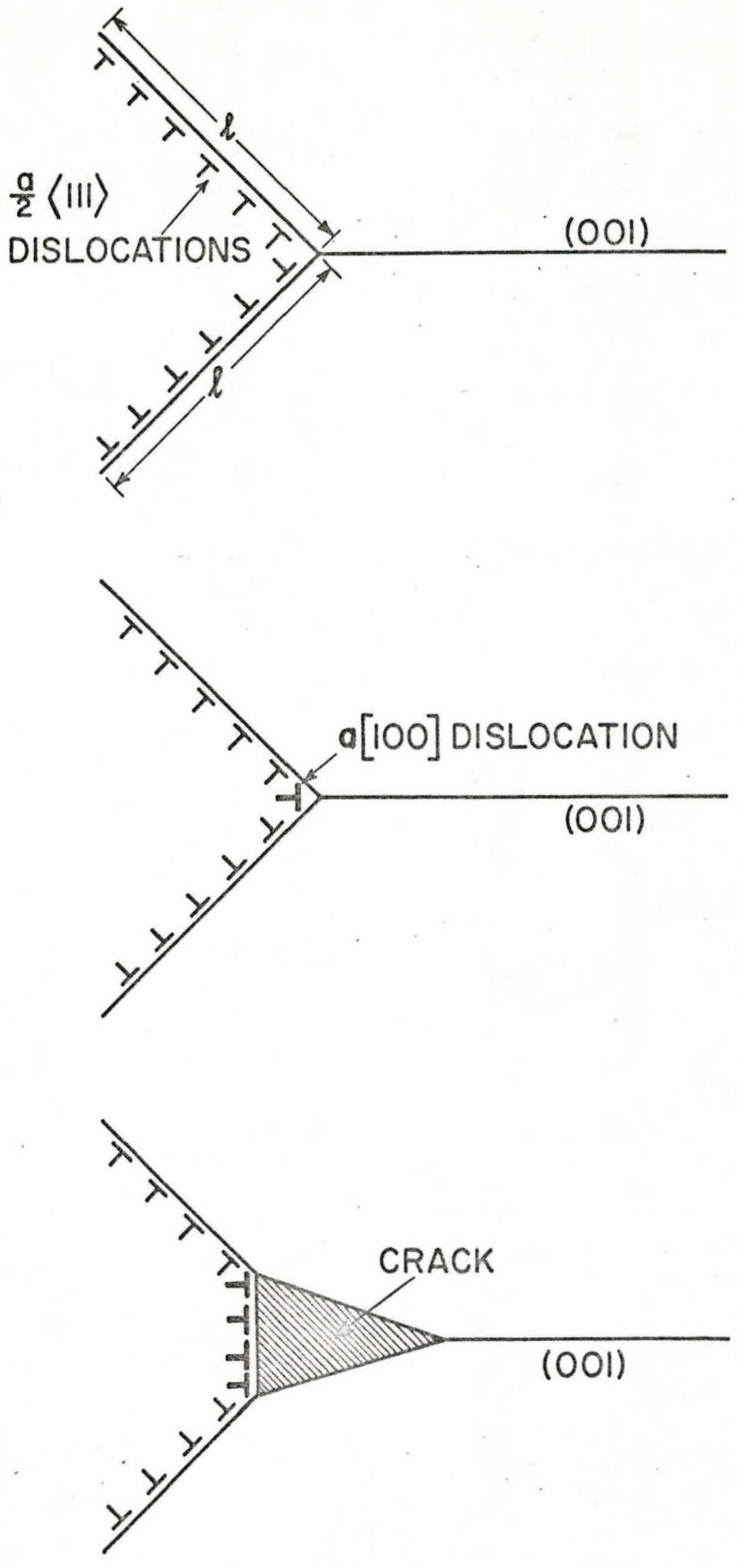

Figure 1: Coalescence of two slip dislocations to form a cracked dislocation on a cleavage plane (Cottrell 1958).

crack is normal to the applied stress, its length is c, then the energy of the cracked dislocation, W, can be written in the form,

$$W = \frac{n^2 a^2 G}{4\pi(1-\nu)} \ln\left(\frac{4R}{c}\right) + 2\gamma c - \frac{\pi(1-\nu)p^2 c^2}{8G} - \frac{pnac}{2} \qquad (5)$$

where (following Stroh) the first term is the energy of the stress field of the dislocation, R being the effective radius of this field, G the shear modulus and ν Poisson's ratio; the second term is the surface energy of the crack faces; the third term is the elastic energy of the crack in the applied stress field; and the fourth term is the work done by the applied stress (p) due to the increase in volume on opening up the crack. Equation 5 has stationary values when

$$\frac{dW}{dc} = 0 \qquad (6)$$

which then gives Equation 5 either two positive roots, in which case the smaller gives the stable crack length, or imaginary roots, in which case the crack grows indefinitely (cracks unstable).

The transition between these two cases occurs when

$$p = \frac{2\gamma}{na} = \tau_F \qquad (7)$$

in terms of the specific surface energy γ, and n the number of coalesced a{100} dislocations. Using the calculations of Eshelby et al. (1951) and Head and Louat (1955) for estimating the number of dislocations, n, in a pile-up of length ℓ,

$$n = \frac{l \tau_s}{G a} \tag{8}$$

where G is the shear modulus, and τ_s is the effective shear stress acting on the pile-up of dislocations (the effective stress is equal to the applied stress minus the stress opposing dislocation motion). Then using the experimental observations for the stress at which yielding and crack nucleation occur simultaneously (Low 1963, Petch 1953), the following criterion was derived for crack propagation to occur as soon as the material yields

$$k_y (k_y + \sigma_o l^{1/2}) \geq \beta G \gamma \tag{9}$$

where β is a parameter that measures the relation between tensile and shear stresses for a particular condition of loading (1 for tension, 2 for torsion, 1/3 for the condition at the root of a notch). When simplified, Equation 9 becomes (when yield and fracture are coincident)

$$\sigma_F > \frac{\beta G \gamma}{k_y} l^{-1/2} \tag{10}$$

Petch (1959) derived a very similar expression for the change from ductile to cleavage fracture on lowering the temperature. In the case of a notched bar this change will occur when the yield stress and fracture stress are coincident and is given by

$$\sigma_F > \frac{4 G \gamma}{k_y} l^{-1/2} . \tag{11}$$

In both the Cottrell and Petch equations the material is ductile when the left side of the equation is smaller than the right and brittle

when the reverse is true.

The Cottrell-Petch theory can therefore readily explain the effects of temperature, strain rate, grain size, and the degree of tensile stress intensification on the ductile-brittle transition. It can also explain how twinning is more effective in nucleating a cleavage crack, since the Hall-Petch slope for twinning (k_{tw}) is much higher than that for yielding (Worthington and Smith 1966, Hull 1960, Hahn et al 1962), and so reduces the right side of the equation relative to the left side.

Thus the Cottrell-Petch approach was to calculate the stress required to propagate a crack of length equal to the grain diameter and compare it with the yield stress.

However, this approach has several limitations. Firstly, as Stroh (1957) and more recently Smith (1966) have shown, that fracture is only controlled by crack growth if the effective surface energy required for propagation is increased sufficiently above the value of the surface energy required for initiation of the crack. From a comparison of the available experimental data with the expression in Equation 10, Cottrell concluded that the effective surface energy was of the order of 1.8×10^4 ergs/cm^2 which is much higher than the expected true surface energy (2000 ergs/cm^2 Price et al.1964). Cottrell attributed this discrepancy to plastic relaxation of the dislocation pile up. However, no detailed mechanism was advanced to explain the value of surface energy operative during crack growth relative to that operative during initiation. Secondly, one of the main assumptions of the Cottrell approach was that all the constituent dislocations present in the intersecting slip bands coalesce to form a wedge type crack; this was convenient but unrealistic since there is no driving force to coalesce all the dislocations and hence the magnitude of term n a in Equation 8 would clearly be overestimated. Thirdly, no account was taken of the

effect of microstructure, particularly second phase particles on the mechanism of fracture initiation and propagation although the detailed microstructure was considered with respect to the yield stress through the parameters σ_o and k_y in the Hall-Petch relationship. Thus the Cottrell approach would predict that steels with equivalent yield characteristics should exhibit similar brittle fracture characteristics in both uniaxial and notched tensile tests whereas the recent investigations of Hahn et al (1962), McMahon and Cohen (1965), Oates (1968, 1969), Lindley (1969) have demonstrated that this is not the case. These latter workers have shown that even when the only metallurgical difference between steels is one of grain boundary carbide size, there are marked differences in cleavage fracture characteristics even though the yield stresses of the two materials may be very similar.

Hahn and Rosenfield (1966) have re-examined the Cottrell dislocation coalescence model with particular reference to the values of surface energy, the number of coalesced dislocations and the interpretation of the effective shear stress. These authors modified the coalescence theory by considering that only those dislocations at the head of the array are coalesced, that is, only those dislocations whose average spacing is equal to a (the a$\langle 100 \rangle$ Burgers vector) are considered to coalesce. Using this criterion together with the computer calculations of Chou et al.(1960) for the distribution of the dislocations in a double pile-up, Hahn and Rosenfield obtained an expression for the number of coalesced dislocations to be

$$n_a \approx 5 L \left(\frac{\tau_s}{G}\right)^{3/2} \qquad (12)$$

where L is the length of dislocation array, τ_s is the effective shear stress and G is the shear modulus. Hahn and Rosenfield also question Cottrell's (1958) use of the Hall-Petch relation to estimate τ_s:

$$\tau_s = \tau - \tau_o = 1/2\ k\ \ell^{-1/2} \qquad (13)$$

where τ is the applied stress, τ_o is the friction stress, k is regarded as an unpinning parameter, and ℓ is the average grain size. This view of yielding regards the grain boundaries as extremely short-range obstacles and identifies τ_s as a relatively large stress that is strongly grain size dependent. They question this interpretation since the Hall-Petch interpretation claims that the pile-ups responsible for crack initiation are present when $\sigma_o < \sigma < \sigma_y$ where σ is the applied stress and σ_y the yield stress. This is consistent for observations of slip in isolated grains at stresses below the yield stress but is not consistent with fracture experiments which show that cleavage tends to occur after yielding (Low 1954, Petch 1953). They suggest that the Hall-Petch relation overestimates both the effective stress and its grain size dependence and propose an alternative method of calculating the effective stress on a slip band. They introduce calculations which show that the effective stress on a pile-up depends on the stress sensitivity of dislocation velocity. Furthermore, the calculations show that dislocation velocity and hence effective stress varies with distance along the pile-up and as a result, the rate of stress build up at a pile-up depends markedly on the strain rate sensitivity of the material. This consideration gives substantially smaller values than the Hall-Petch analysis. Hahn and Rosenfield claim that these two modifications lead to a better description of single phase materials than Cottrell's (1958) assumptions and use their modified equation to explain Low's (1954) fracture results of iron at $-196^{\circ}C$. However, Hahn and Rosenfield in formulating their model assumed that the operative value of the surface energy is of the order of 1500 ergs/cm^2 which is very near the true surface energy of iron (2000 ergs/cm^2). This is clearly contrary to Orowan's (1949)

observations in which the fracture surfaces of mild steel were examined by X-rays and indicated the presence of extensive plastic deformation at the fracture surface. This suggested that even for brittle metals the energy of plastic deformation at the tip of a propagating crack might be orders of magnitude greater than the intrinsic surface energy of the material. Further, the experimental observations of Tetelman and Robertson (1963) and Tetelman (1962) on the interrelationship between plastic deformation by dislocation motion and crack propagation are in accord with Orowan's results. These investigators used etch pitting techniques to reveal the extent and distribution of plastic deformation by slip occurring during crack propagation in silicon iron single crystals. They found extensive dislocation etch-pit patterns located around crack tips and along the crack path indicating the spatial distribution of plasticity occurring.

A second feature of the Hahn and Rosenfield (1966) model is their extension of the double pile-up model to estimate the cleavage stress of alloys containing dispersed particles. For hard dispersed particles, they limit the maximum length of the dislocation pile-up length L to

$$L = \frac{(\lambda + 2r)^2}{2r} \tag{14}$$

where λ is the interparticle spacing and r is the mean planar particle radius.

The Orowan model (1948), described previously, can then be used to estimate the yield stress, and accordingly, the total shear stress for the dispersed alloy system will be altered due to the dispersion of second phase particles; thus the effective shear stress will be

$$\tau_m = \tau_s + \frac{Gb}{2\lambda} \tag{15}$$

where τ_m is total shear stress acting on the dislocation pile-up between adjacent particles, and τ_s is the effective stress in the matrix. Consequently then, using this modification for L and τ_s they obtain the following value for the fracture stress for dispersion strengthened materials.

$$\sigma_F = \frac{4\gamma r}{5(\lambda + 2r)^2} \left(\frac{G}{\tau_s + \frac{Gb}{2\lambda}}\right)^{3/2} \qquad (16)$$

However, they do place two limitations on their model. Firstly, small precipitates whose diameters are less than 200 Å, are likely to be coherent with the matrix and will not serve as strong obstacles to dislocations. Secondly, particles greater than 5000 Å may crack internally or at their interfaces and thus become the equivalent of Griffith cracks equal to the diameter of the particle. Such cracks would put an upper limit on the cleavage strength. However, in developing this model for the enhanced cleavage strength of a dispersion strengthened material, they do not consider the possible occurrence of secondary slip in the region of the particle. This secondary slip was postulated to explain the increased work hardening rate due to second-phase particles.

Hahn and Rosenfield have used this criterion to explain the influence of a fine dispersion of thoria particles on the cleavage strength of iron and show that the dispersion of thoria does increase the fracture resistance. They do not mention however, if the dispersion strengthened material has a dislocation substructure. This could also limit the pile-up length.

These authors have also considered the case when soft particles are present in the matrix. Soft particles are weak obstacles by definition and permit the dislocations to pass through them. In this case the length of the slip bands will not be restricted to the interparticle spacing and can be equated with the grain diameter. Thus soft particles would not be expected to enhance the resistance to cleavage and alloys strengthened by

soft particles would, in fact, be less cleavage resistant than a particle free matrix because of the increase in the yield stress due to the particles.

In summary, Hahn and Rosenfield's (1966) model is limited on two accounts. Firstly, it does not allow for plastic relaxation of the pile-up by secondary slip (this criticism is valid for all existing models including that advanced later in this work). Secondly, it is based on the assumption that the effective surface energy is that of the free surface throughout the growth stage. Further the model would not account for the presence of stable microcracks observed in some mild steels. In effect the Hahn and Rosenfield model really considers initiation rather than growth and may be more applicable to cases where nucleation is more critical than growth, such as in the case of extremely brittle solids (ceramic type materials) or for some of the more ductile materials at very low temperatures. Hull's (1965) work on tungsten and Bullen's (1965) on chromium has shown that at low temperatures the crack surface energy is equal to the free surface energy.

Stroh (1957) has also derived a crack nucleation criterion assuming that the concentrated stresses (an extension of Zener's (1948) shear crack) at the tip of a pile-up are not relaxed by further plastic deformation before nucleation occurs. Stroh assumes that the crack nucleates by a pile-up of positive edge dislocations, these being held against a barrier by a uniform externally applied shear stress. With the aid of certain simplifying assumptions, in particular neglecting the effect of local shear stresses in assisting the spread of a crack, Stroh uses an energy balance method in determining the most favourable orientation relationship for nucleation of cracks with respect to the slip plane. Smith and Barnby (1967) have discussed Stroh's analysis and shown

that Stroh's calculations were only marginally in favour of nucleation being the critical event. Smith revises Stroh's analysis by using a corrected version of the original Griffith formula, as well as introducing the effect of local shear stresses to assist in the formation of a crack. Smith then reveals that nucleation is easier than envisaged by Stroh.

It has been recognized for many years that in mild steels cracks can form within grain boundary carbide particles (Allen et al.1953, Bruckner 1950, Oates 1968, Lindley 1969) and the recent comprehensive investigations by McMahon and Cohen (1965) have convincingly demonstrated that cracks formed within grain boundary carbide particles can propagate into the surrounding ferrite as cleavage cracks and thereby causing complete fracture of a steel. Particle cracking has also been observed in a 3% silicon iron (Gell and Worthington 1966).

The interrelationship between grain boundary particle thickness, degree of tensile stress intensification and cleavage fracture in mild steel has been recently investigated by Oates (1968). He compared the behavior of two mild steels, one having a low manganese content (0.36%) and containing large grain boundary carbide films and the other having a high manganese content (1.44%) and containing much thinner carbide films. The two mild steels had identical grain sizes and yield characteristics but their cleavage fracture characteristics were completely different. Although metallographic studies revealed that twins were responsible for cleavage in the high manganese steel while slip bands caused cleavage in the low manganese steel, the only non propagating microcracks observed were those that had formed within the grain boundary carbide films and had a length equal to the grain boundary carbide thickness. Since the high manganese steel fractured at a much lower temperature than the low manganese steel and in view of the fact that the only metallographical difference was in the carbide thicknesses, it was

concluded that the marked differences in cleavage fracture characteristics must be associated with the propagation of these cracks from particles into the surrounding ferrite matrix.

Smith (1966) has developed a fracture model which takes into account the relevant parameters involved in the formation of cleavage cracks in mild steel. He postulated that inhomogeneous plastic deformation (slip or twinning) was responsible for the fracture of grain boundary carbides and that the critical event in the formation of a cleavage crack is its growth and not its nucleation. The growth process can be associated with the propagation of cracks from the brittle second-phase particles into the surrounding matrix. Factors such as effect of grain size and temperature are also considered in the model.

Smith's model is illustrated in Figure 2 where edge dislocations representing the nucleating deformation process are emitted by a source s and lie along a plane that makes an angle of 45^{o} with the tensile axis. Cracks are nucleated at a distance d from the source which is centrally situated, 2 d being representative of the grain diameter ℓ of the material under consideration. It is assumed that cracks of length t, which represent the thickness of the brittle second-phase particles in the material, form along the plane containing these dislocations and are subject to a normal stress (σ_n) and a shear stress. To make the approach general, Smith has added a superimposed hydrostatic tensile stress p so that extension of the theory to notched specimens becomes a natural development. Using a continuum approach, that is, assuming that the dislocations in a slip band can be smeared into an array of infinitesmal dislocations and allowing for the discontinuity in the displacement across the cracks, Smith obtained the following equation for two-phase materials (Equation 17).

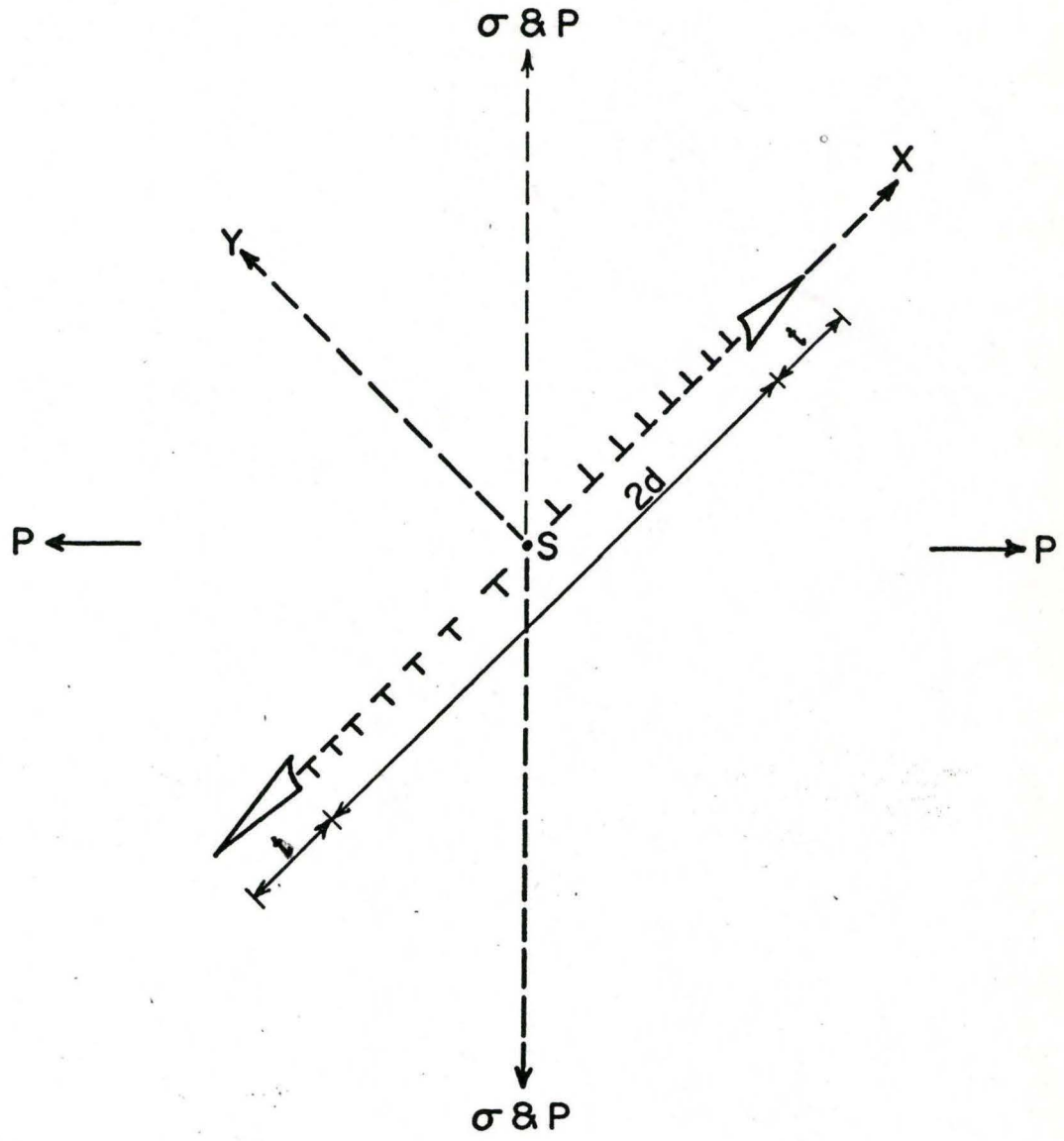

Figure 2: Schematic representation of Smith's (1966) model used for discussing the fracture process when grain boundary carbides are present.

$$\frac{t}{2d}\ (\sigma_n + p)^2 + \tau_s^2\left[1 + \frac{2}{\pi}\left(\frac{2t}{d}\right)^{1/2}\frac{\tau_o}{\tau_s}\right]^2 > \frac{4\gamma G}{\pi(1-\nu)d} \qquad (17)$$

Smith considered two conditions for Equation 17, depending on whether

$$\frac{2}{\pi}\left(\frac{2t}{d}\right)^{1/2}\frac{\tau_o}{\tau_s} \gg 1 \quad \text{(slip)} \qquad \text{or} \ll 1 \quad \text{(twin)} \qquad (18)$$

The former case is for slip induced fracture and the equation reduces to

$$\frac{t}{2d}\left[(\sigma_n + p)^2 + \tau_o^2\ \frac{16}{\pi^2}\right] > \frac{4\gamma G}{\pi(1-\nu)d} \qquad (19)$$

while the second case is for twin induced fracture and reduces to

$$\frac{t}{2d}\ (\sigma_n + p)^2 + \tau_s^2 > \frac{4\gamma G}{\pi(1-\nu)d} \qquad (20)$$

It was assumed in this case that τ_s, the effective shear stress for twinning, is much greater than τ_o, the friction stress for twinning (Worthington and Smith 1966).

Smith's model, while being a very general one to account for grain size and carbide thickness is limited on geometrical

considerations alone, in that once the crack in the second phase particle has been produced, only the applied stress is acting on the length of the particle sized crack. The shear stress which supposedly nucleated the crack does not assist in opening up the crack which is contrary to Smith's original proposition. This is because in the model as proposed by Smith, the nucleated cracks are parallel with the slip band and not at some angle to it. Smith (1966) considers that the model is primarily concerned with the temperature region where twins nucleate fracture and thus is limited to explaining brittle fracture at low temperatures (-196^{o}C). It appears then that further modification of Equation 17 would be necessary before the model could be extended to a region of practical technological importance.

In summary, it appears that the available fracture models, while considering the relevant features involved in the fracture process, are too limited in that they do not account for a change in surface energy between the initiation and propagation event and do not account for the effect of microstructure for conditions of technological importance. Further there is little quantitative data available in regard to the dependence of fracture stress on the microstructure of two-phase systems. With these limitations in mind, the first part of the present investigation was conducted to examine the role of second-phase particles on the yielding and fracture behavior of low carbon steel.

In addition to the transgranular mode of fracture discussed above, ferrous materials are also observed to fracture by an intergranular mode. The literature pertinent to this second mode of fracture is reviewed below.

INTERGRANULAR FRACTURE

2.3 Introduction

Intergranular fracture in ferrous materials can be classified into two basic types: those due to the presence of a thin film of second phase at the grain boundaries, such as iron sulfide in iron, and those due to the segregation of an impurity which occurs without any metallographic evidence of a second phase at the boundaries, for example, iron embrittled with oxygen. It is the latter case, which is of interest in the present work.

The pertinent literature will be reviewed in regard to the effects of composition, mechanical properties and metallographic data, and mechanisms.

2.3.1 Composition

It has been shown by many investigators (Rees and Hopkins 1952, Low and Feustel 1953, McMahon 1966, Richards et al.1968, Honda and Taga 1968) that the mode of fracture in polycrystalline high purity iron at low temperatures can be changed from transgranular to intergranular when the carbon content is reduced sufficiently. Honda and Taga have recently reported that the critical carbon level below which intergranular fracture occurs in slowly cooled specimens is about 0.0021 wt.%. Low and Feustel report intergranular fracture occurred in decarburized iron specimens when the carbon content was approximately 0.001 wt.% whereas recarburizing to a carbon level of 0.014 wt.% restored ductility and alters the fracture mode to transgranular. Richards et al.and McMahon carried out work on iron specimens with higher levels of carbon (0.0025 wt.% and 0.005 wt.%), respectively. They showed that the fracture mode depended on the rate at which the specimen was cooled from 700^{o}C to room temperature;

the faster the rate of cooling, the greater tendency towards intergranular fracture. Rees and Hopkins detected intergranular fracture in samples with carbon levels ranging from 0.0014 to 0.0082 wt.%.

Although the removal of carbon, and more specifically the removal of carbon from the grain boundary area (Richards et al, McMahon), leads to severe embrittlement it appears that the segregation of oxygen to the grain boundaries is of paramount importance in causing the embrittlement. It has been proposed that the embrittlement is caused by the presence of oxygen at ferrite grain boundaries and it appears to require a low ratio of segregated carbon to segregated oxygen at these boundaries (McMahon et al.1969). In fact, several authors (Rees et al. 1951, Rees and Hopkins 1952, Tomalin and Stein 1965, Stein and Low 1966) report that oxygen is the cause of intergranular embrittlement. Tomalin and Stein found on working with high purity iron single crystals (carbon reported as less than 0.005 wt.%) that the low temperature ductility could be improved by lowering the oxygen level to less than 0.0006 wt.%. Stein and Low (1966) found that fracture nucleation in single crystals of iron tested at 78^{o}K could be traced back to an occluded grain. The carbon composition of the single crystals of iron was reported to be less than 0.005 wt.% but the oxygen level was about 0.0020 wt.%. When they added 0.9 ppm of carbon, the iron sample had a higher fracture stress and the fracture could not be traced to an occluded grain. This agrees with the work of Fast (1950) and Smith and Rutherford (1957) who state that the grain boundaries in very high purity iron are not inherently weak, but that in the absence of carbon there is usually sufficient oxygen segregated to cause embrittlement.

Honda and Taga (1968) report that provided the carbon content is above a critical amount, the fracture properties are independent of the oxygen content. However, their lowest oxygen level reported is

about 0.0020 wt.%.

McMahon et al (1969) carried out an investigation to see whether the additions of alloying elements (aluminum and titanium), which interact with oxygen, would eliminate the intergranular fracture and thus support the hypothesis that the effect is caused by residual oxygen at the grain boundaries. An aluminum addition of 0.04 wt.% did succeed in eliminating the embrittling effect whereas titanium did not. The authors attributed this to the fact that titanium is a better getter for carbon and nitrogen and as a consequence the titanium was not able to interact with the oxygen.

Thus the evidence for iron indicates the intergranular fracture is caused by the presence of a low carbon to oxygen ratio at the grain boundaries with the high residual oxygen level at the boundaries causing the embrittlement. However, the carbon level is the most important deterrent to embrittlement and even though the iron may contain segregated oxygen at the boundaries, small additions of carbon over and above a critical amount which when allowed to segregate to the grain boundaries will greatly reduce the embrittling effect.

2.3.2 Mechanical Properties and Metallographic Data

When intergranular fracture occurs at low temperatures it is generally characterized by a low fracture stress; well below the stress required for cleavage fracture, and with essentially zero ductility occurring. If the temperature is raised, a point is reached at which the fracture stress coincides with the yield stress and signs of ductility appear (Honda and Taga, 1968). A further increase in temperature results in greater ductility and, depending on the operative carbon level, a normal ductile fracture may be obtained. Honda and Taga (1968) report an almost 100% intergranular surface at 22^{o}C in specimens with less than 0.0012 wt.% carbon but do not report the

mode at temperatures greater than 22°C. For higher levels of carbon, at similar temperatures, the iron specimens fractured in a ductile manner.

McMahon (1966) has reported a large variation in fracture stress, fracture mode, and elongation to fracture at -196°C in low carbon ferrite depending on rate of cooling from 705°C. When the iron (containing about 0.005 wt.%C) is quenched from 705°C, severe embrittlement occurred. As the temperature from which the iron samples were quenched was decreased, the fracture mode progressively changed to transgranular. Maximum ductility and fracture stress occurred when samples were quenched from 485°C. This was the highest temperature at which no grain boundary carbides were observed and the fracture surface was almost 90% transgranular. Richards et al. (1968) showed that the fracture mode was dependent on the rate of cooling from 720°C. Quenching iron samples containing 0.0025 wt.% carbon from 720°C and testing at -196°C showed no observable elongation with a fracture surface predominantly intergranular in nature. However, if the specimens were furnace-cooled, some plastic elongation was recorded before fracture with about 90% of the surface exhibiting the river patterns characteristic of cleavage fracture.

Rees and Hopkins (1952) observed both a decrease in brittle fracture strength in uniaxial tension at -196°C and a progressive increase in transition temperature in notched impact tests with increasing oxygen content (carbon 0.0025 - 0.0080 wt.%).

The intergranular fracture surface is characterized by its very smooth grain boundary facets portraying a three-dimensional effect of the grains, contrasting with the characteristic river lines on the cleavage facets observed in transgranular fracture. Sometimes the intergranular facets show what appear to be small particles embedded in the surface (Richards et al. 1968, McMahon 1966). Richards et al has suggested that these particles are iron oxide but no diffraction evidence has thus

far been produced to substantiate this suggestion.

When embrittled specimens are sectioned perpendicular to the fracture surface, decohesion of the grain boundaries is often observed away from the fracture surface (Richards et al, 1968, Low and Feustel 1953). Also, it has been observed (Low and Feustel, Richards et al) that when intergranular fracture occurs twins are only visible on sectioned samples within one or two grains immediately adjacent to the fracture surface. This substantiates the observations that in embrittled specimens, no twinning bursts are heard, nor load drops seen in the early stages of deformation (Richards et al, 1968) and suggests that twins are produced during crack propagation.

McMahon (1966) and Richards et al (1968) have observed that intergranular microcracks are often associated with twins. This led McMahon to suggest that the microcracks were nucleated by the twins. Richards et al have rationalized this observation by considering the stress distribution at the tip of a twin.

In summary then, when the mode of fracture changes from transgranular to intergranular the fracture stress is generally very low and very little plastic deformation appears to be involved in the fracture propagation.

2.3.3 Mechanisms of Intergranular Fracture

While the evidence on purity and temperature, as they effect the mechanical properties, and the resulting microstructure is now fairly well documented, little consideration has been given to the detailed mechanisms for the initiation and propagation of intergranular fracture.

Since intergranular fracture involves the loss of cohesion along the grain boundaries, the phenomenon has been attributed to simply a lowering of the interfacial energy γ_{GB} of the grain boundaries

due to the segregated oxygen. Although there is evidence that oxygen is adsorbed on the surface of delta iron (Hondros 1968) and in view of the fact that in all the cases where intergranular fracture occurs, the oxygen content is in excess of the solubility limit, it can be postulated that oxygen segregation will occur at the grain boundaries. However, the segregation to the grain boundaries is a very localized phenomena and thus it is extremely difficult to produce experimental evidence to substantiate the models based on oxygen segregation. It is not clear whether the segregation of oxygen to the grain boundaries is by Gibbsian adsorption or whether it is a non-equilibrium segregation of the type proposed by Floreen and Westbrook (1969). To date little direct evidence for segregation exists although the development of techniques such as Auger electron microscopy and energy loss electron microscopy may aid this in the future.

It was mentioned in the previous section that McMahon (1966) and Richards et al.(1968) observed twins associated with intergranular microcracks, prompting McMahon to conclude that the microcracks were nucleated by the twins. This provides a possible mechanism for the initiation of fracture by the high stresses produced at the tips of the twins. However, Richards et al.(1968) proved quite conclusively that the twinning stress was consistently higher than the intergranular fracture stress over a range of grain sizes. They suggested it was more likely that the twins were formed during the propagation of fracture as suggested previously by Low and Feustel (1953) and Hull (1961).

Two alternative mechanisms have been proposed by Richards et al; either propagation of pre-existing Griffith-type flaws or crack nucleation by micro-slip in the pre-yield region, which can then spread under the influence of the applied stress. In the former case, although no grain boundary microcracks were observed in their

quenched material, they estimated that any microcracks must be less than 10 microns in length to avoid detection. Using the Griffith fracture criterion, they calculated the surface energy necessary to propagate the 10 micron crack length to be 230 ergs/cm^2. For intergranular failure this energy value should be equal to $2\gamma_s - \gamma_{GB}$, where γ_s is the energy of a new surface and γ_{GB} is the grain boundary energy. Now the true surface energy of pure iron is about 2000 ergs/cm^2 (Price et al, 1964) and if the grain boundary energy is about one third this value (Inman and Tipler 1963) a very large oxygen effect on the surface energies of the pure iron would be necessary to obtain the value of 230 ergs/cm^2. However, there appears to be an arithmetic error in the estimate reported above because applying the reported fracture stress of 26,000 psi and using a crack length of 10 microns, the calculated surface energy value should be 2300 ergs/cm^2 instead of 230 ergs/cm^2.

The alternative mechanism for initiation is for some micro-slip to occur in the specimens and nucleate a crack which propagates with a low surface energy value. If this is the mechanism, then it should be possible to use the Cottrell-Petch fracture relation,

$$\sigma_F = \frac{4G\gamma}{k} \ell^{-1/2} \qquad (21)$$

where σ_F = fracture stress

G = shear modulus (for iron 8×10^3 Kg/mm^2 - Hahn and Rosenfield 1966)

k = Hall-Petch parameter

ℓ = average grain diameter

γ = the effective surface energy

However, as this formula applies to the ductile-brittle transition

condition, it can only be applied where fracture and yield coincide. The only available data, which satisfies this condition, comes from the work of Honda and Taga (1968), who report fracture coinciding with the lower yield stress at -75°C. This data was for their critical carbon content and their values for elongation to fracture vary considerably at this carbon level. As a result the fracture may not in fact be 100% intergranular. Nevertheless, using their fracture - lower yield stress value at this point (25 Kg/mm^2) gives an effective surface energy value equal to about 2.9×10^4 $ergs/cm^2$. This value was obtained with a k value of 2.2 $Kg/mm^{3/2}$ (Cottrell 1963) which may be incorrect in view of the fact that intergranular fracture is usually observed to occur in material under conditions where dislocation sources are not heavily locked. Reducing the k value to 1 $Kg/mm^{3/2}$ (Armstrong et al (1962) reported for partly decarburized Swedish iron a k value equal to 0.99 $Kg/mm^{3/2}$) gives an effective surface energy of 1.3×10^4 $ergs/cm^2$.

Richards et al.(1968) provide evidence for dislocation movement in their quenched compression samples which when pulled in tension to the stress at which dislocation movement was first observed, fractured intergranularly. On the other hand, for their furnace-cooled specimens no slip was detected before twinning which is in accordance with their load-elongation observations where twinning bursts are observed in the pre-yield region and some elongation occurs before fracture. The critical event then seems to be in assessing the role of slip and in particular the slip in the pre-yield region.

One other important aspect to be considered in regard to the transferrence of slip from one grain to another concerns the evidence of increased grain boundary hardness associated with intergranular fracture (Westbrook and Wood 1961). This increase was observed in specimens which had a low carbon to oxygen ratio at the grain

boundaries. Although electron transmission microscopy has not revealed any structural differences to account for the hardness difference (Phillips 1963), compositional or thermal treatments which eliminate the hardness difference also eliminate intergranular fracture. This increase in the grain boundary hardness may be associated with the difficulty in transmitting slip from one grain to another resulting in premature failure along the grain boundaries. If there is a difficulty in transferring slip it will be seen in an alteration in the Hall-Petch parameter k, as k by definition is a measure of the resistance of the grain boundary to the passage of dislocations and/or the creation of new dislocations in unyielded grains. There is evidence that heat treatments have a significant effect on the Hall-Petch parameter (Smith et al. 1963, Cottrell 1963) but these measurements have been made under conditions where carbon contents are sufficiently high to offset any embrittling effect due to the oxygen, or at temperatures where ductility would be observed even for embrittled material.

Thus, in summary, although much effort has been directed towards delineating the role of composition and in particular the carbon-oxygen ratio on intergranular fracture, the detailed mechanisms of initiation and propagation remain undefined.

CHAPTER 3

MATERIALS AND EXPERIMENTAL PROCEDURES

3.1 Introduction

As outlined in the literature review much attention has been paid to the influence of microstructure on the yielding processes in metals but to date few quantitative descriptions have been developed concerning the influence of microstructure on the fracture process. Much evidence has accumulated to indicate that second phase particles play an important role in the initiation of brittle fracture and in the determination of the transition from ductile to brittle behavior in structural materials. It is thus of value to attempt to develop a quantitative description of the role of second phase particles on the fracture behavior of well characterized materials and to examine the implications of this description when applied to more complex materials such as structural steels.

The purpose of the present work was to examine the yield and critical fracture stress in low carbon iron as a function of grain size and as a function of the carbide distribution both within the grain and at the grain boundary. Detailed consideration has been given to delineating the role the second phase particles play in both the initiation and subsequent propagation of cleavage cracks. The experimental program utilized specimens tested in various states of stress. It is thus pertinent to comment on the influence of the state of stress on yielding and fracture behavior.

3.2 Effect of the State of Stress on Yielding and Fracture

One of the easiest methods of obtaining the critical fracture

stress in low carbon ferrous materials is to establish when fracture and yielding coincide by means of notch bar bend tests. The presence of a notch serves to develop tri-axial stresses around the notch and does not alter the intrinsic mechanical properties or fracture characteristics of the material around the notch. The tri-axial stresses developed at a notch are composed of two parts: a hydrostatic component which contains no shear stresses; and a deviatoric component which consists entirely of shear stresses and is responsible for the yielding processes. In an ideal plastic rigid solid containing a notch, the largest tensile stress in this region exceeds the yield stress in shear by the magnitude of the hydrostatic component. It has been shown by Green and Hundy (1956) using slip-line field theory that for a notched bar the maximum tensile stress (σ_{max}) at general yield* may be expressed in terms of the shear yield stress τ_y, and Θ the included notch angle in radians by the relation

$$\sigma_{max} = 2\,\tau_y \left(1 + \frac{\pi}{2} - \frac{\Theta}{2}\right) \tag{22}$$

The shear yield stress τ_y can be expressed in terms of the uniaxial yield stress σ_y by means of the von Mises or the Tresca yield criterion.

$$\sigma_y = \sqrt{3} \cdot \tau_y \quad \text{von Mises} \tag{23}$$

$$\sigma_y = 2 \cdot \tau_y \quad \text{Tresca} \tag{24}$$

Figure 3 is a schematic diagram of a load-deflection curve illustrating the condition for general yield in a notch bar.

Thus, in notch bend tests material is constrained at the

* General yield is defined as the state when plastic yielding is just able to propagate across the minimum section in notched bars.

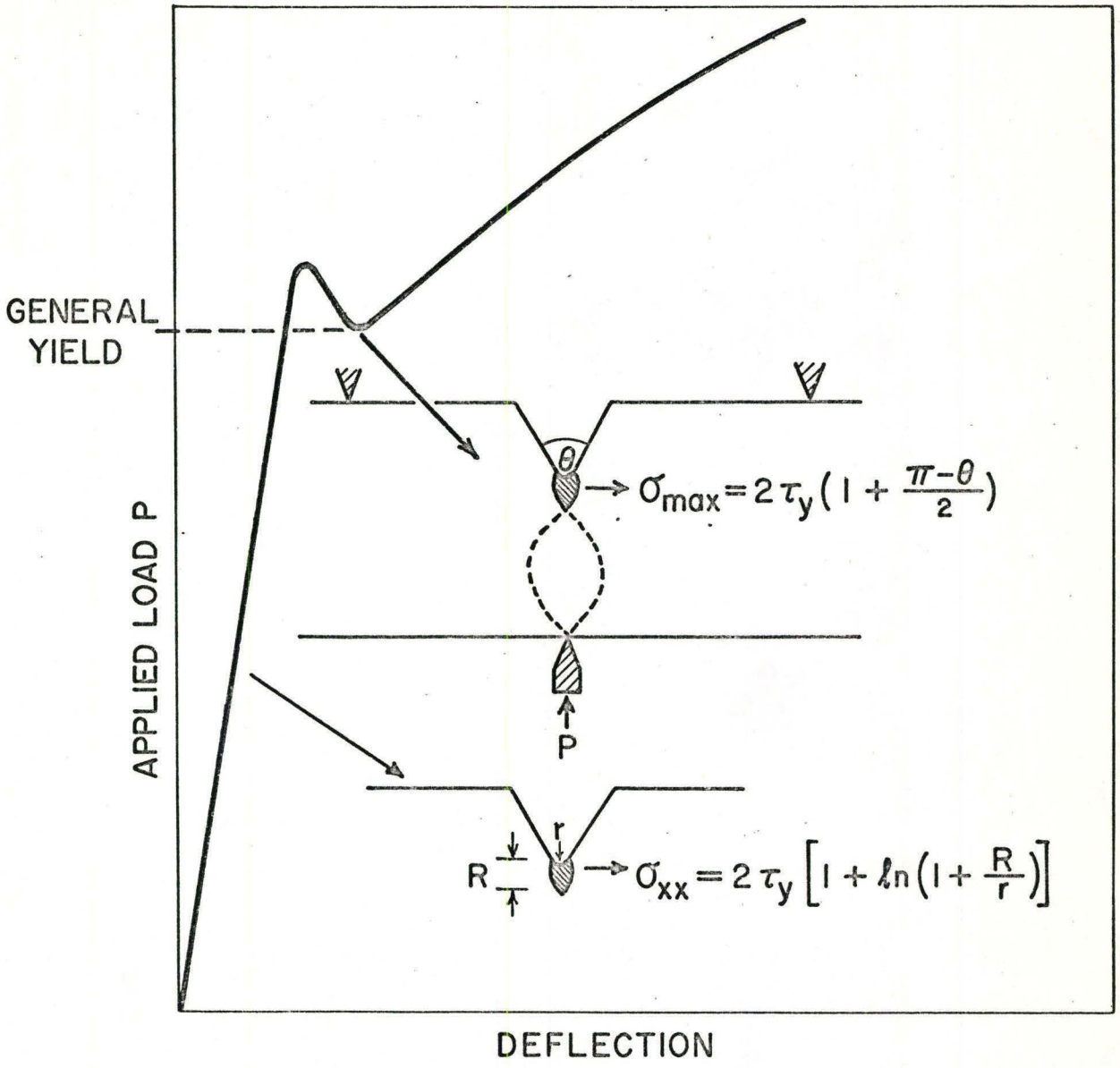

Figure 3: Schematic load-deflection curve for a notched specimen in three-point bending.

notch root so that in order for slip to propagate the longitudinal tensile stress below the notch is raised to R times the yield stress in uniaxial tension (Knott 1966). R is known as the stress intensification factor and reaches its maximum value at general yield. If the testing temperature is varied until fracture occurs at general yield, the critical fracture stress can be determined by the expression

$$\sigma_F = \sigma_{max} = R\,\sigma_y \qquad (25)$$

In this work most of the notch bars have an included angle of 45° so R is equal to 2.18 using the Tresca criterion and 2.52 for the von Mises criterion. The temperature at which fracture occurs at general yield is known as the transition temperature. Thus by measuring the uniaxial yield stress at the transition temperature the critical fracture stress can be obtained.

3.3 Composition and Heat Treatment of Materials

The compositions of the materials used in this work are listed in Table 1. The NPL and Armco iron was received in the form of 1/2 inch diameter rod; the commercial structural steel in 1/2 inch plate.

To obtain a suitable range of grain sizes the annealing treatments listed in Table 2 were used.

It is perhaps pertinent at this point to discuss the portion of the iron-carbon phase diagram relevant to this work.

Figure 4 shows a portion of the iron-carbon phase diagram (Smith 1962) on which the compositions of the various materials used in this work are shown. The equilibrium microstructures of low carbon ferrous materials at room temperature would show a structure consisting of ferrite, as the matrix, in which iron carbide particles, cementite, or pearlite (a mixture of ferrite and cementite) are embedded.

TABLE 1

LIST OF MATERIALS

Alloy	Composition						
	C	N	0	Si	Mn	P	S
NPL	.018	.0006	.0006	.003	0.01	.002	.003
Armco Iron	.022	-	-	.003	.028	.005	.018
Mild Steel (1018)	.171	.003	-	.004	.35	.004	.014

TABLE 2

The heat treatments used to obtain the various grain sizes.

Heat Treatment	Grain size, mm
NPL	
Reduced 75% by cold swaging, annealed at 925°C for 6 hrs.	0.105
ARMCO	
Reduced 25% by cold swaging, annealed at 720°C for 1 hour	0.0145
Annealed at 720°C for 1 hr., 25% reduction, annealed 750°C for 12 hours	0.0230
Annealed at 720°C for 1 hr., 25% reduction, annealed 720°C for 5 hours	0.0234
Annealed at 720°C for 1 hr., 25% reduction, annealed 720°C for 15 hours	0.0370
Reduced 25%, annealed 920°C for 1 hr.	0.0860
Reduced 25%, annealed 1200°C for 3 hrs.	0.144
Reduced 25%, annealed 1200°C for 6 hrs.	0.276
COMMERCIAL STRUCTURAL STEEL	
50% reduction by cold rolling, annealed at 925°C for 1 hr.	0.0209

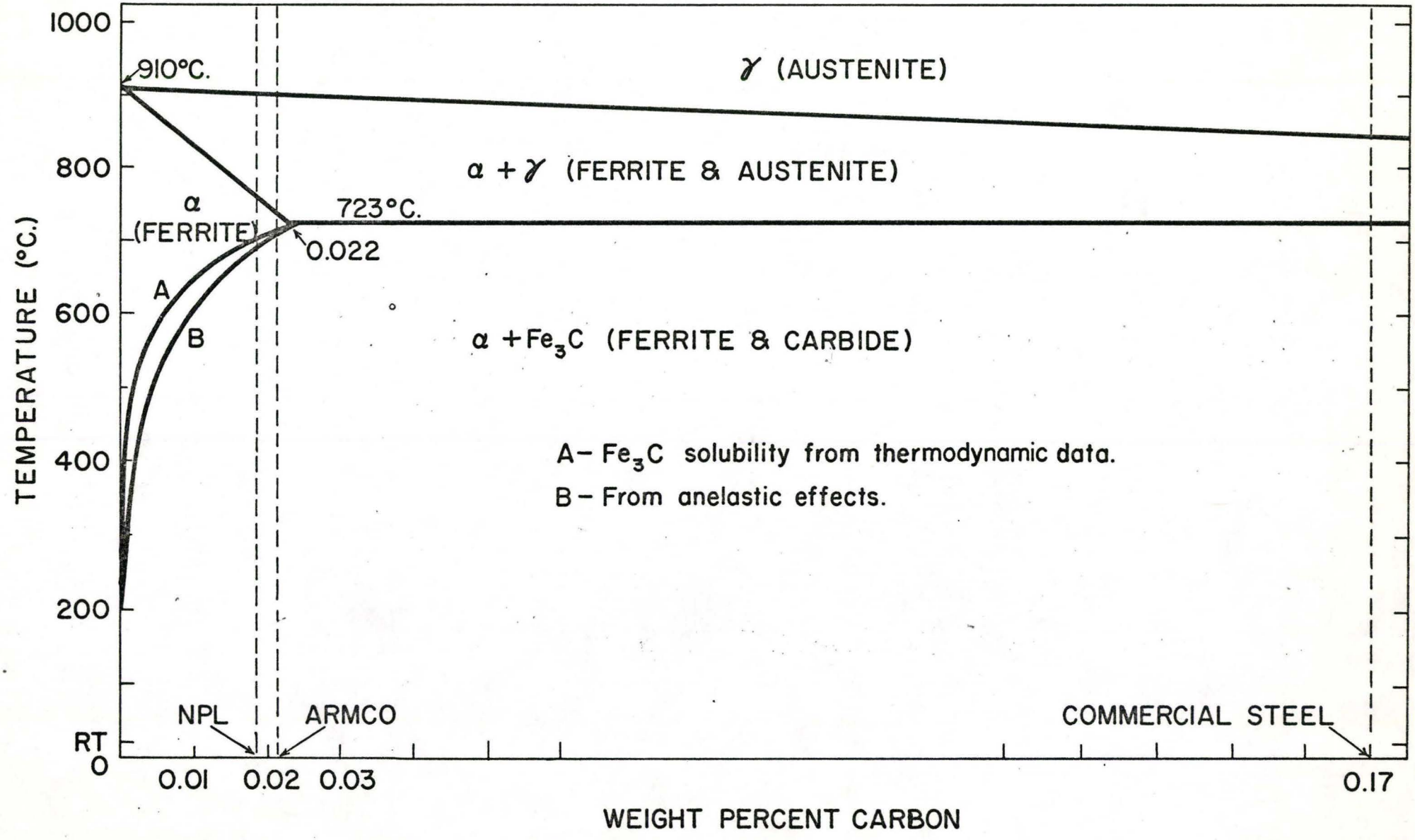

Figure 4: Low carbon portion of the iron-carbon phase diagram.

In the case of NPL or Armco iron, if these materials are slowly cooled from the ferrite region of the phase diagram the microstructure would consist of ferrite and cementite, the latter generally present as a discontinuous film along the grain boundaries of the ferrite. However, if either NPL or Armco iron is cooled rapidly (quenched) from the ferrite region and subsequently aged at a temperature in the range 100°C to 300°C the microstructure would now consist of ferrite with most of the carbon present as a dispersed carbide within the matrix. The type of dispersed carbide depends on ageing time and temperature (Leslie et al. 1959 , Keh and Leslie 1962 , Wells and Butler 1966).

In the case of the commercial steel, containing 0.17%C , when slowly cooled, the microstructure would consist of ferrite and pearlite, the latter present as a characteristic lamellar structure. If the commercial steel is now heated up to a temperature just below 723°C (see Figure 4) then quenched and aged at temperatures similar to that for NPL or Armco, the microstructure would not be significantly altered, although that portion of the carbon (approximately 0.02%) that went into solid solution in the ferrite would precipitate out as a dispersed carbide within the ferrite matrix. Thus, the structure would consist of ferrite (with a dispersed carbide) and pearlite.

3.4 Test Specimens

Tensile and notch bend bars were fabricated to the dimensions shown in Figures 5 and 6 , respectively. The notch bars served as specimens for both impact bar tests and slow bend tests. For the NPL material, only tensile specimens were fabricated; for the commercial steel only notch bars were fabricated. All of the test specimens were fabricated and notched before the final annealing treatment. The specimens were furnace-cooled to room

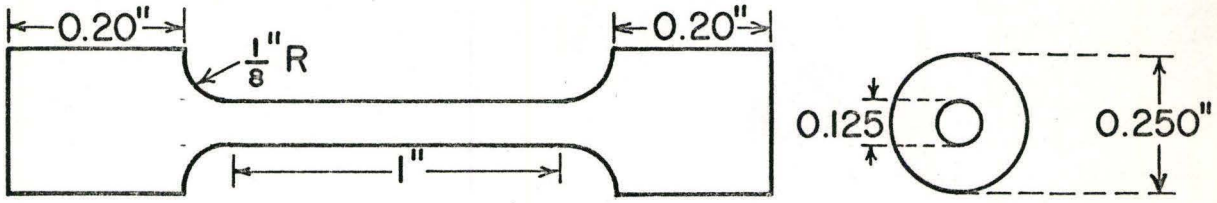

Figure 5: Design of tensile specimens.

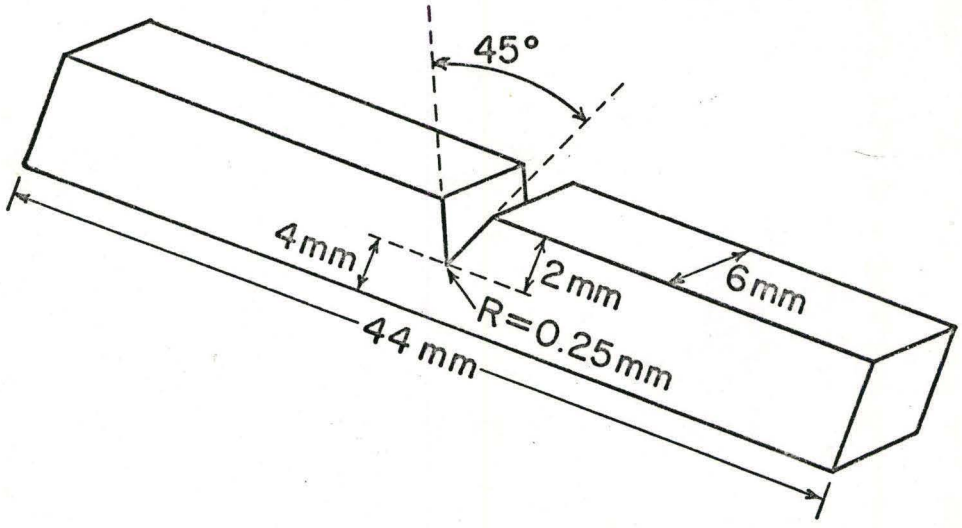

Figure 6: Design of notched bar specimens.

temperature from the final annealing temperature at a rate of 50 deg C/hour. Some of the tensile and notched bars were then heated to 720°C for one hour and quenched into ice water (0°C). Some of the quenched test specimens were subsequently aged at 100°C for 6 hours, the remaining were aged at 300°C for 8 hours. Between the time of the quench from 720°C and the subsequent ageing treatment, the test specimens were kept in liquid nitrogen. All the tensile specimens were electropolished in Morris' (1949) solution before testing to remove any surface irregularities.

All heat treatments were carried out in a vacuum furnace evacuated to a pressure of 1×10^{-5} torr.

3.5 Testing Procedure

The notched specimens were deformed in three-point bending and the tensile specimens in unaxial tension inside a metal cage suspended from the cross head of an Instron testing machine driven at a speed of 0.2 in/min. Tests were conducted at various temperatures from room temperature down to -196°C by immersing the metal cage in a bath of liquid.

The low temperature liquid baths consisted of either a mixture of acetone and solid carbon dioxide (temperature range from room temperature to - 78°C) or a mixture of Freon 12 and liquid nitrogen (temperature range from -30°C to -155°C). Some tests were made at liquid nitrogen but no tests were made between -155°C and -196°C.

Each specimen was maintained to within $\pm$ 2 deg C of the desired temperature for 10 minutes prior to testing, by hand mixing the liquid solution. The temperatures were determined by means of a chromel-alumel thermocouple and a Honeywell portable potentiometer using a cold junction maintained at 0°C.

Figure 7 shows the testing machine, with the three point bend

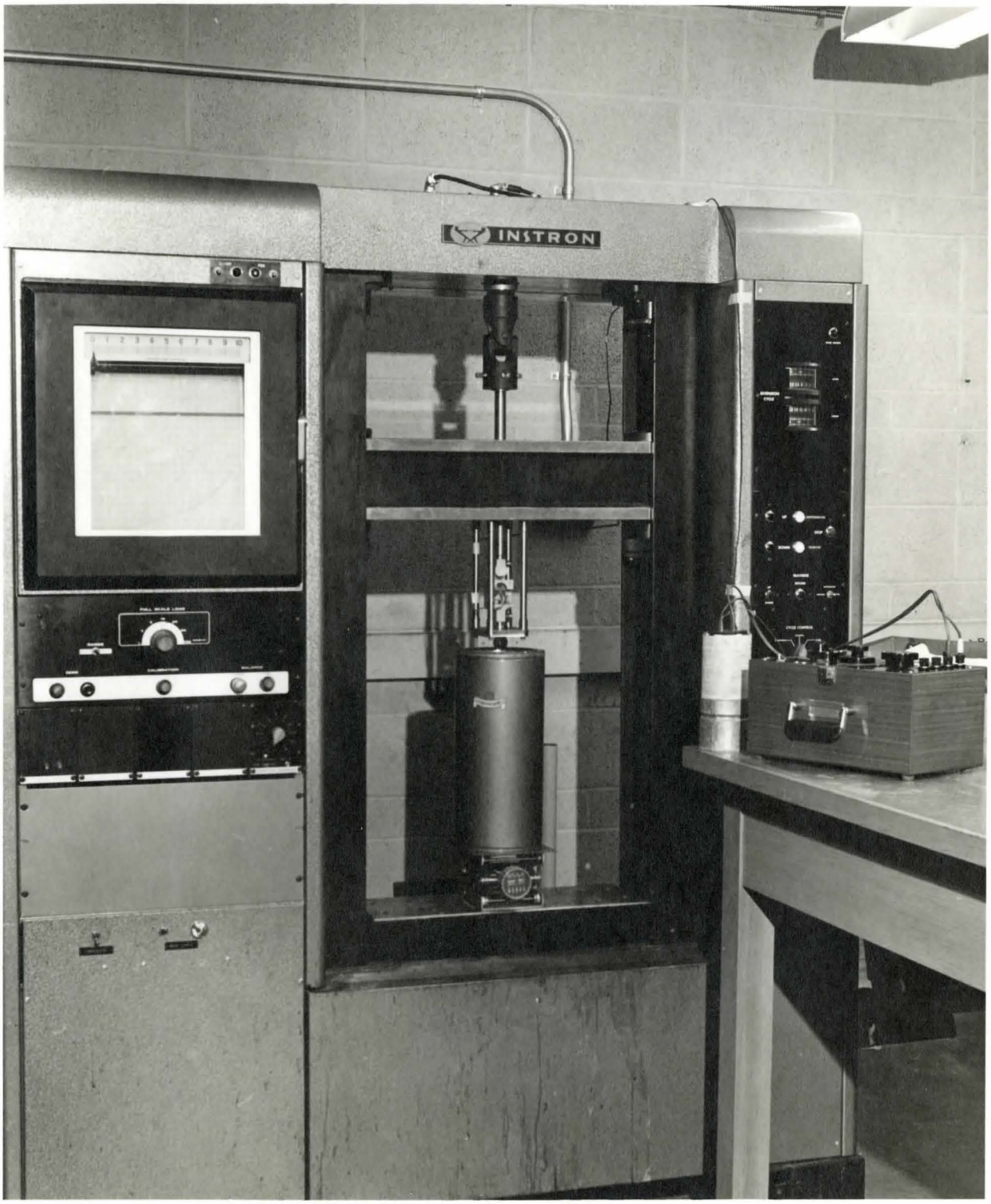

Figure 7: Photograph of testing apparatus.

jig in place, the dewar for holding the liquid baths, and the portable potentiometer and thermocouple for measuring the temperature.

For the notch impact tests the test temperatures above room temperature were obtained by heating a detergent solution (Kyrol L) on a hot plate and monitoring the temperature with a mercury in glass thermometer. The low temperatures were obtained as explained above for both the three-point bend and uniaxial yield tests.

The notch impact tests on the commercial structural steel specimens were obtained on a Tinius-Olsen pendulum impact machine of 264 ft-lbs capacity while the notch impact tests for Armco iron were obtained on a Zwick pendulum impact machine of 500 Kilogram-centimeter capacity (36.15 ft-lbs.).

3.6 Metallographic Techniques

3.6.1 Carbide Measurements

In the furnace-cooled specimens, grain boundary carbides in the low carbon materials, and coarse lamellar pearlite in the commercial steel, could readily be seen in metallographically prepared sections by optical microscopy. In order to obtain an idea of the sizes and distributions of the grain boundary carbides in the low carbon materials, 100 randomly observed carbides were measured and recorded for each of the different grain sizes. For each grain boundary carbide measured, the maximum thickness was recorded.

The presence of grain boundary carbides in the quench-aged low carbon materials could only be established by examining carbon replicas in the electron microscope of sections taken from test specimens. In this case, only about ten measurements of the carbides from the electron micrographs were made for each grain size.

The fine dispersion of carbides within the ferrite grains of the

quench-aged low carbon specimens were examined in thin films by transmission electron microscopy. Measurements of the mean planar spacing was obtained by a random line technique and the results from a number of micrographs were averaged. The carbides within the grains could not be identified by electron diffraction.

For the commercial steel, the microstructures of the furnace-cooled and quench-aged materials showed that the proportion of pearlite was approximately the same.

3.6.2 Grain Size Measurements

Sections from two notched bars and/or heads of two tensile test specimens from each heat treatment were examined metallographically and grain sizes obtained by using the linear intercept method of Lement et al (1954).

In order to obtain a representative grain size and to overcome any anisotropy of grain shape five different traces were made in the horizontal and vertical directions across the total section of each specimen. This was particularly desirable for the smaller grain size material as they tended to show more grain shape anisotropy than the larger grain size material. The results were then averaged to express a mean grain size for each specific heat treatment.

3.6.3 Electron Microscopy

Transmission electron microscopy was used to examine the fine dispersion of carbides within the ferrite grains. Thin wafers about 1/16 of an inch thick were cut from the test specimens by means of a fine-toothed jeweller's saw, then mechanically polished on 200 grit Emery paper to about 0.01 inches. In the case of tensile specimens, the thin wafers were cut from the heads of the tensile specimens. The mechanically thinned sections were then chemically thinned to about

0.003 inches using a solution of 80 ml hydrogen peroxide (30%), 15 ml of distilled water, and 5 ml of hydrofluoric acid maintained at a temperature around -10°C. For the final stages of thinning, the standard window technique (Nicholson et al 1958) and Morris' (1949) solution was found to produce good thin foil specimens.

The sizes and distributions of grain boundary carbides in quench-aged material was examined by means of carbon extraction replicas taken from surfaces of sectioned test specimens using the following experimental procedure. Sectioned specimens were mounted in lucite, mechanically polished to a 0.3μ finish, and then etched in a 2 percent solution of nitric acid in methyl alcohol long enough to give slight relief of the grain boundaries. The sample was then ultrasonically cleaned, washed in methyl alcohol and coated with carbon in a vacuum coating unit. So that carbon would be deposited only on the sectioned specimen, the exposed area of the lucite mount was masked off. The carbon was stripped off by immersing the sample first into a solution of 10 percent bromine and 90 percent ethyl alcohol at room temperature for 5 - 10 minutes, then into distilled water.

Both the thin films and extraction replicas were examined in a Siemens Elmiskop I electron microscope. The thin films were examined at 100 kV, the carbon replicas at 80 kV.

CHAPTER 4

OBSERVATIONS ON CLEAVAGE FRACTURE

This chapter is divided into three sections: a preliminary survey of the fracture characteristics of both low carbon irons and a commercial structural steel; a detailed investigation of the yield and fracture behavior of low carbon ferrite containing various carbide distributions, and the development of an elementary quantitative model to describe the fracture of two phase materials.

4.1 Preliminary Survey

The fracture properties of a low carbon ferrite and a commercial structural steel were surveyed using notched bar impact tests.

4.1.1 Notched Bar Impact Tests

A very rapid and widely used test for measuring the total energy absorbed in both the initiation and propagation of fracture is the notch impact test. While the test gives little information regarding the intrinsic properties of materials, it provides a useful basis for comparison of materials in that it provides a simple method of following the change in the fracture mode of a steel as a function of temperature.

Figures 8 and 9 show the variation of impact energy with testing temperature for the commercial structural steel and the Armco iron respectively, in the furnace cooled and quench-aged

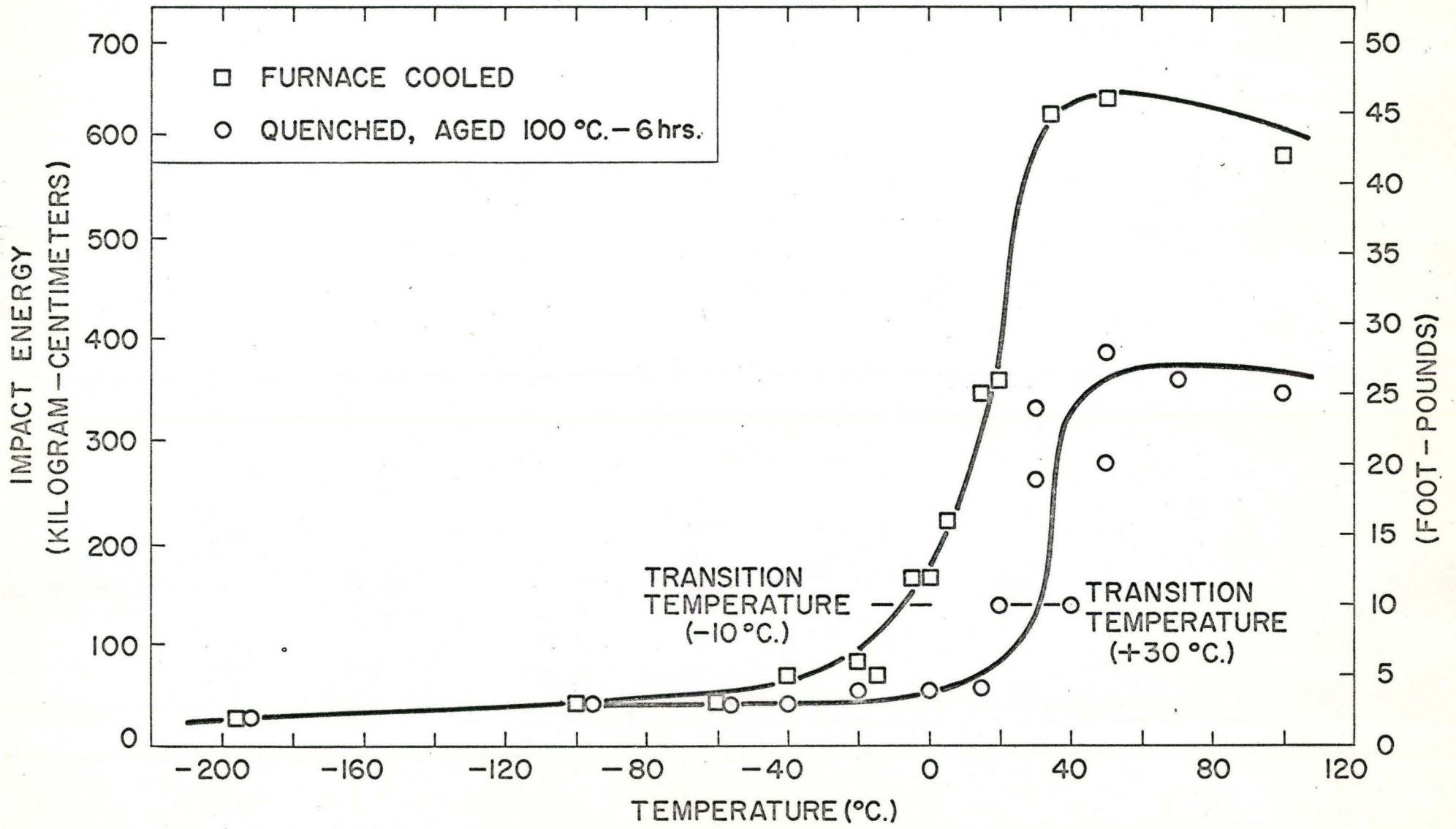

Figure 8: The variation of impact energy with testing temperature for the commercial steel specimens in the furnace-cooled and quench-aged condition.

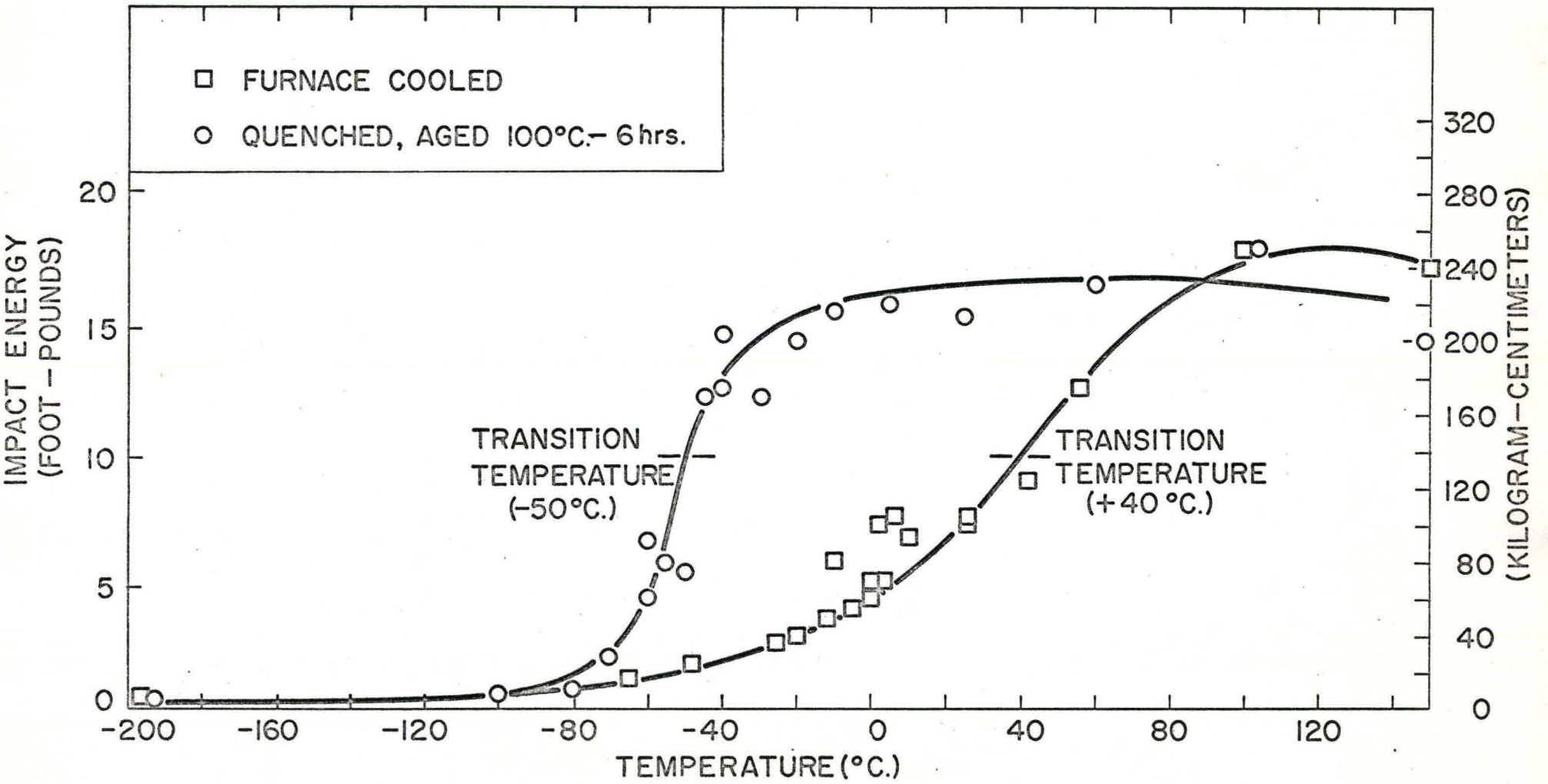

Figure 9: The variation of impact energy with testing temperature for Armco iron specimens in the furnace-cooled and quench-aged condition.

condition (100°C for 6 hours). One of the important features of these curves is the extent of the temperature range in which the energy expended in breaking the specimens decreases from a maximum to a minimum value. Closely associated with this range of energy absorption values is the amount of the cross section that has broken in a ductile fashion. The higher energy values correspond to a ductile fracture and the low energy values correspond to a brittle (cleavage) fracture. The intermediate energy values correspond to a mixed mode.

As seen in the figures there is no single temperature where the two materials suddenly become brittle and the transition occurs over a finite temperature range. The transition temperature for the notched bar impact tests in this work has been arbitrarily taken at that temperature coinciding with an energy absorption value of 10 ft-lbs. Equally valid comparisons could be made on the basis of the temperature corresponding to 50 percent of the shelf energies or on the observation of 50 percent crystallinity in the fracture surface.

The results indicate that for the commercial steel an increase in transition temperature occurs on quench ageing while for the Armco iron a decrease in transition temperature occurs on quench ageing.

4.1.2 Microstructural Observations

Microstructures of the commercial structural steel and the Armco iron in the furnace-cooled and quench-aged condition are shown in Figures 10 and 11 respectively. The important feature of these optical micrographs lies in the different second phase distributions. For the commercial structural steel the microstructures do not differ significantly and the proportion of pearlite content is approximately the same in both cases although the quench-aged specimen has a greater amount of dispersed carbide within the ferrite matrix (Figure 12).

In the case of the low carbon material, the microstructures differ

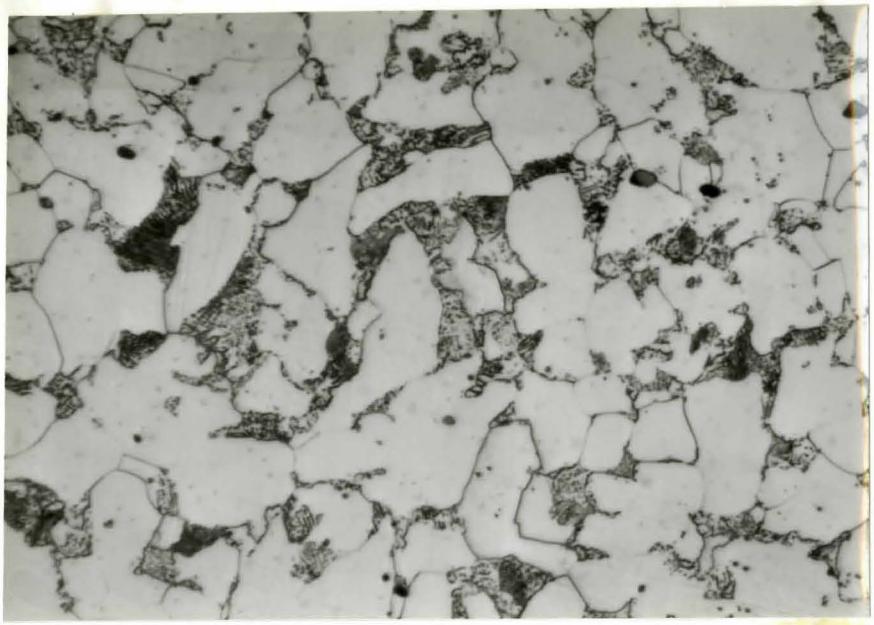

FURNACE COOLED

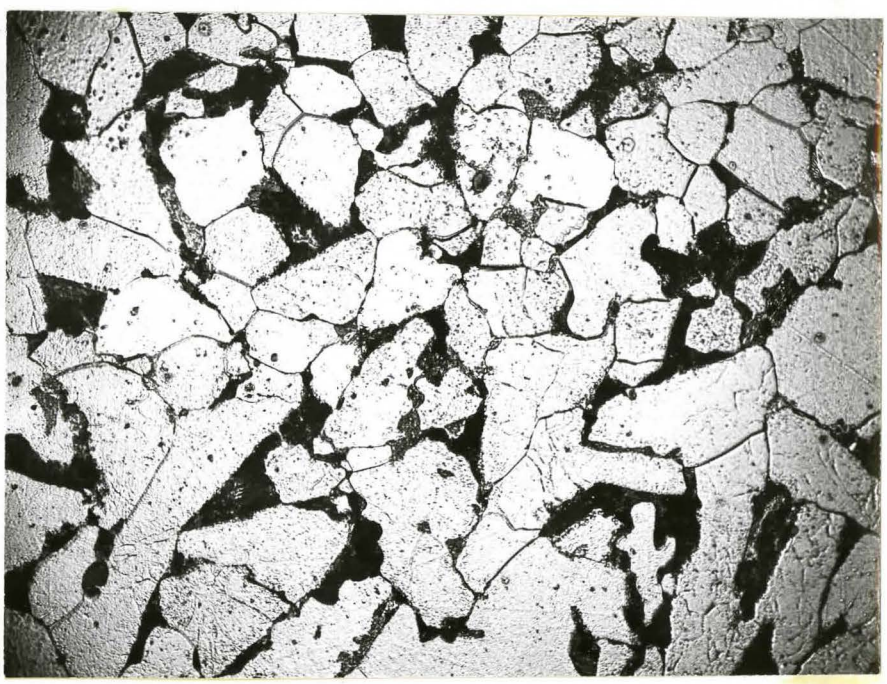

QUENCH AGED

Figure 10 Optical micrographs of the commercial steel in the furnace-cooled and quench-aged condition. X400

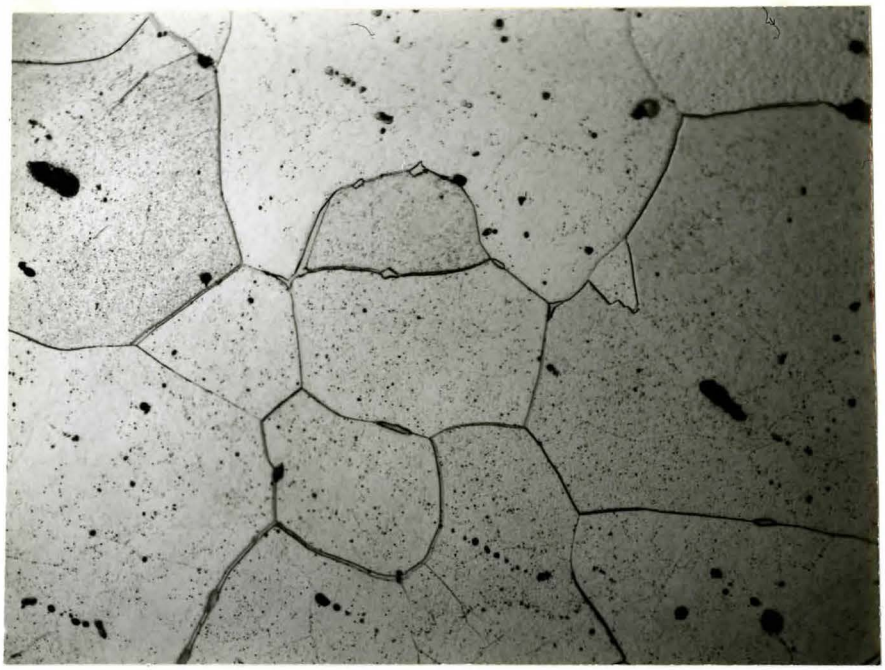

FURNACE COOLED

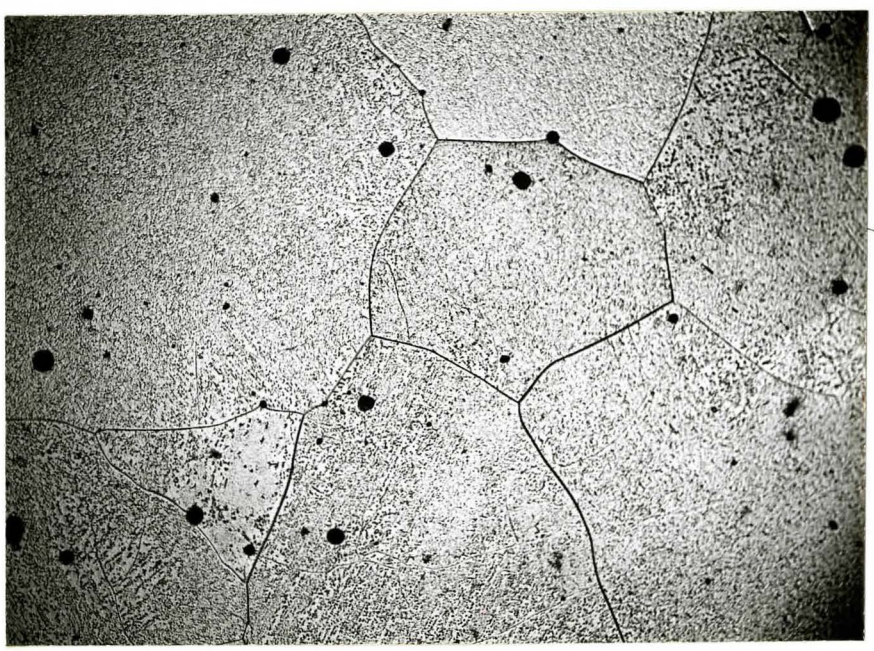

QUENCH AGED

Figure 11 Optical micrographs of Armco iron in the furnace-cooled and quench-aged condition. X400

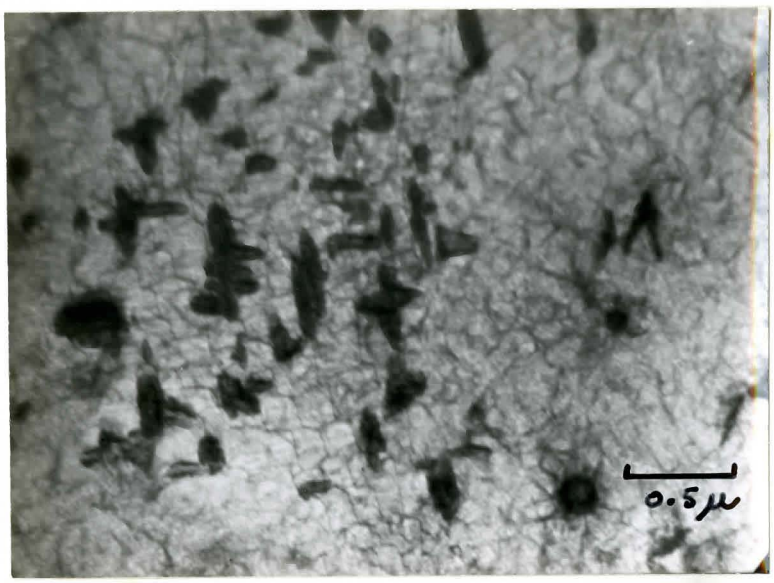

Figure 12: Transmission electron micrograph showing dispersed carbides in the commercial steel quenched from 700°C and aged 6 hours at 100°C.

markedly in the distribution of the second phase carbide particles. For the furnace cooled specimens, massive carbides were seen at the grain boundaries but none were observed optically in the quench-aged specimens. The grain boundary carbides present in the furnace-cooled materials are replaced by a fine dispersion of carbides within the ferrite grains as shown in Figure 13.

It is thus apparent that the distribution of the second phase then is of vital importance in considering the difference in brittle behavior of the two materials.

4.2 Investigation of the Mechanical Properties of Low Carbon Iron

In this section the results are reported in two sections: those concerning the tensile properties, and those describing the important microstructural features of the materials.

4.2.1 Tensile Properties

It was shown earlier that a variety of carbide distributions could be obtained by furnace cooling and quench ageing irons of various carbon contents. For clarity and for ease of comparison, quench ageing in the following sections refers to ageing at 300°C for 8 hours. The effect of quench ageing on the mechanical properties of low carbon iron is best illustrated by comparing Figures 14, 15, 16 and 17. These figures show the lower and upper yield stress, the fracture stress, and the reduction in area as a function of testing temperature for furnace cooled and quench-aged Armco and NPL iron respectively.

A comparison between the fracture properties of the two materials in the furnace cooled and quench-aged conditions show they are quite dissimilar. The ductility transition temperature (DTT) of Armco iron when furnace cooled is about -100°C, while that of the

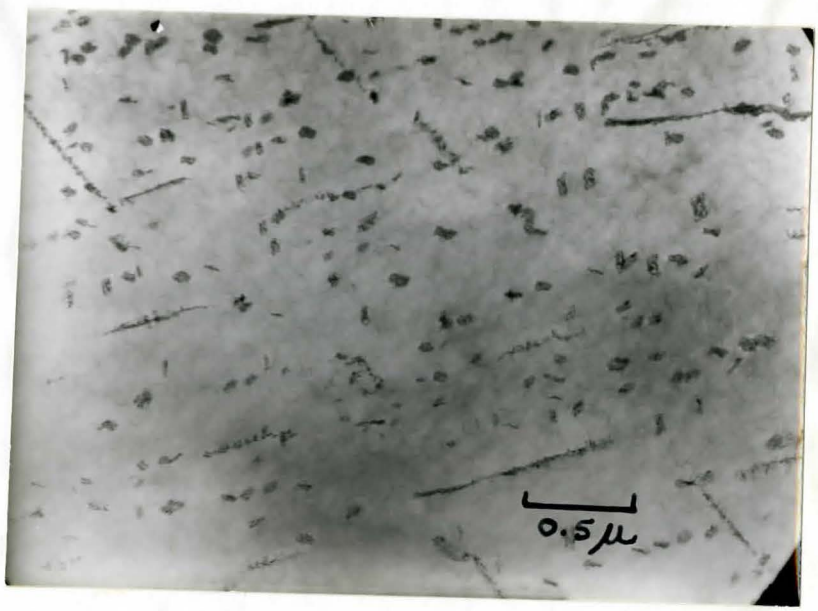

Figure 13: Transmission electron micrograph showing dispersed carbides in Armco iron quenched from 700°C and aged 6 hours at 100°C.

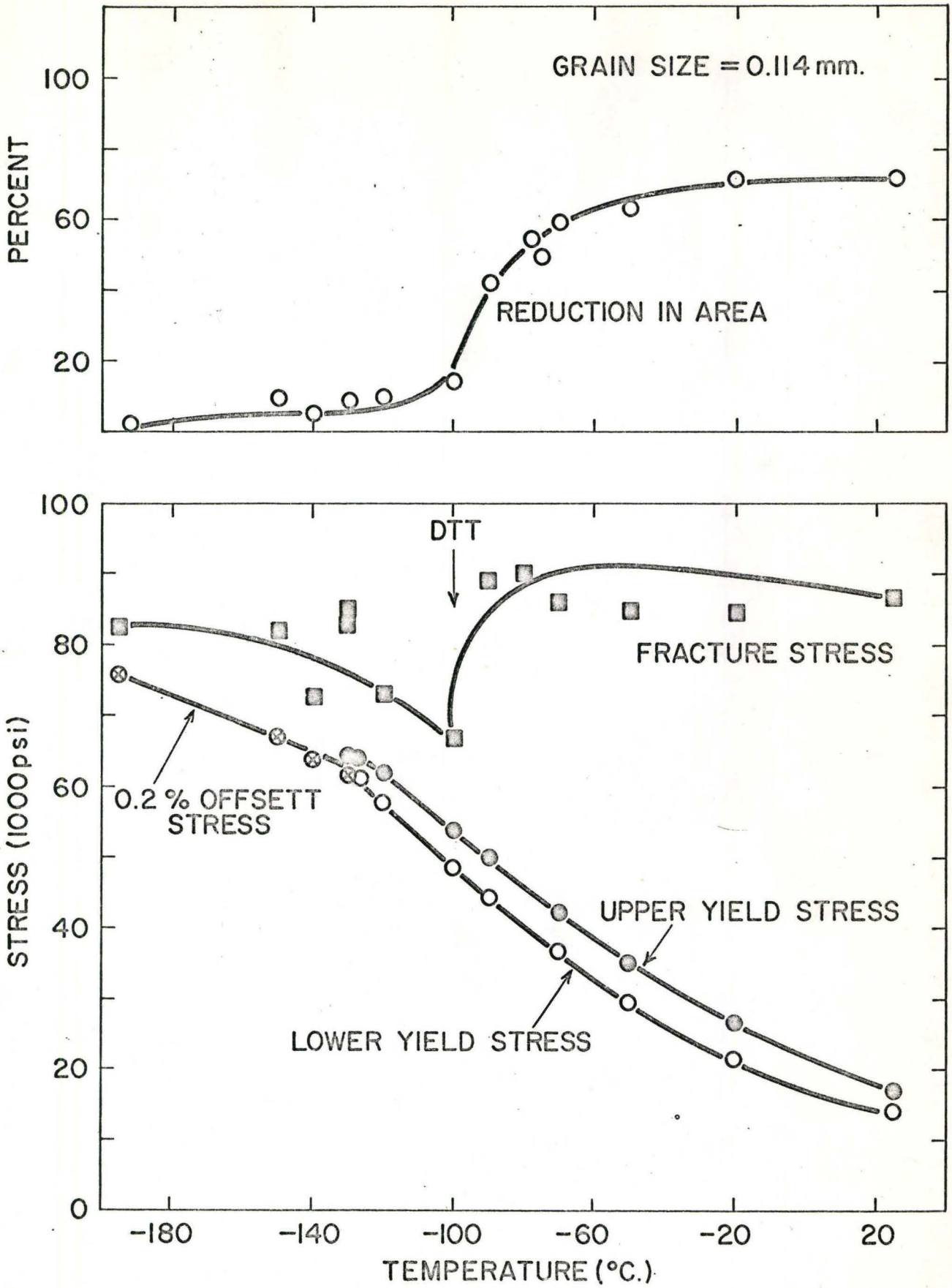

Figure 14: Tensile properties of furnace-cooled Armco iron.

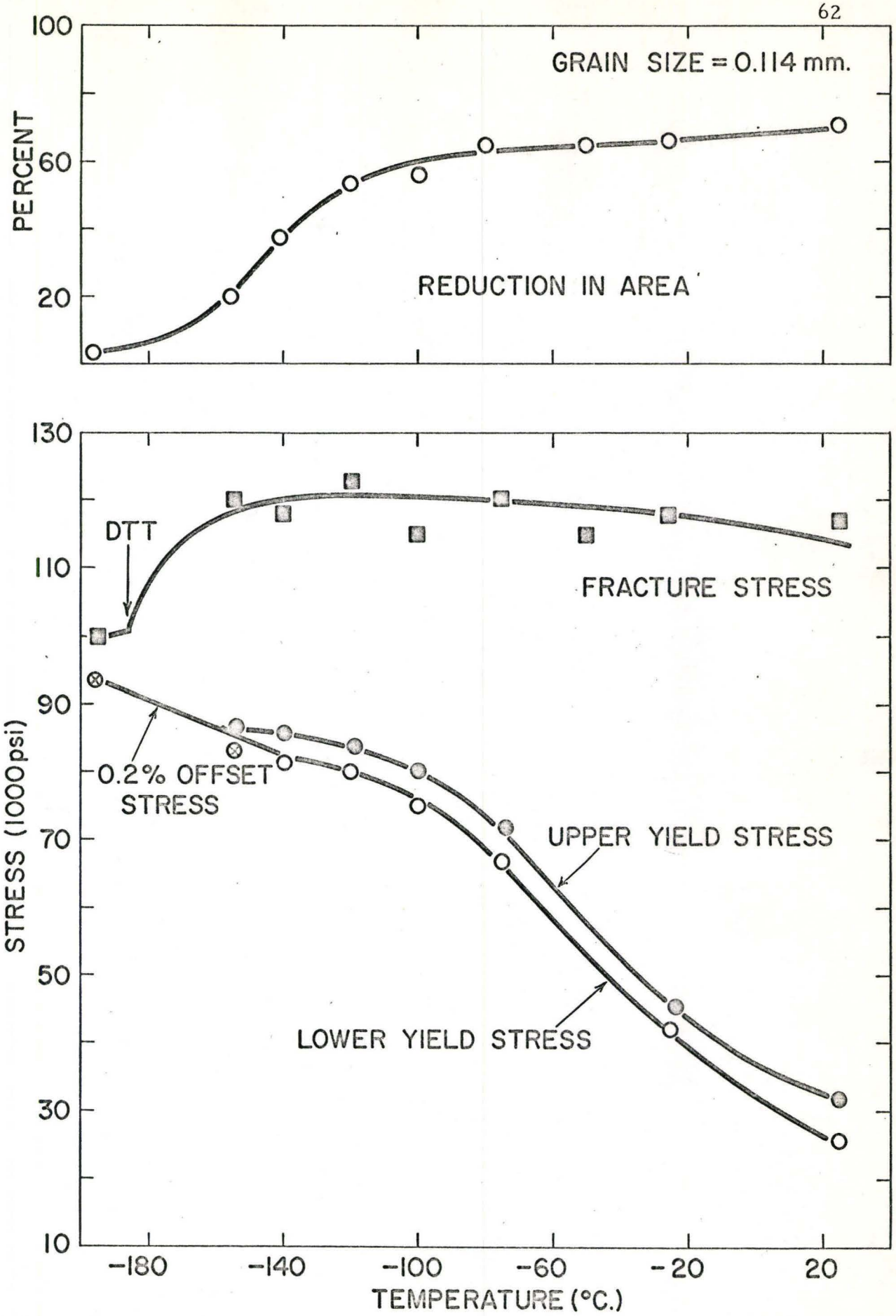

Figure 15: Tensile properties of quench-aged Armco iron.

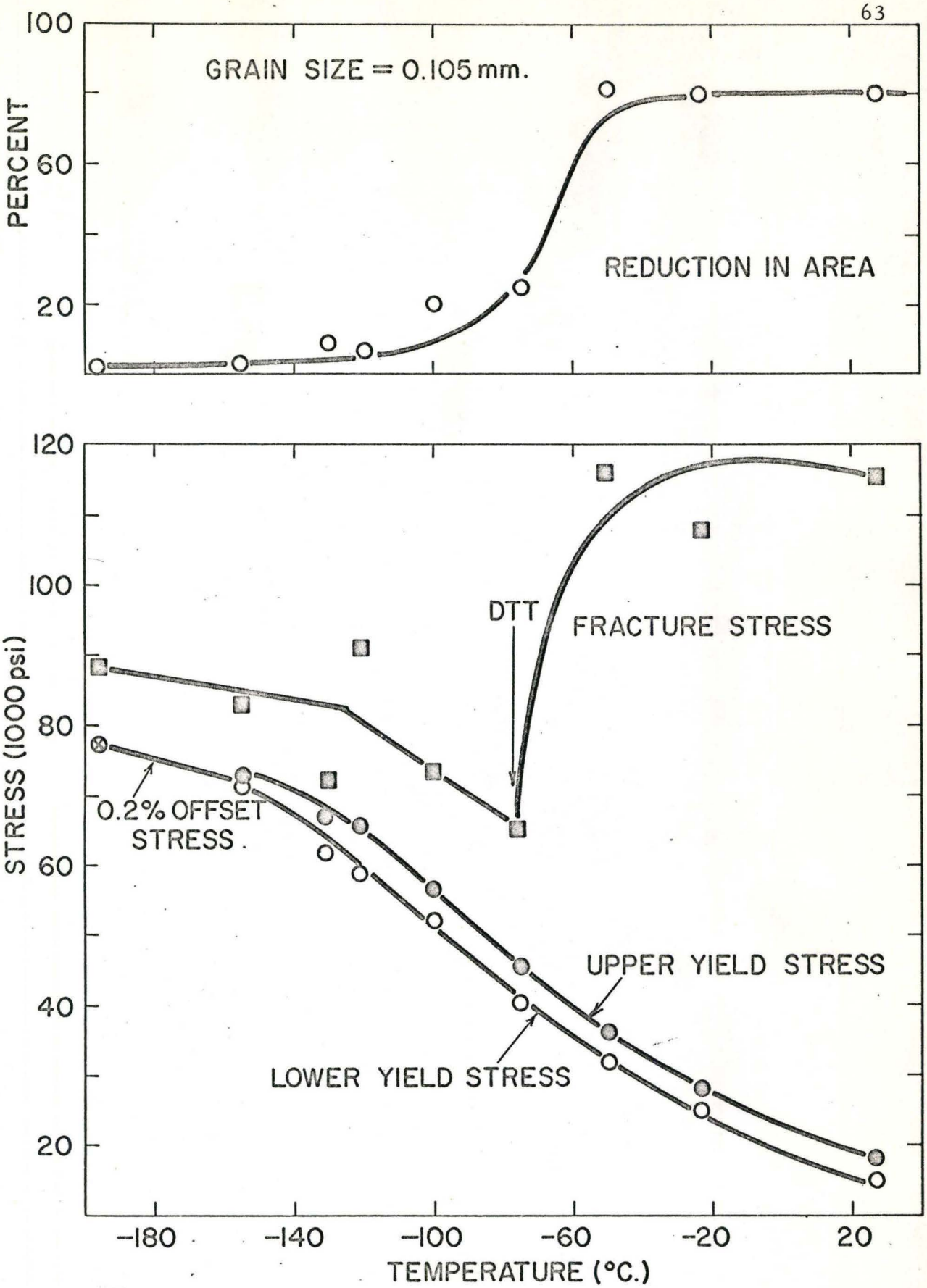

Figure 16: Tensile properties of furnace-cooled NPL iron.

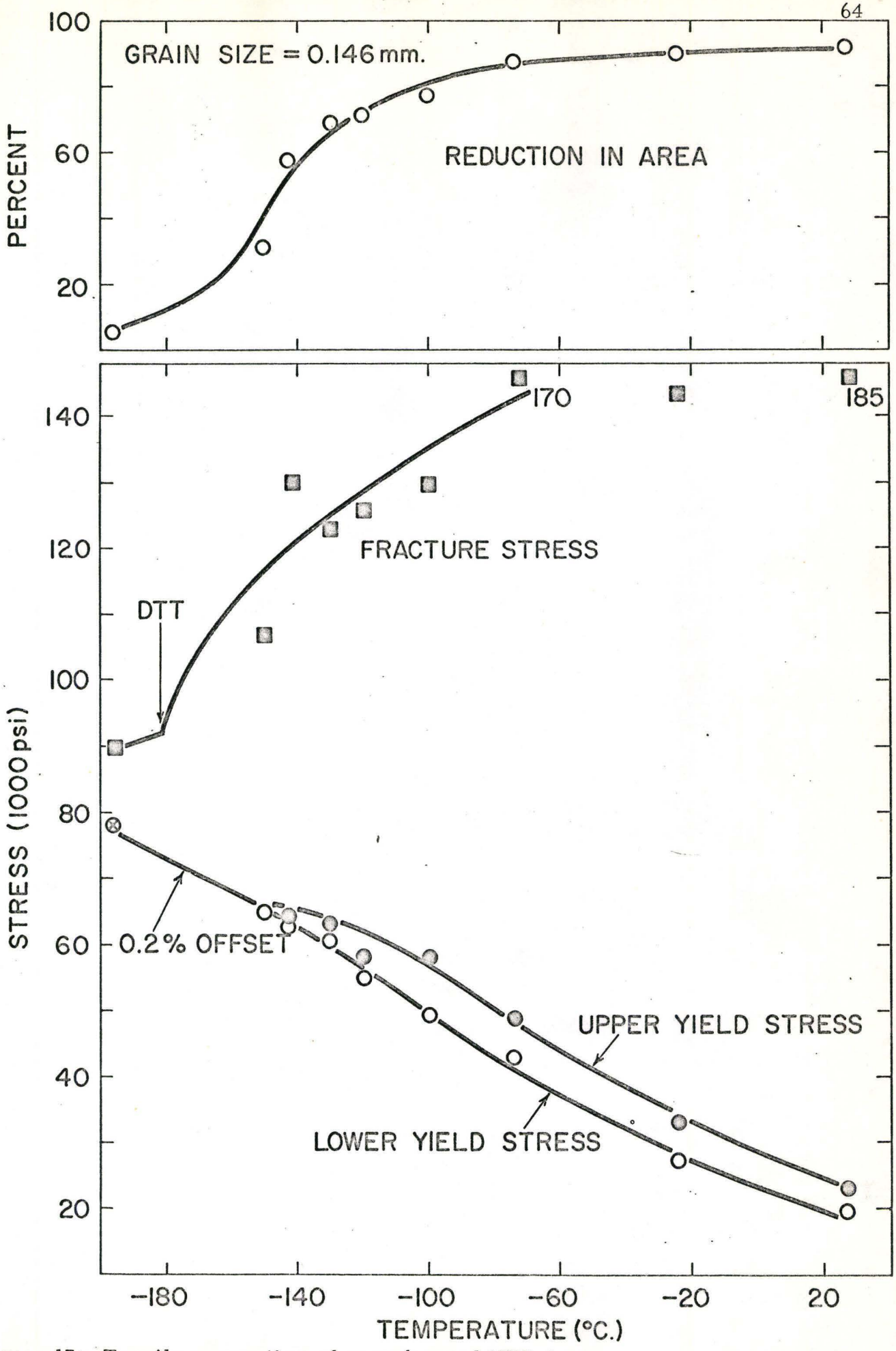

Figure 17: Tensile properties of quench-aged NPL iron.

quench-aged material is about -180°C. The DTT for NPL iron in the furnace cooled and quench-aged conditions is about -80°C and -180°C respectively.

The yield stress values in the quench-aged condition for both low carbon materials are proportionally higher than those in the furnace cooled case at each of the test temperatures.

Also, at the lower test temperatures the quench aged material is appreciably more ductile than the furnace cooled material (using reduction in area as a measure of ductility). At test temperatures below the ductility transition temperature, all specimens failed by cleavage fracture.

At the very low test temperatures, -140°C and below, mechanical twinning occurred and a 0.2% offset stress was used to indicate macroscopic plastic flow.

The quantities which are of particular interest are the lower yield stress at room temperature σ_y(rt), and the fracture stress (σ_F) at the ductile transition temperature (DTT).

A comparison of the mechanical properties is given in Table 3 where the values of σ_y(rt), σ_F and DTT are tabulated. It can be seen from this data that the effect of quench ageing was to raise both the fracture stress and room temperature yield stress and to reduce the transition temperature.

4.2.2 Microstructural Aspects

In the furnace-cooled condition large grain boundary carbides were observed in the Armco and NPL irons similar to those illustrated previously in the preliminary survey (Figures 11 and 18 respectively). In the quench-aged specimens the presence of grain boundary carbides could only be firmly established by observing surface replicas in the electron microscope. Figure 19 is electron micrograph of a carbon

TABLE 3

Grain and Carbide Sizes, Yield Stress, and Fracture Stress Values

Material	Condition	Grain Size (mm)	Grain Boundary Carbide Range (μm)	Dispersed Carbide Size (mean) (μm)	σ_y(rt) (psi)	σ_F (psi)	Transition Temperature (^{o}C)
Armco	furnace-cooled	.114	1-3	-	13,000	68,000	-100
	quench-aged	.114	< 1	0.3	25,000	100,000	-180*
NPL	furnace-cooled	.105	1.5-3.5	-	15,000	65,000	-80
	quench-aged	.146	< 1	0.4	20,000	90,000	-180*

* The transition temperature for the quench-aged materials has been estimated. The fracture stress value quoted is an average value obtained on samples tested at -196^{o}C.

Figure 18. Large grain boundary carbides in furnace-cooled NPL iron.

Figure 19: Grain boundary carbides in quench-aged NPL iron.

replica illustrating a grain boundary carbide in NPL iron. The sizes of the grain boundary carbides in the furnace-cooled and quench-aged condition for the two low carbon materials are shown in Table 3.

Examination of thin films from the quench-aged Armco and NPL test specimens showed a fine dispersion of carbides within the grains. Figure 20 is an electron micrograph showing dispersed carbides in Armco iron quenched from 720°C and aged at 300°C. The dispersed carbides could not be identified by electron diffraction but their (110) habit plane (Leslie 1961) suggests they are cementite rather than epsilon carbide. The mean planar spacing of the dispersed carbides were measured from a number of electron micrographs and the values are given in Table 3.

Some indication of the role of grain boundary and dispersed carbides in the deformation process was obtained by examining sections taken from the gauge length of tensile specimens. Furnace-cooled specimens tested in the ductile transition temperature region contained numerous fractured carbides as shown in Figure 21. Further, examination of specimens in the transition region showed a number of stable microcracks in the ferrite matrix which originate from the grain boundary carbides (Figure 22) in accord with previous observations of McMahon and Cohen (1965), Bruckner (1950), Allen et al. (1953)and Lindley (1969). No stable ferrite microcracks were seen in quench-aged material nor was any cracking of the ferrite-carbide interface in furnace-cooled material observed.

To establish the role played by dispersed carbides, strip tensile specimens were deformed at -80°C after quench ageing. A typical microstructure is shown in Figure 23 in which tangled groups of dislocations can be observed around the carbides. There was no evidence of broken carbides within the grains or of non propagating microcracks associated with these carbides.

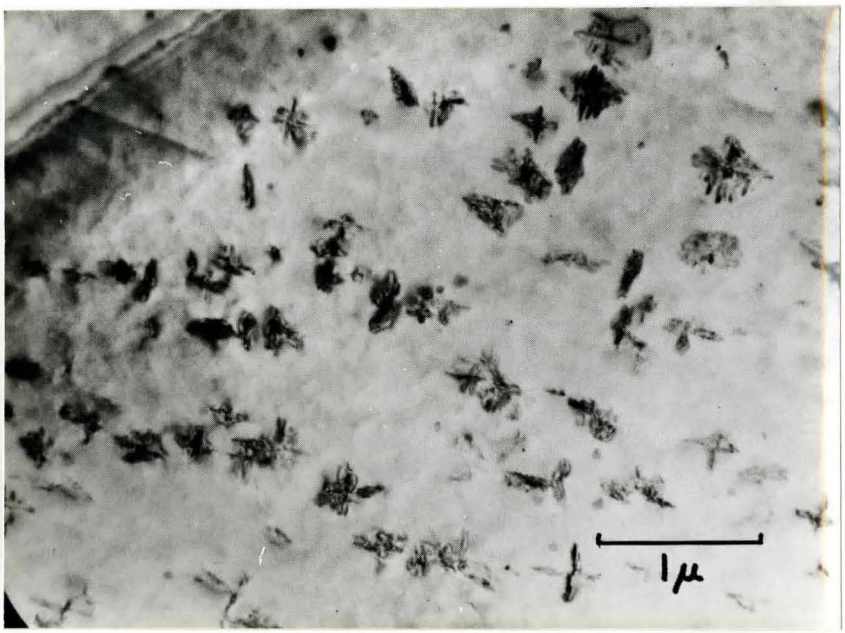

Figure 20. Transmission electron micrograph showing dispersed carbides in Armco iron quenched from 720°C and aged 8 hours at 300°C.

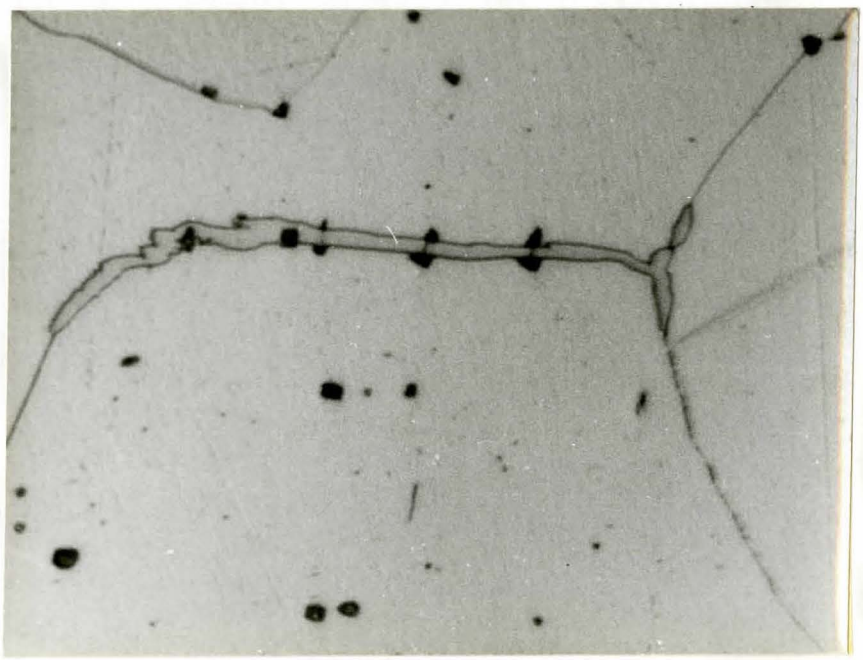

Figure 21: Cracks confined within the thickness of a grain boundary carbide. X2000

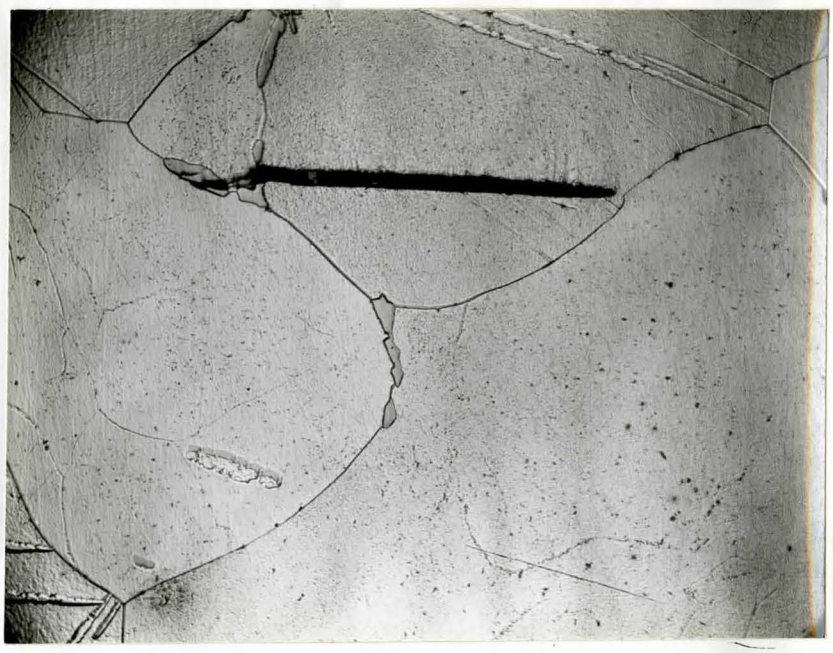

Figure 22: Example of a stable microcrack in the ferrite matrix originating from a grain boundary carbide. X600

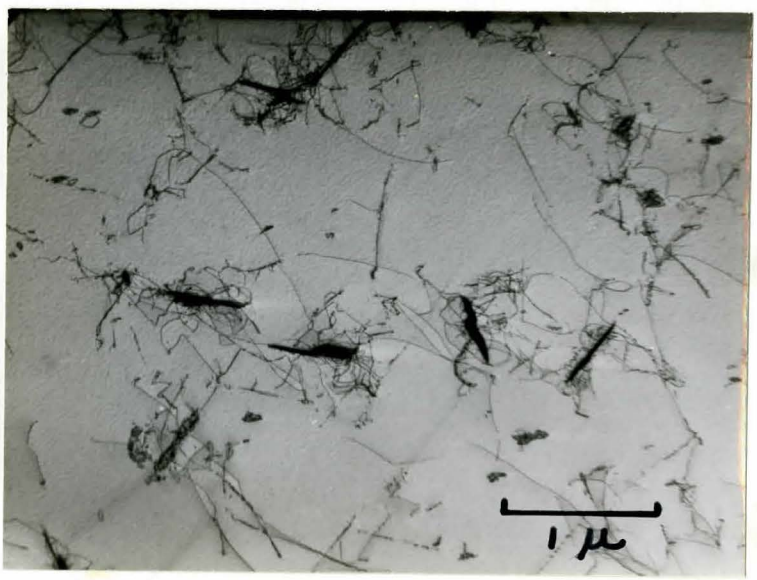

Figure 23 Transmission electron micrograph of the structure of quench-aged Armco iron deformed in tension at -80°C showing complex dislocation tangles formed at the carbides.

Thus, the dispersed carbides within the grains appear to promote localized dislocation tangling whereas the larger grain boundary carbides fracture during plastic deformation of the matrix. Under favorable conditions of stress and temperature fractured grain boundary carbides may subsequently initiate fracture in the ferrite matrix.

4.3 Fracture in Two Phase Material

The previous two sections have demonstrated the importance of microstructural inhomogeneties in the initiation and propagation of cleavage cracks in low carbon steels. This section will be divided into two parts. In the first part a simple energy balance method will be used to derive the condition for crack propagation accounting for the influence of hard second phase particles. In the second part the model will be examined in two respects: firstly, from the dependence of the fracture behavior on the thickness of the grain boundary carbide, and secondly, from the dependence of the fracture stress on grain size for material containing various sizes of grain boundary carbides.

4.3.1 Fracture Model

Consider a material such as Armco iron in the furnace cooled condition in which large carbides at the grain boundaries are observed (Figure 11). When inhomogeneous plastic deformation takes place in the material a slip band can be envisaged to impinge on the grain boundary particle as shown schematically in Figure 24 . The situation is thus similar to Stroh's (1957) model for a dislocation pile-up against a grain boundary.

Since these grain boundary particles (cementite) are brittle, a crack can be formed (due to the large stress concentration at the head of a pile-up) with an effective surface energy γ_p equal to the true surface

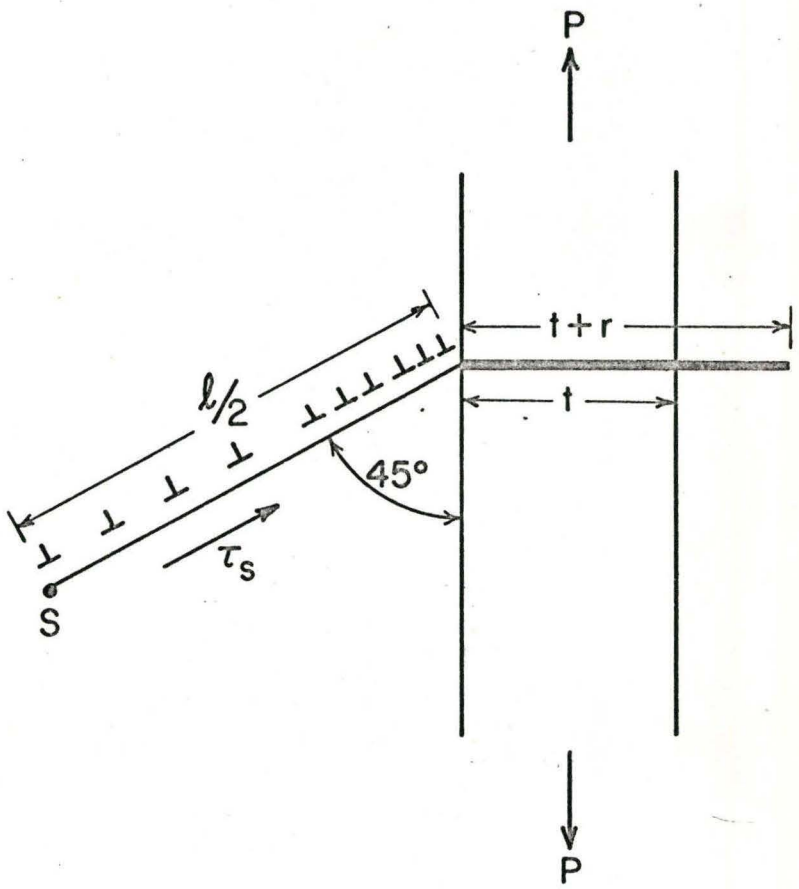

Figure 24: Schematic representation of a crack in a grain boundary carbide being assisted in propagation by the applied normal stress and the stresses due to the slip band.

energy value of the particle and much less than γ the effective surface energy of a cleavage crack in the ferrite. The matrix now contains a crack of length t which is acted upon both by the applied stress system and the stresses due to the pile up of dislocations in the slip band which is assumed to be unrelaxed by the failure of the particle, that is, the crack in the hard particle is less than one Burgers vector.

The crack will either be relaxed by plastic deformation in the neighbouring ferrite grain or propagate as a cleavage crack. Following the failure of the particle the wedging action of the dislocation pile up is effectively transferred to the tip of the crack and the energy considerations for extending the crack into the ferrite will be similar, to those for the formation of a cracked dislocation at the tip of the pre-existing crack (Stroh 1957).

The energy (W) involved in extending the crack of length t to a length (r + t) under the action of an applied normal stress p will be,

$$W = \frac{n^2 a^2 G}{4\pi(1-\nu)} \ln\left(\frac{4L}{r}\right) + 2\gamma r - \frac{pna(r+t)}{2} + \frac{\pi(1-\nu)\, p^2 t^2}{8G} - \frac{\pi(1-\nu)\, p^2 (r+t)^2}{8G} \qquad (26)$$

where the first term is the energy of a cracked dislocation of strength n a (Stroh 1954), L being the effective radius of the stress field of the dislocation and G the shear modulus, the second is the effective surface energy γ of the ferrite, the third is the work done by the applied stress due to the increase in volume on opening up the crack, and the fourth and fifth terms describe the change in the elastic energy of the growing crack in the applied stress field.

For ease of calculation, let

$$C_1 = \frac{n^2 a^2 G}{8\pi(1-\nu)\gamma} \quad ; \quad C_2 = \frac{8G\gamma}{\pi(1-\nu)p^2} \quad ; \quad \left(\frac{C_1}{C_2}\right)^{1/2} = \frac{pna}{8\gamma}$$

We now can write W in the following form

$$W = 2\gamma C_1 \ln\left(\frac{4L}{r}\right) + 2\gamma r - \left(\frac{C_1}{C_2}\right)^{1/2} 4\gamma(r+t) + \frac{\gamma t^2}{C_2} - \frac{\gamma(r+t)^2}{C_2} \qquad (27)$$

Equation 27 has stationary values when

$$\frac{dW}{dr} = 0 \qquad (28)$$

that is, when

$$-\frac{2\gamma C_1}{r} + 2\gamma - \left(\frac{C_1}{C_2}\right)^{1/2} 4\gamma - \frac{2\gamma}{C_2}(r+t) = 0 \qquad (29)$$

By multiplying through by r and C_2 and rearranging we obtain a quadratic in r

$$2\gamma\left[-\frac{C_1}{r} + 1 - 2\left(\frac{C_1}{C_2}\right)^{1/2} - \left(\frac{r+t}{C_2}\right)\right] = 0 \qquad (30)$$

$$r^2 - r\,C_2\left[-\frac{t}{C_2} + 1 - 2\left(\frac{C_1}{C_2}\right)^{1/2}\right] + C_1 C_2 = 0 \qquad (31)$$

Thus when both the applied stress system and the stresses due to a pile up in an unrelaxed slip band are present Equation 31 has real positive roots (positive stable crack lengths) when

$$\left[-\frac{t}{C_2} + 1 - 2\left(\frac{C_1}{C_2}\right)^{1/2}\right]^2 C_2^2 > 4\,C_1 C_2 \qquad (32)$$

or imaginary roots (cracks unstable) when

$$\left[-\frac{t}{C_2} + 1 - 2\left(\frac{C_1}{C_2}\right)^{1/2} \right]^2 C_2^2 < 4 C_1 C_2 \qquad (33)$$

The transition between these cases occurs when

$$\left[1 - \frac{t}{C_2} - 2\left(\frac{C_1}{C_2}\right)^{1/2} \right]^2 C_2^2 = 4 C_1 C_2 \qquad (34)$$

$$\left[1 - \frac{t}{C_2} - 2\left(\frac{C_1}{C_2}\right)^{1/2} \right]^2 = 4 \frac{C_1}{C_2} \qquad (35)$$

$$1 - \frac{t}{C_2} - 2\left(\frac{C_1}{C_2}\right)^{1/2} = 2\left(\frac{C_1}{C_2}\right)^{1/2} \qquad (36)$$

or,

$$1 = \frac{t}{C_2} + 4\left(\frac{C_1}{C_2}\right)^{1/2} \qquad (37)$$

then,

$$1 = \frac{t\,\pi(1-\nu)p^2}{8G\gamma} + \frac{pna}{2\gamma} \qquad (38)$$

Since $na = \left\{ \frac{\pi(1-\nu)\ell}{2G} \right\} \tau_s$ (Eshelby et al. 1951) (39)

where τ_s is the effective shear stress on the pile up in a grain of diameter ℓ. At the yield condition $\tau_s = \tau_{applied} - \tau_{friction} = \frac{k_y \ell^{-1/2}}{2}$ where k_y is the slope of the Hall-Petch equation for the lower yield stress in uniaxial tension,

then

$$\frac{p^2 t\,\pi(1-\nu)}{8G\gamma} + \frac{p}{8\gamma}\,\frac{\pi(1-\nu)}{G}\,k_y \ell^{1/2} = 1 \qquad (40)$$

Thus brittle behavior is expected when

$$p^2 t + p\, k_y \ell^{1/2} > \frac{8G\gamma}{\pi(1-\nu)} \tag{41}$$

If the carbide thickness t = 0, Equation 41 reduces to the Petch condition for the ductile-brittle transition

$$p = \frac{8G\gamma}{\pi(1-\nu)\, k_y} \ell^{-1/2} \tag{42}$$

If the grain size ℓ is very small, the expression tends to the Griffith's equation

$$p = \left(\frac{8G\gamma}{\pi(1-\nu)t}\right)^{1/2} \tag{43}$$

For finite values of carbide thickness t, fracture occurs when

$$p = \left(\frac{k^2 \ell}{4t^2} + \frac{8G\gamma}{\pi(1-\nu)t}\right)^{1/2} - \frac{k\ell^{1/2}}{2t} \tag{44}$$

and when fracture occurs at the yield stress

$$p = \sigma_y = \left(\frac{k^2 \ell}{4t^2} + \frac{8G\gamma}{\pi(1-\nu)t}\right)^{1/2} - \frac{k\ell^{1/2}}{2t} \tag{45}$$

In notch bend tests when general yield and fracture coincide the maximum tensile stress below the notch is $R\sigma_y$ where R is the plastic constraint factor appropriate to the notch geometry (Knott 1966). Thus crack propagation can occur at the general yield stress under the notch when

$$R\sigma_y > \left(\frac{k^2 \ell}{4t^2} + \frac{8G\gamma}{\pi(1-\nu)t}\right)^{1/2} - \frac{k\ell^{1/2}}{2t} \tag{46}$$

The model predicts that the fracture stress will decrease when either the grain size or carbide thickness is increased. Further, grain size dependence of the fracture stress should be modified by the presence of brittle particles, such that at fine grain sizes of the order of a few microns the criteria for propagation will become increasingly dependent on carbide thickness t, rather than the grain size. The variation of fracture stress with grain size and grain boundary carbide thickness becomes apparent when plotted graphically as in Figure 25. It can be seen that as the grain size decreases there is an increased divergence from the Cottrell-Petch relationship. This divergence is greater as the carbide thickness t increases.

In Figure 25, the grain size and the fracture stress have been normalized with respect to the carbide thickness t. By allowing the grain size, expressed in terms of $\ell^{-1/2}$, to vary as a function of

$$\left(\frac{k^2 \pi (1-\nu)}{32 G \gamma t}\right)^{1/2}$$

the fracture stress of both the Cottrell-Petch relationship and the derived equation (Equation 45) from the fracture model proposed in this work can then be expressed in similar terms and as a function of

$$\left(\frac{8 G \gamma}{\pi(1-\nu) t}\right)^{1/2}$$

This latter expression is similar to a modified form of Griffith's fracture equation where the carbide thickness t has been treated simply as a pre-existing crack of length t.

Of the latter two expressions, the former has been obtained by manipulating both the Cottrell-Petch fracture relationship and Equation 45, so that the fracture stresses from both relationships could be expressed as similar functions irrespective of the carbide thickness. Hence, by expressing the grain size in this manner it can be seen

that increasing the carbide thickness t then has an effect similar to increasing the relative grain size, which in turn results in a decrease in the fracture stress. This normalization of the grain size with respect to the carbide thickness is particularly desirable for the Cottrell-Petch relationship, as their fracture model does not consider the effect of microstructural inhomogeneities on the initiation and propagation of cleavage cracks.

By utilizing this method of normalization, both the divergence of the derived equation (Equation 45) from the Cottrell-Petch relationship, and the variation of the fracture stress obtained from both fracture relationships with grain size can be readily visualized.

In order to make a quantitative estimate of the accuracy of the model, tensile, notch bend and impact tests were performed on Armco iron specimens. By observing the temperature at which general yield and fracture coincided in the notch bend tests and measuring the uniaxial yield stress at this temperature, a value for the fracture stress can be obtained directly. This value could then be checked against a value obtained by measuring the parameters k, l, t and γ.

4.3.2 Experimental Results

The experimental results will be divided into two sections: those showing the dependence of the fracture stress on grain size for coarse grain boundary carbides, and those showing the dependence of the fracture behavior on thickness of the grain boundary carbide for a range of grain sizes.

The results of the bend tests at various temperatures on specimens of different grain sizes for furnace-cooled Armco iron are shown in Figure 26, and the temperature (T_{Gy}) at which fracture coincided with general yield is tabulated in Table 4. At this temperature the

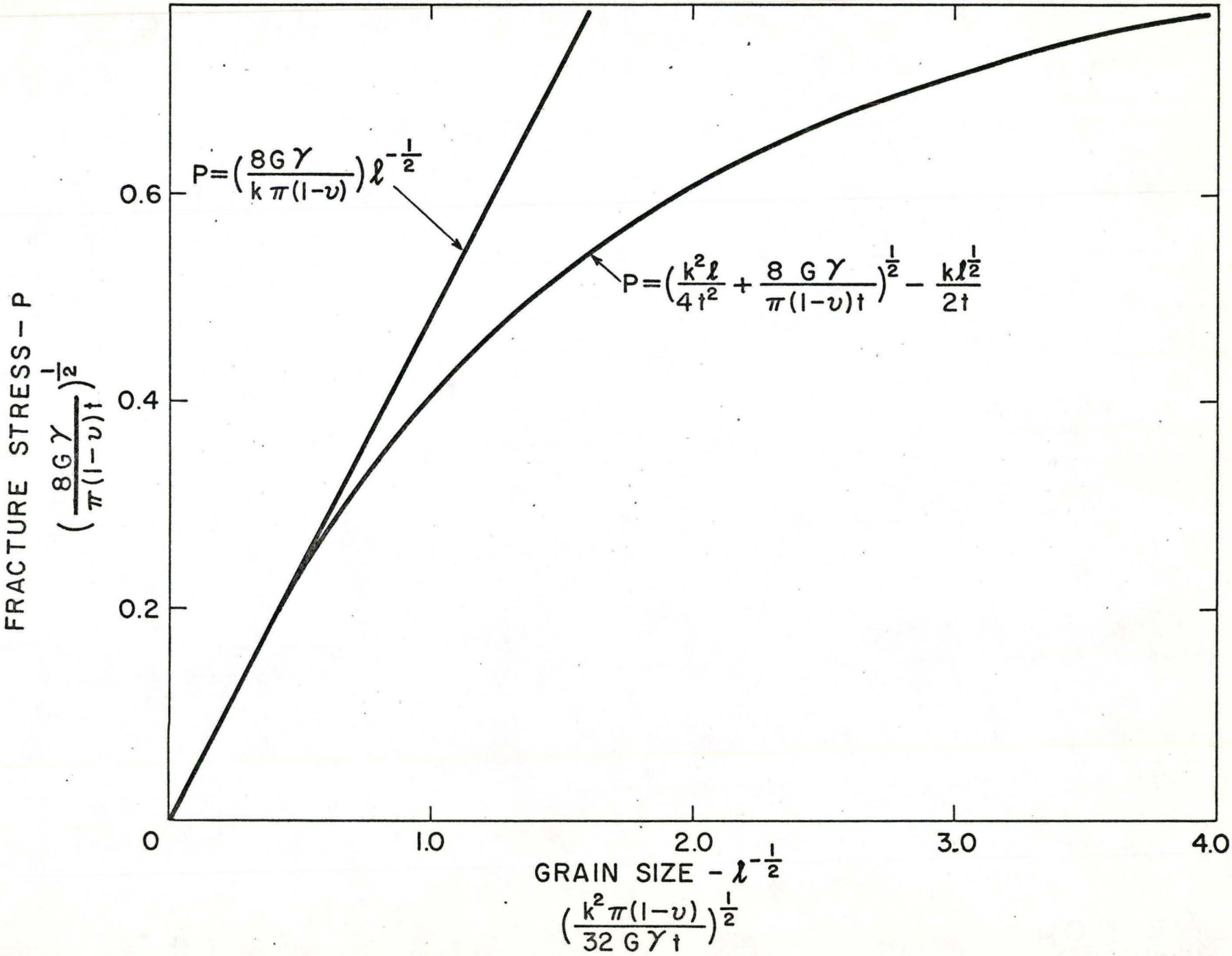

Figure 25: The effect of brittle carbides on the variation of fracture stress with grain size.

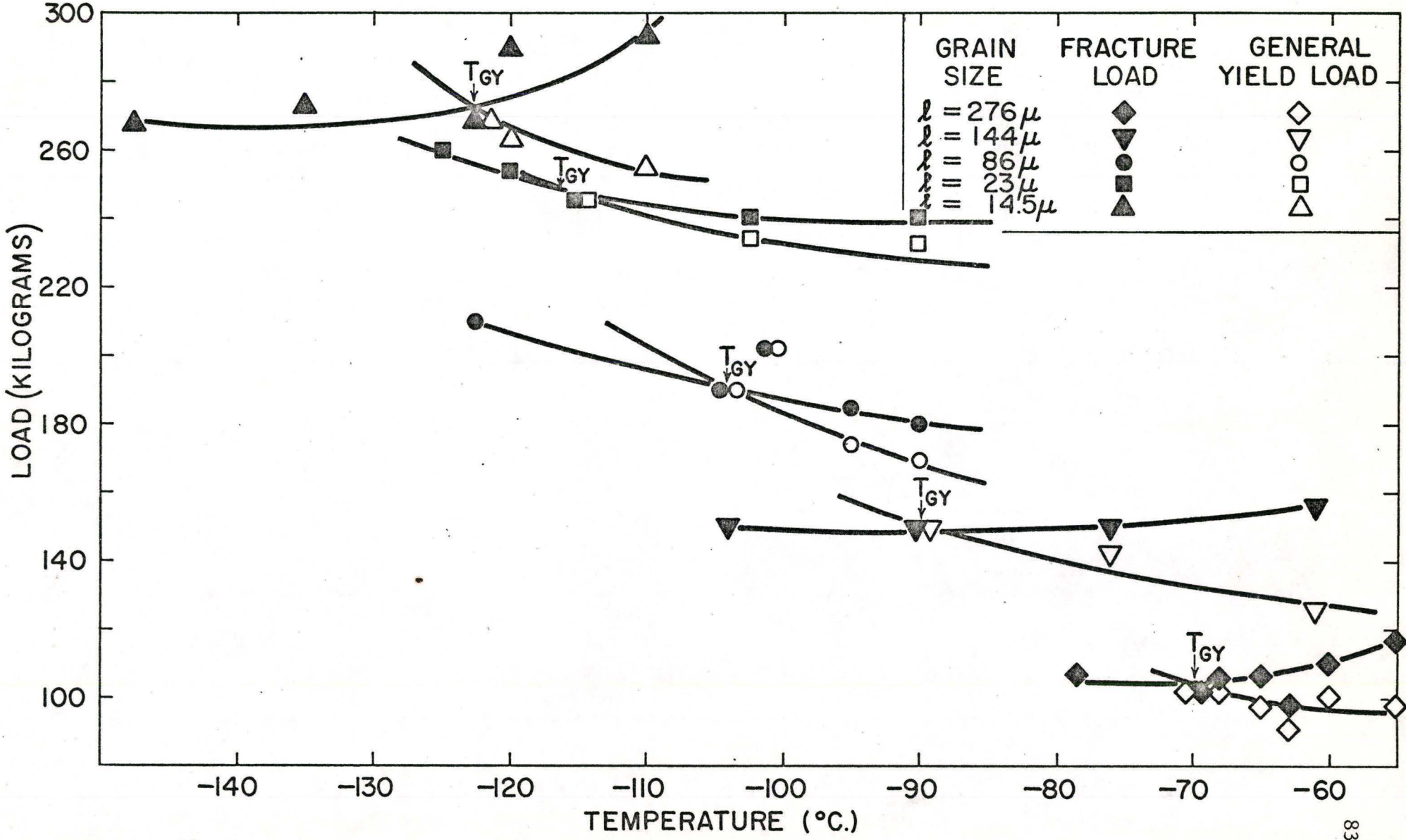

Figure 26: Fracture load and general yield load of notch bend furnace-cooled Armco iron specimens with different grain sizes as a function of temperature.

TABLE 4

Values of the yield stress, the fracture stress and k, at the temperatures when fracture coincides with general yield. The values of the yield stresses and k were obtained from uniaxial tensile tests.

Armco Iron, Furnace-Cooled

(45^{o} notch)

Grain Size mm	Transition Temperature ^{o}C	Yield Stress Kg/mm^2	Fracture Stress Kg/mm^2		k $Kg/mm^{3/2}$
			Tresca	von Mises	
.276	-70	20.4	44.5	51.4	2.40
.144	-90	29.5	64.5	74.5	2.43
.086	-102	33.0	71.8	84.7	2.35
.0234	-110	44.5	97.0	114.3	2.45
.0230	-115	47.0	102.3	120.8	2.40
.0145	-122	52.4	114.2	134.7	2.44
		(90^{o} notch)			
.144	-110	35.8	64	73.7	2.45

maximum tensile stress below the notch is directly related to the tensile yield stress of the material by the stress concentration factor R described previously in Chapter 3. Thus, by determining the yield stress at the transition temperature the fracture stress can be calculated. Values of the yield stress at the relevant temperatures were determined by uniaxial tensile tests for a range of grain sizes as shown in Figure 27 , and the pertinent values at the transition temperatures are listed in Table 4 . The fracture stress was then calculated from the product of the stress intensification factor R and the relevant uniaxial yield stress. The fracture stress values are shown in Table 4 and have been calculated using both the Tresca and von Mises yield criteria.

The results for the variation of fracture stress with grain size calculated from both the Tresca and von Mises yield criterion are plotted in Figure 28, where it can be seen that for the smaller grain sizes there is a considerable deviation from the Cottrell-Petch fracture relationship as predicted by the model in the previous section.

A numerical fit to the experimental data can be made using a simpler version of Equation 45.

$$p = \left(\frac{k^2 \ell}{4t^2} + \frac{4G\gamma}{t}\right)^{1/2} - \frac{k\ell^{1/2}}{2t} \qquad (47)$$

once the experimentally determined values for grain boundary carbide thickness t, grain size ℓ , Hall-Petch parameter k, and the effective surface energy γ are determined.

The sizes and distributions of grain boundary carbides for a range of grain sizes in furnace-cooled Armco iron are listed in Table 5. Values of k were obtained from the grain size dependence of the yield stress (Figure 27) and they are listed in Table 4 . A value for

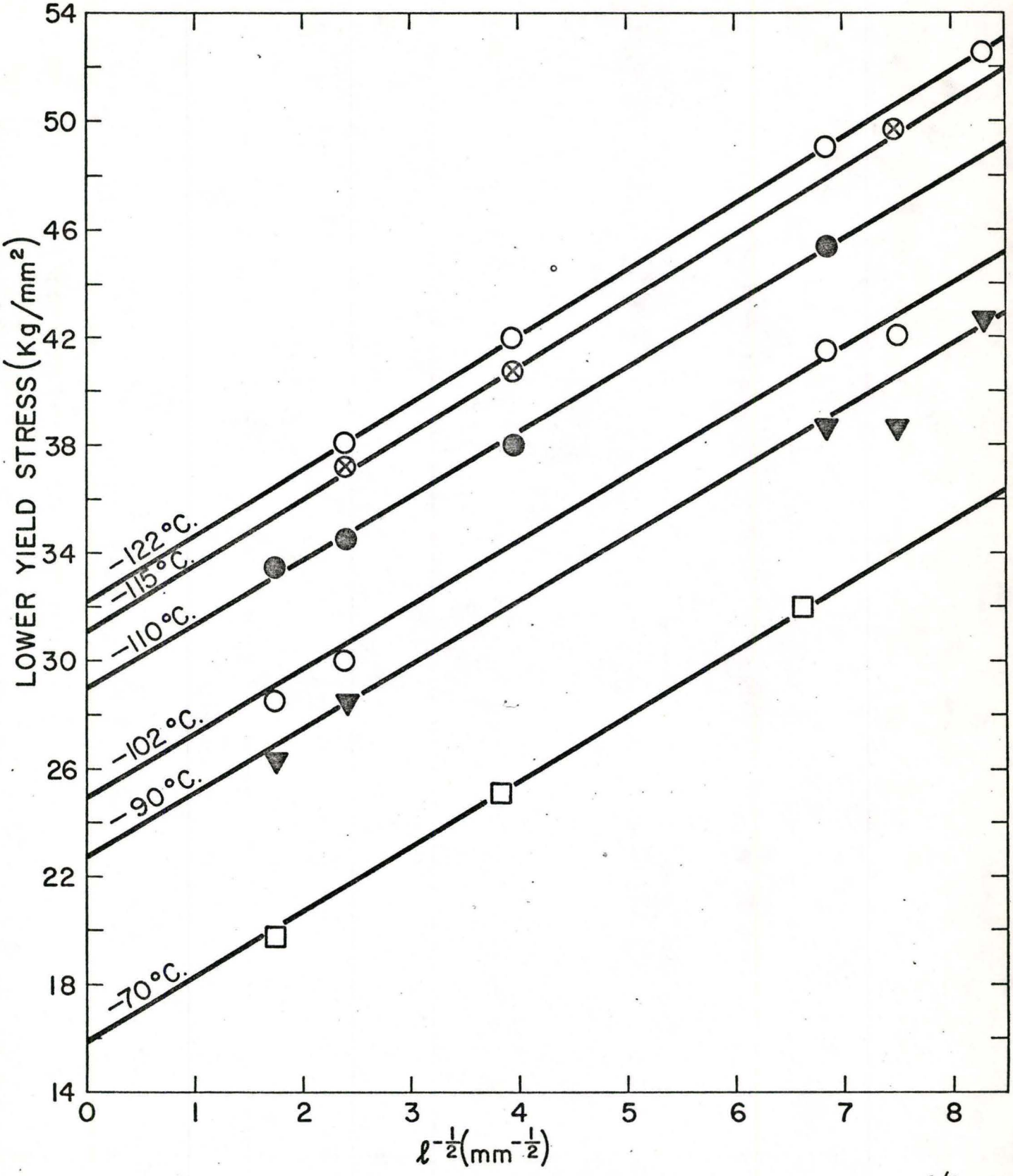

Figure 27: The relationship between lower yield stress and (grain size)$^{-1/2}$ for furnace-cooled Armco iron at various temperatures.

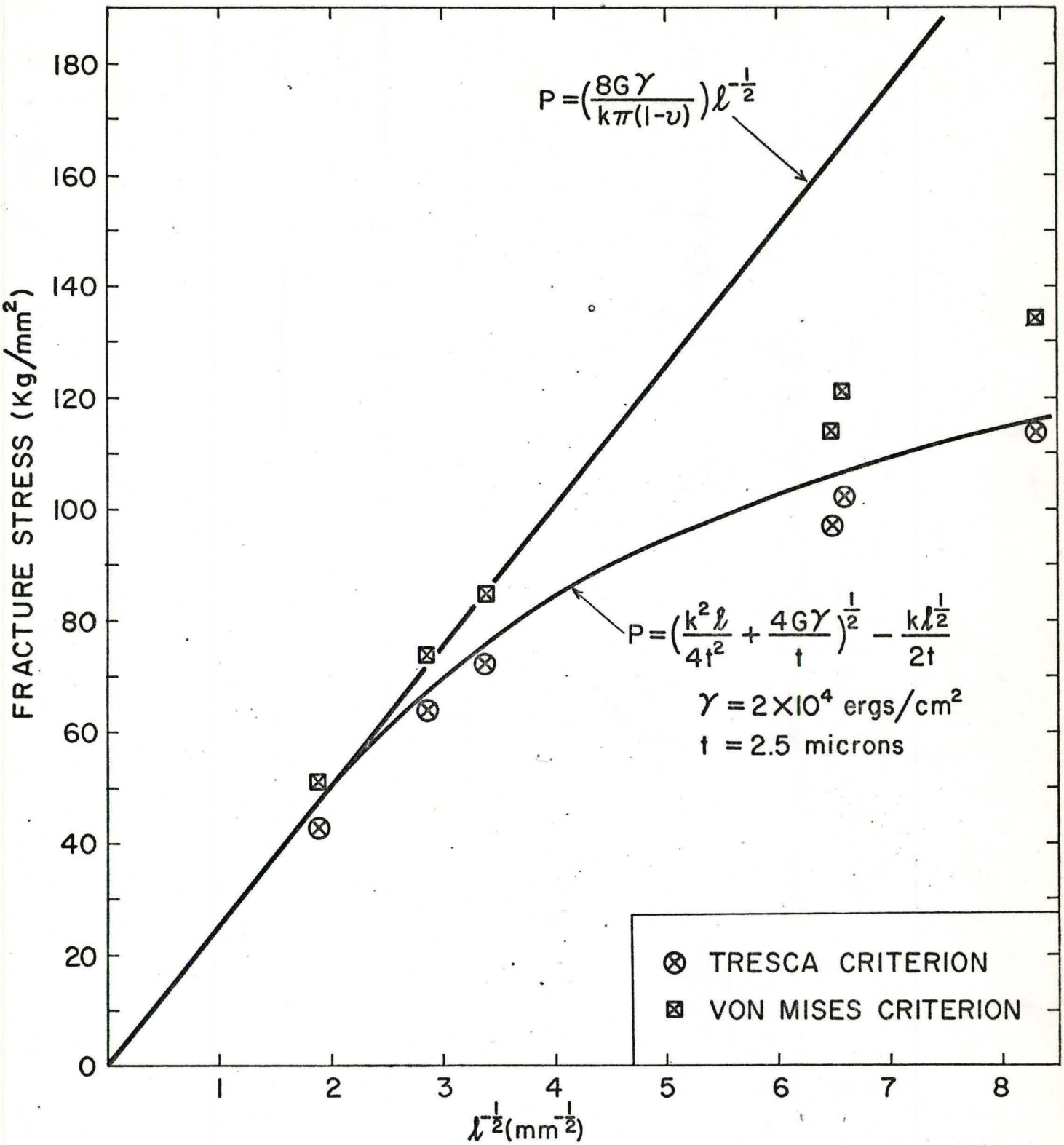

Figure 28: The variation of fracture stress with grain size for furnace-cooled Armco iron. The Petch fracture relationship is illustrated for comparison.

TABLE 5

Grain boundary carbide distribution in furnace-cooled Armco Iron (100 examples).

Grain Size (mm)	Thickness (Microns)					
	<1	1	1.5	2.0	2.5	>2.5
.276	12	15	34	20	14	5
.144	13	22	36	17	11	1
.086	7	29	29	22	11	2
.0234	14	37	11	13	15	4
.0230	6	35	23	24	11	1
.0145	9	23	24	24	15	5

the effective surface energy has been taken to be 2×10^4 ergs/cm^2 (Cottrell, 1958) and the relevance of this value will be discussed more fully in Chapter 5.

Thus, if an average grain boundary carbide of 2.5 microns is used for all grain sizes, and the mean k value is taken as 2.4 Kg/mm$^{3/2}$, the fracture stress may be derived using Equation 47. As seen in Figure 28, for a mean carbide size of 2.5 microns and Cottrell's (1958) value for the effective surface energy, the derived curve lies very close to the experimentally determined fracture values. If a mean grain boundary carbide size of 1 micron was used instead of 2.5 microns the derived curve would vary slightly for the larger grain sizes ($\ell^{-1/2}$ = 2.8 mm$^{-1/2}$, where the derived fracture stress p goes from 64 to 67 Kg/mm^2 Tresca) but at the smaller grain sizes ($\ell^{-1/2}$ = 8.3 mm$^{-1/2}$) the derived fracture stress p varies from 115 Kg/mm^2 to 154 Kg/mm^2. Thus, for the smaller grain sizes the criteria for crack propagation becomes increasingly more dependent on carbide thickness rather than the grain size as predicted by the model.

Notch bend tests were also performed on furnace-cooled specimens with a 90° notch angle and the results compared with those for specimens of the same grain size with a 45° notch, these are shown in Figure 29.

In order to examine the effect of grain boundary carbide size on the fracture behaviour, a comparison was made between furnace-cooled Armco iron specimens and specimens which had been quenched from 720°C and aged at 300°C for 8 hours. Tensile and notch bend tests were performed and the size and distribution of grain boundary carbides was measured by carbon replica techniques.

The results of the bend tests at various temperatures on specimens of different grain sizes for quench-aged Armco iron are shown in Figure 30, and the temperatures (T_{Gy}) at which fracture

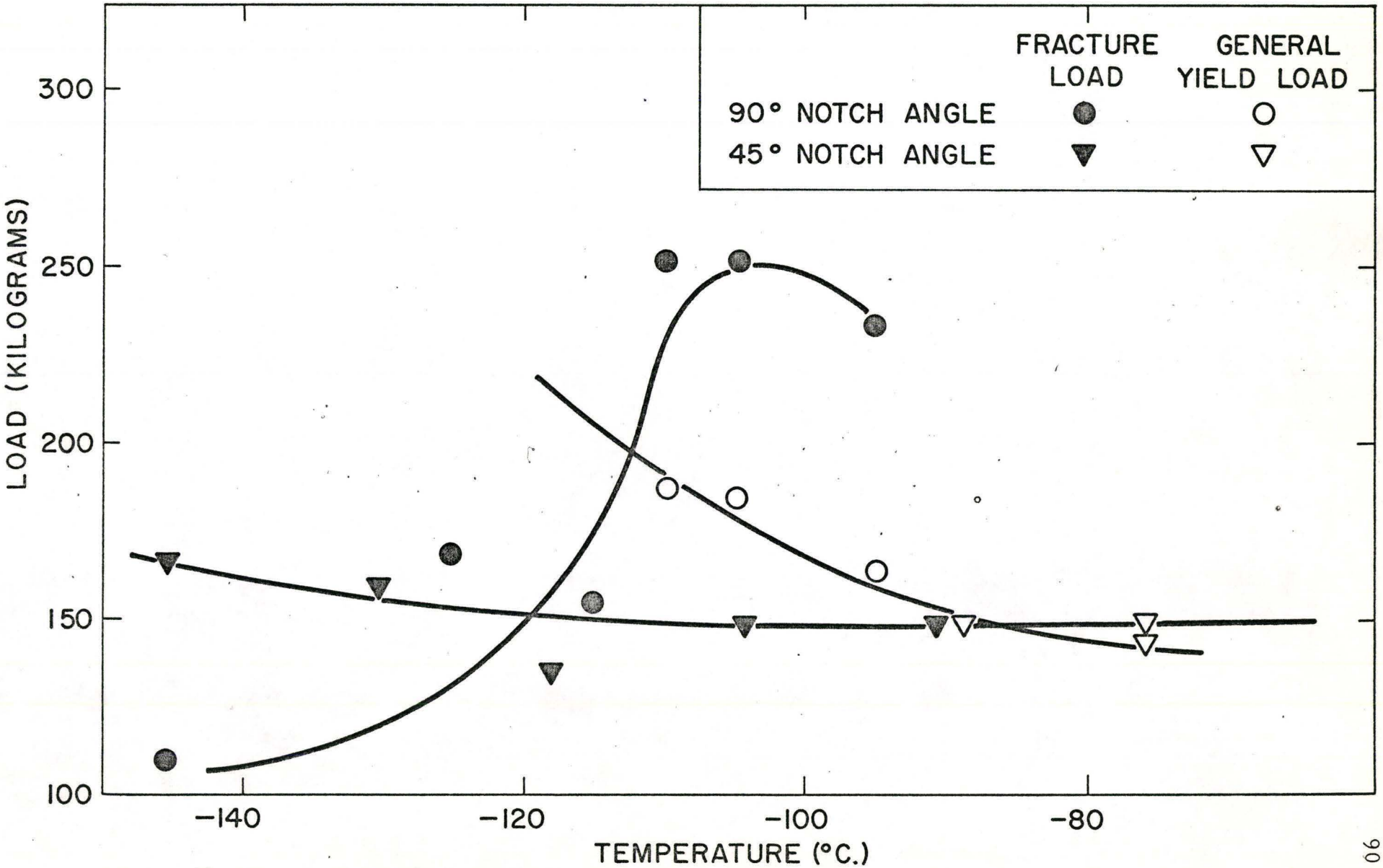

Figure 29: Fracture load and general yield load of notch bend furnace-cooled Armco iron specimens with 45° and 90° notch angles as a function of temperature.

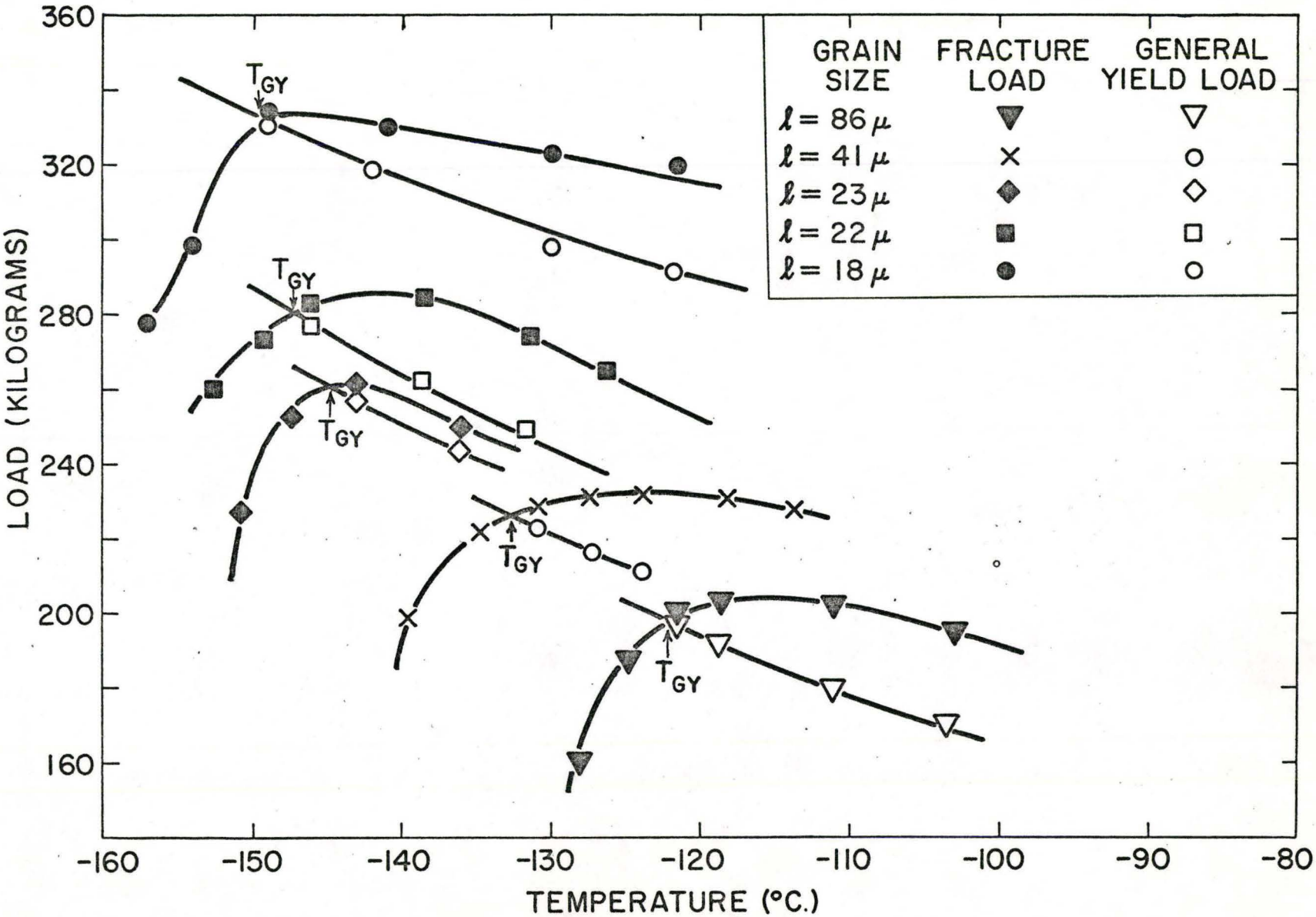

Figure 30: Fracture load and general yield load of notch bend quench-aged Armco iron specimens with different grain sizes as a function of temperature.

coincided with general yield are tabulated in Table 6 . Lower yield stress values were determined at various temperatures for a number of grains and the results are plotted against (grain size)$^{-1/2}$ in Figure 31 . The fracture stress was calculated by interpolating the yield stress data and the values are shown in Table 6 . As in the case of the furnace-cooled specimens, values for the fracture stress were calculated using both the Tresca and von Mises yield criterion.

The results for the variation of fracture stress with grain size for the quench-aged Armco iron are plotted in Figure 32 . Also shown on the figure are the fracture stress results obtained from the furnace-cooled specimens obtained by using the Tresca yield criterion. It can be seen that at the finer grain sizes for the quench-aged material there is still a deviation from the fracture stress-(grain size)$^{-1/2}$ relationship although not as pronounced as in the case for the furnace-cooled specimens. This was predicted by the model, where it was shown that as the carbide thickness tends to zero the condition for crack propagation reduces to the Cottrell-Petch fracture relationship.

A numerical fit to the experimental data for the quench-aged material can be made and the precedure used was identical to that explained previously for the furnace-cooled specimens.

The sizes and distributions of carbides in the quench-aged material was established by examining carbon replicas, in which it was found that the mean grain boundary thickness was about 0.3 microns. The Hall-Petch parameter k was obtained from the slope of the grain size dependence of the lower yield stress values and the results are shown in Table 6 . Again, if Cottrell's value for the effective surface energy is used, a numerical fit to the data can be made. As can be seen in Figure 32, there is a considerable deviation from the derived curve and the experimental fracture results obtained by the Tresca

TABLE 6

Values of the yield stress, the fracture stress and k at the temperature when fracture coincides with general yield for quench-aged Armco Iron.

Armco Iron, Quench-aged

45° notch

Grain Size (mm)	Transition Temp $^{\circ}C$	Yield Stress Kg/mm^2	Fracture Stress Kg/mm^2		k $Kg/mm^{3/2}$
			Tresca	von Mises	
.086	-123	43.8	95.5	110	2.0
.084	-123	44.0	96	111	2.0
.0415	-133	50.6	110	127	2.03
.0234	-145	58.6	128	148	2.03
.0223	-148	60.0	131	151	2.14
.0189	-145	60.2	131	151	2.03
.0189	-150	62.4	136	157	2.14

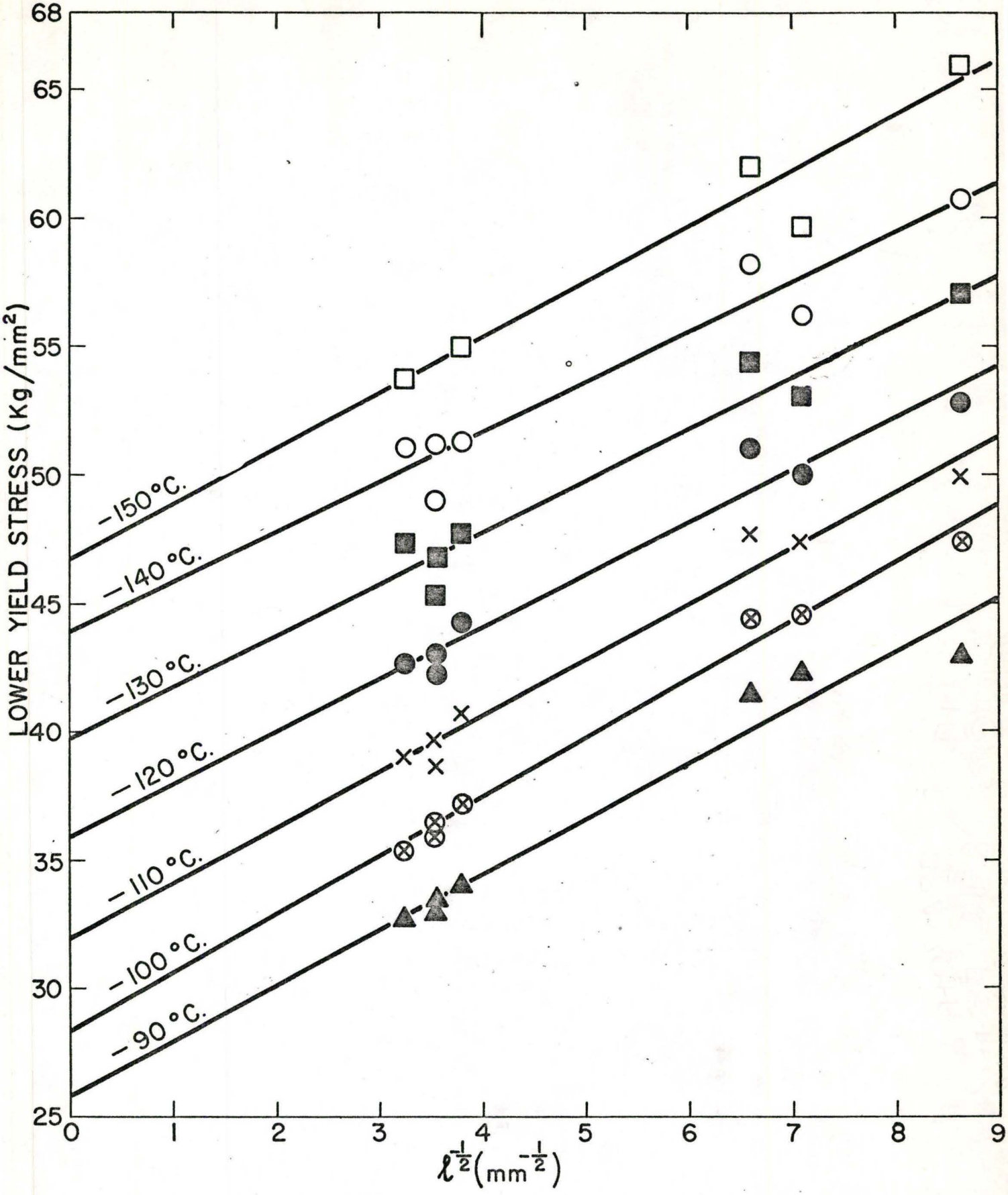

Figure 31 : The relationship between lower yield stress and (grain size)$^{-1/2}$ for quench-aged Armco iron at various temperatures.

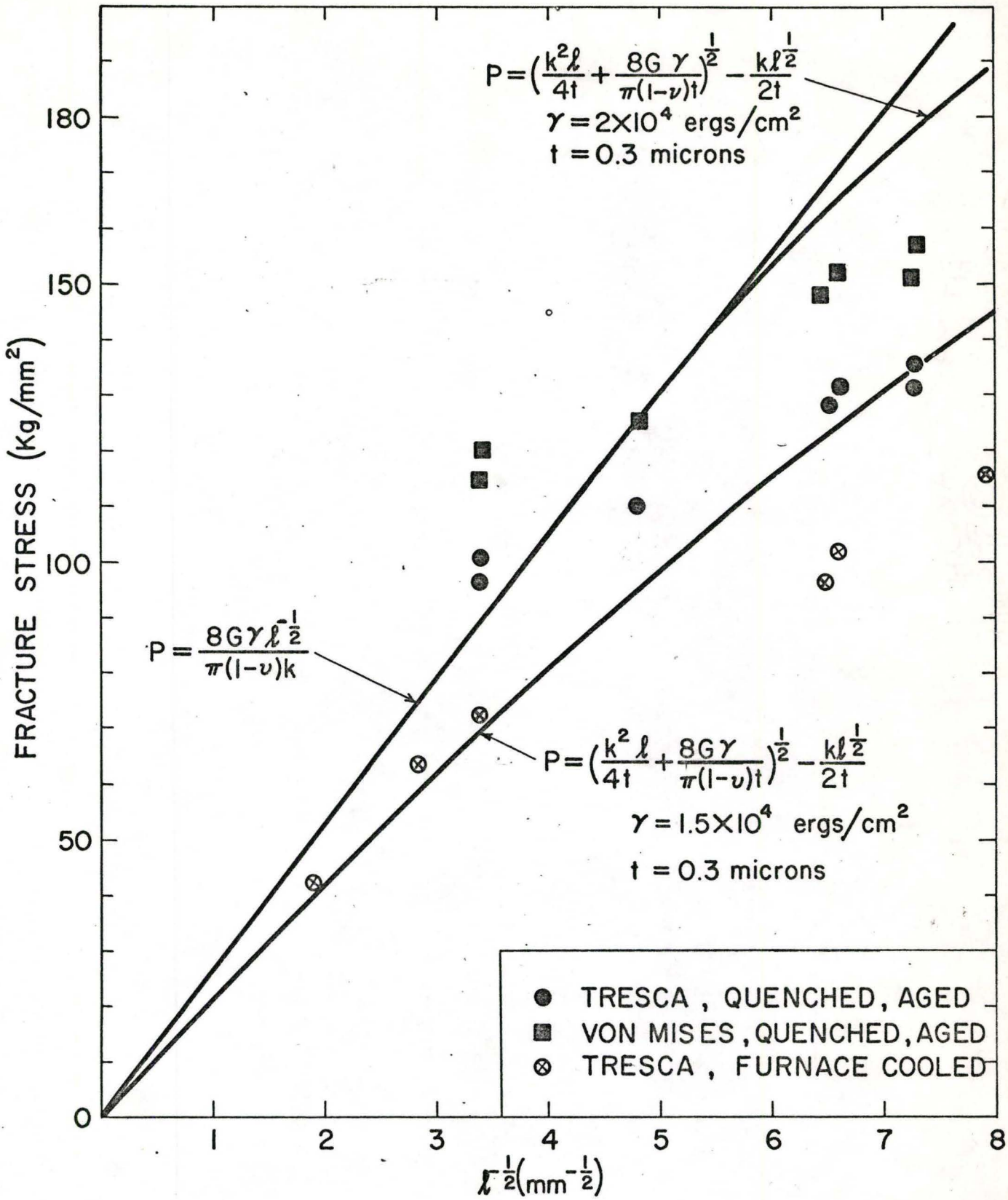

Figure 32: The variation of fracture stress with grain size for quench-aged Armco iron. The Petch fracture relationship and the fracture stresses from the furnace-cooled results are illustrated for comparison.

yield criterion. The fracture results obtained by the von Mises yield criterion fit much better although there is some deviation at the larger grain sizes. More important however, is that by reducing the grain boundary carbide thickness from a mean value of 2.5 microns to 0.3 microns the fracture stress has been increased from about 20 - 25 Kg/mm^2 (28,000 psi - 35,000 psi) for grain sizes smaller than $\ell^{-1/2} = 3$. It would be expected that at grain sizes greater than $\ell^{-1/2} = 3$, the fracture stresses would begin to coincide as the presence of grain boundary carbides at large grain sizes becomes increasingly less important in initiating and propagating cleavage cracks.

The results of the impact tests on furnace-cooled and quench-aged Armco iron are shown in Figure 33, where it is shown that the transition temperature was reduced by approximately 60°C after quench ageing.

4.4 Summary of Results

The results indicate that in low carbon steels, quench ageing may produce a simultaneous increase in both yield strength and fracture resistance provided the coarse carbide particles present in the furnace-cooled material are replaced by a fine dispersion of carbides within the ferrite matrix. It was shown in low carbon irons that grain boundary carbides may fracture due to inhomogeneous yielding of the ferrite matrix and provide important sources of cleavage cracks. Also, it was observed that the dispersed carbides within the grains act only as rigid barriers to dislocation motion thus promoting localized work hardening around the dispersed carbides and are not associated with the formation of non-propagating microcracks.

A simple energy balance criterion was proposed for the propagation of a micro-crack in a grain boundary carbide into the surrounding ferrite matrix under the combined action of the applied

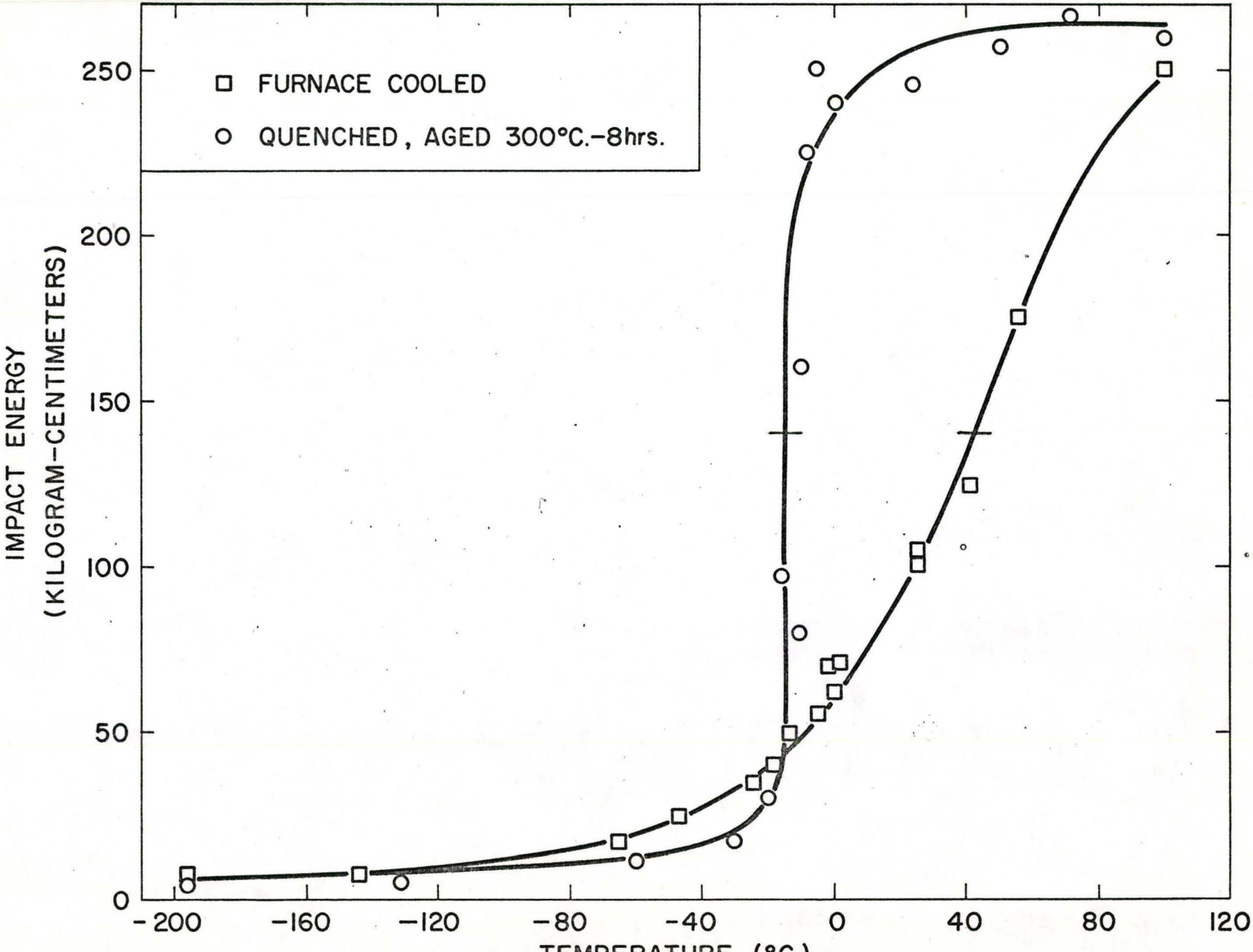

Figure 33: The variation of impact energy with testing temperature for Armco iron specimens.

stress and the stress concentration at the tip of an unrelaxed dislocation pile-up. The experimental results provide a limited confirmation of the model by demonstrating its ability to explain the effect of variations in both carbide thickness and grain size on the fracture stress. It was shown in low carbon irons, that in the presence of brittle grain boundary particles the grain size dependence of the fracture stress deviates from the Cottrell-Petch fracture relation and that for small grain sizes the fracture stress is increasing dependent on carbide thickness rather than grain size.

CHAPTER 5

FRACTURE TOPOLOGY

5.1 Introduction

During the propagation of a crack in metals and alloys the high stresses developed at the crack tip are usually sufficient to cause some plastic deformation to occur in the material adjacent to the fracture surface even though the fracture may appear quite brittle. Orowan (1955) recognized that the work done in causing plastic deformation during crack propagation should be included in the effective surface energy to create the new fracture surface and so, the effective surface energy required for crack propagation may be considered as the sum of the true surface energy of the solid and the work required to produce the plastic deformation. Although the true surface energy of most solids can be estimated with a fair degree of accuracy the magnitude of the plastic deformation term will depend on the temperature, the velocity of the crack and the detailed nature of dislocation motion in the material. Thus, it should vary in magnitude during the transition from brittle to ductile behavior.

The results described in Chapter 4 indicate that for the fracture criterion used in the present work, that is, that fracture be coincident with the general yield condition, the apparent values of surface energy are of the order of 2×10^4 ergs/cm^2. This is greater than the current estimate of the true surface energy of iron (2000 ergs/cm^2, Price et al 1964) and thus it is pertinent to examine the source of this difference in surface energies. The most likely source lies in the plastic work performed during crack propagation and thus an investigation of the detailed topology of the

fracture surfaces was undertaken to investigate this aspect.

The purpose of this chapter is two fold: firstly, to examine the fracture surfaces by scanning electron microscopy to observe topological features which might contribute to the magnitude of the plastic deformation term, and secondly, to estimate the extent of plastic deformation on cleavage surfaces by a micro-focus X-ray back reflection Laue technique.

5.2 Testing Apparatus and Procedure

5.2.1 Scanning Electron Microscopy

Scanning electron microscopy has a number of advantages in studying fracture surfaces over both light optical microscopy and surface replica methods in electron microscopy. The great advantage of scanning electron microscopy relative to the use of surface replicas is that the surfaces may be directly examined with little or no surface preparation, although the resolution (150-200Å) is less than that from a good replica (20-50Å). Also, much more irregular surface topologies can be examined by the scanning electron microscope. Compared to light optical microscopy the scanning electron microscope offers many advantages, the most valuable being its great depth of focus, approximately 300 times greater than from an optical microscope due to the shorter wavelength of the electrons.

In this work the scanning electron microscope has been used to compare the fracture surfaces of notch impact specimens in the furnace-cooled and quench-aged condition over a range of temperatures. The surfaces were examined to reveal features which may alter the topology of the cleavage facets or hinder crack propagation and thus contribute to the plastic deformation term.

5.2.2 X-ray Diffraction

A direct method of examining the extent of the plastic deformation involved in crack propagation is to study the diffraction of X-rays from the fracture surface. The basic technique of Laue back reflection of X-rays and its application to deformed materials is described in detail by Barrett and Massalski (1966) and Cullity (1956). The Laue spots from a crystal containing few local imperfections are sharp. In materials which are deformed plastically the lattice planes become distorted and strain gradients are developed in the material. These strain gradients cause the Laue spots to become distorted in shape; a condition generally termed asterism. The extent of asterism can be related to the degree to which the lattice planes are bent, although, the relationship is not a simple one in the Laue technique. With more severe deformation the basic grain structure of the material becomes divided into cells which can diffract X-rays independently and the information in the basic Laue pattern becomes more complex as diffraction processes of the Debye-Scherrer type begin to occur.

In the present work comparative estimates of the extent of plastic deformation on the cleavage fracture surface were made using a Hilger and Watts micro-focus X-ray unit. The X-ray beam of tungsten radiation with a spot size of 100 microns was focussed on various crystals across the fracture surface of notch bend specimens. Various crystals across the surface were examined to establish any differences between the degree of plastic deformation immediately below the notch and that in the bulk of the specimens. In addition specimens were examined which were fractured at various temperatures in both the furnace-cooled and quench-aged condition. All the specimens examined by the micro beam method had large grains of the order of

250 microns in diameter in order to ensure that the diffracted information was obtained from a single cleavage facet.

The specimen to film distance was three centimeters and the film exposure time was four hours.

5.3 Scanning Electron Microscope Observations

The fracture surfaces examined were those obtained from the impact test results shown in Figure 33 in Chapter 4. Scanning electron micrographs of the fracture surfaces of the furnace-cooled and quench-aged Armco iron at various temperatures along the energy absorption curve are shown in Figures 34 and 35 respectively. For the furnace-cooled specimens there is evidence of an increasing amount of plastic tearing at grain boundaries as the testing temperature is increased from -140 to 56°C. The grain boundaries show a pronounced dimpled structure in comparison with the cleavage facets within the grains. In the quench-aged case the amount of plastic deformation present near the boundary region is generally small and deformation only becomes extensive near the shelf energy.

The regions of plastic deformation at the grain boundaries are indicative that a higher effective surface energy is necessary for crack propagation across grain boundaries in the transition temperature region and the extent of this plastic region can be correlated with the shape of the energy absorption curves for the two materials. In the case of the furnace-cooled specimens there is a gradual decrease in energy abosrption values as the test temperature is reduced. This corresponds directly to the decreasing size of the plastic zone which is the reason why the transition region occurs over a broad temperature range. For the quench-aged material very little plastic deformation was evident at the boundaries and the change from ductile to brittle behavior was more abrupt as seen from the impact results in Figure 33.

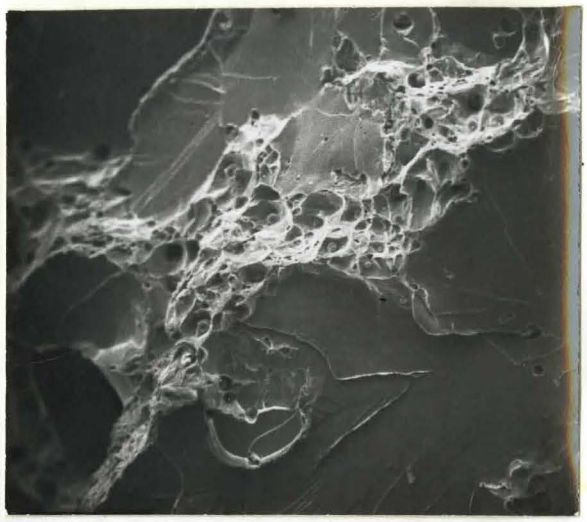

(a)

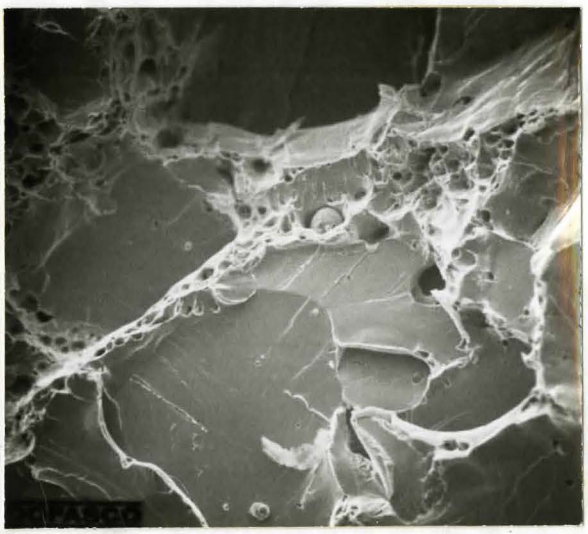

(b)

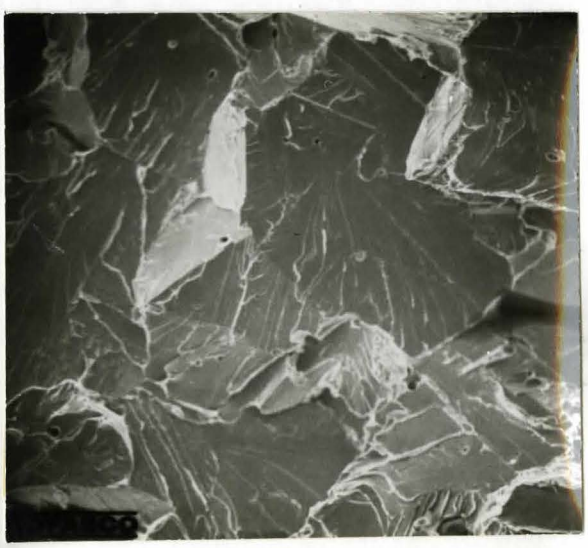

(c)

Figure 34: Scanning Electron Micrographs of the fracture surfaces of furnace-cooled impact specimens tested at (a) 56°C (b) 2°C and (c) -140°C. X200

(a)

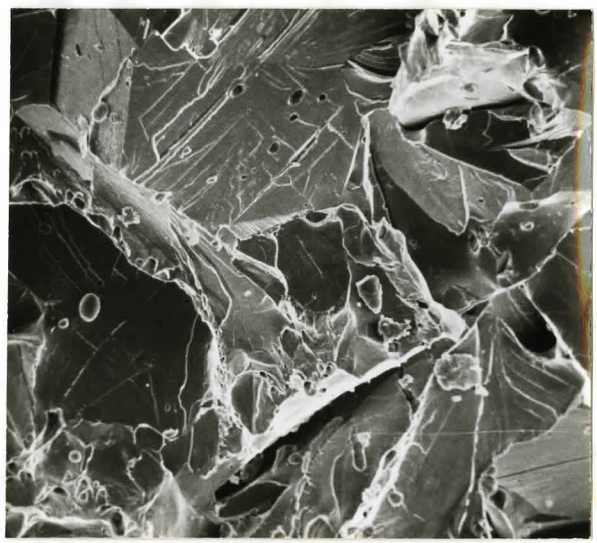

(b)

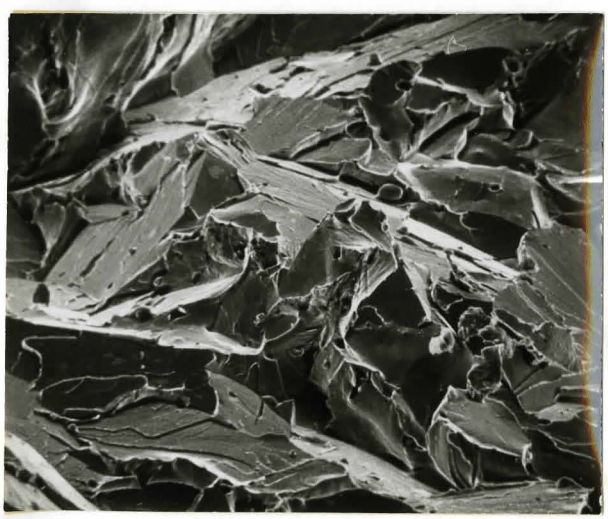

(c)

Figure 35: Scanning electron micrographs of the fracture surfaces of quench-aged impact specimens listed at (a) -2°C (b) -10°C and (c) -130°C. X200

5.4 X-Ray Diffraction Studies

In order to provide a basis for comparing the extent of plastic deformation on the fracture surfaces as indicated by the asterism of the Laue spots a specimen of Armco iron in the furnace-cooled and undeformed condition was examined by the micro beam method. Figure 36 indicates that for the undeformed specimen the Laue spots are relatively sharp.

Two types of experiments were performed using the X-ray micro beam unit. Firstly, back reflection photographs were obtained in the region immediately below the notch, that is, the region in which fracture is initiated, for specimens tested at temperatures where fracture occurred above general yield, at general yield, and below general yield. These observations were made on both furnace-cooled and quench-aged materials. The results are shown in Figures 37 and 38, respectively. It can be seen that for both the furnace-cooled and quench-aged specimens the extent of asterism decreases with decreasing temperatures. In the quench-aged specimen where fracture occurred after general yield plastic deformation is so severe that the Laue spots have almost become enlarged enough to form Debye rings. Also, both the furnace-cooled and quench-aged materials show appreciable asterism at the temperature where fracture is coincident with general yield indicating that some plastic deformation is associated with the initiation and early propagation of cracks at these temperatures.

The second purpose of the micro beam experiments was to explore the extent of plastic deformation in regions away from the notch. Specimens in the quench-aged condition were examined for this purpose with observations being made at the same conditions as those reported in Figure 38 . The results are shown in Figure 39 and in all cases it can be seen that the extent of asterism in the interior of the

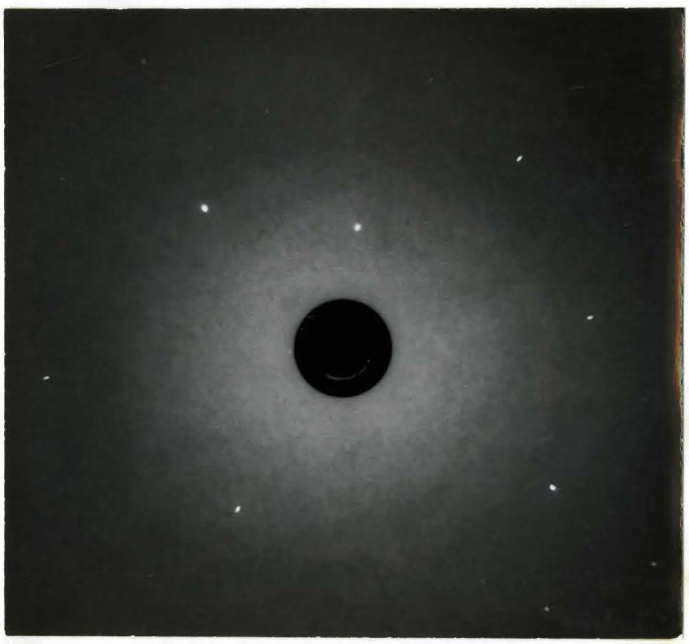

Figure 36: X-ray back reflection photograph from surface of an undeformed Armco iron specimen.

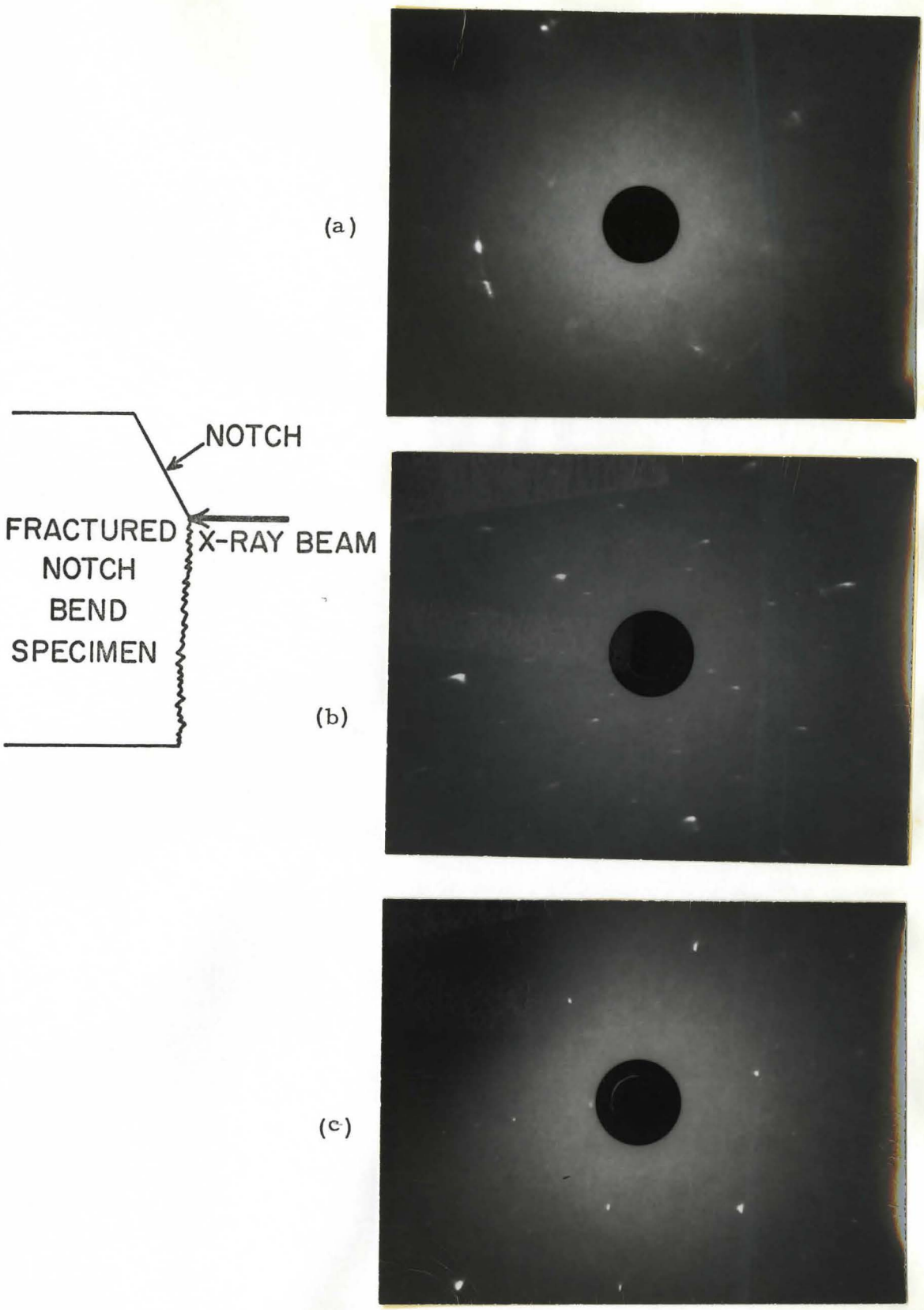

Figure 37: X-ray back reflection photographs from fracture surface immediately below the notch of furnace cooled notch bend Armco iron specimens at conditionswhere fracture occurred a) after general yield b) at general yield c) below general yield.

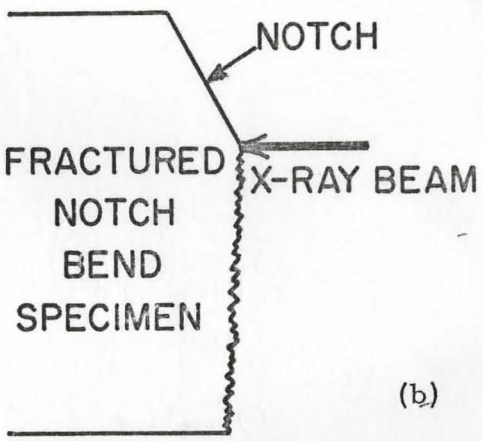

(a)

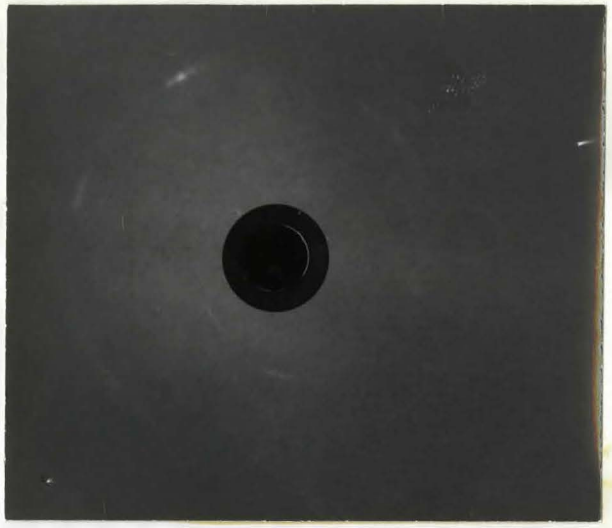

(b)

(c)

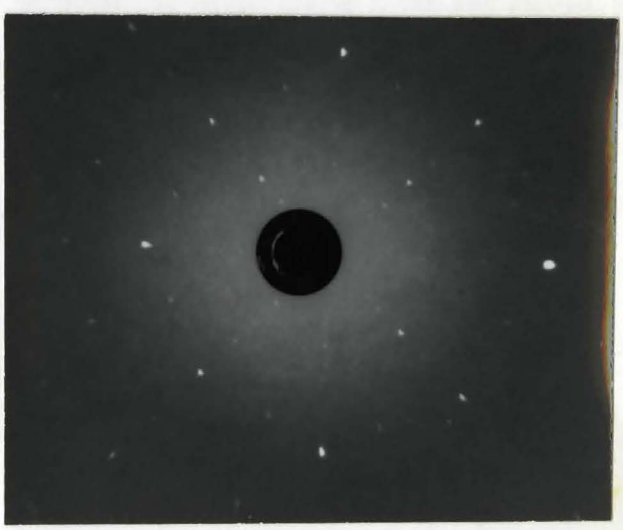

Figure 38. X-ray back reflection photographs from fracture surface immediately below the notch of quench aged notch bend Armco iron specimens at conditions where fracture occurred a) after general yield b) at general yield c) below general yield.

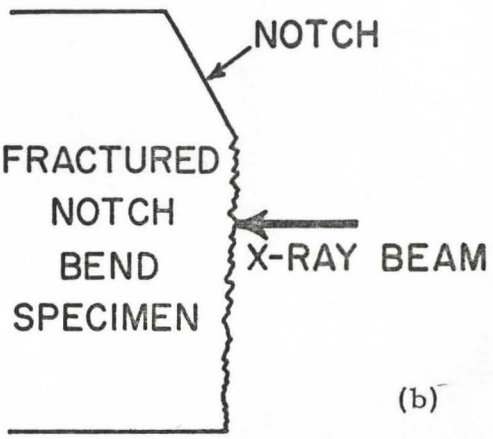

(a)

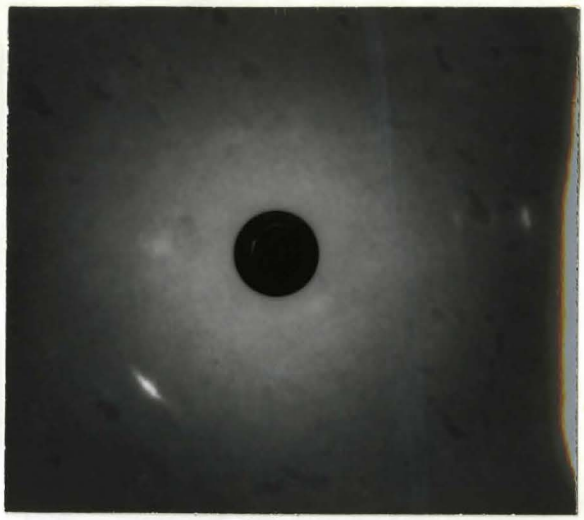

(b)

(c)

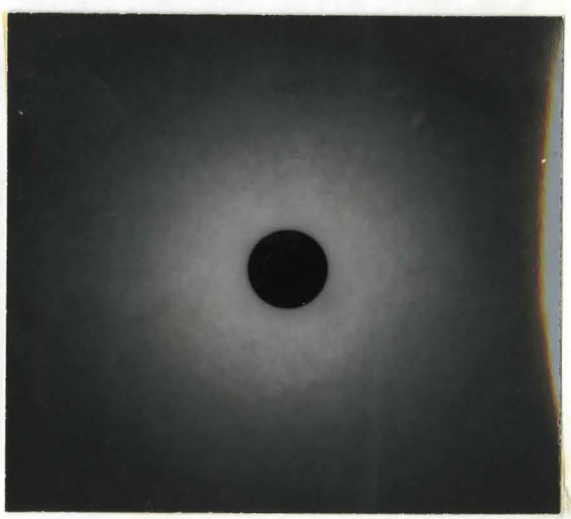

Figure 39: X-ray back reflection photographs from fracture surface away from the notch of quench aged notch bend Armco iron specimens at conditions where fracture occurred a) after general yield b) at general yield c) below general yield.

specimen is less than that observed directly below the notch. This is in accord with the concept of yielding in notch bars outlined in Chapter 3 where the region immediately below the notch deforms first and work hardens prior to the spread of plasticity across the net section of the bar.

Although no attempt was made to measure the depth of the plastic deformation resulting from crack propagation, the fracture surface of a furnace-cooled specimen which broke at general yield was chemically polished in a solution of 80 ml of hydrogen peroxide, 15 ml of distilled water and 5 ml of hydrofluoric acid for about 5 minutes and a Laue photograph taken again of the crystal just below the notch. The result is shown in Figure 40 where it can be seen that the extent of plastic deformation has been reduced considerably.

The results presented above clearly indicate that plastic deformation occurs during the initiation and propagation of cracks in both furnace-cooled and quench-aged materials. This will certainly be a contributing factor to the effective surface energy required for crack propagation.

5.5 Summary of the Results

The evidence from both the scanning electron microscope and the X-ray micro beam methods indicate that considerable plastic deformation occurs during both the initiation and propagation of cracks in the furnace-cooled and quench-aged materials.

The topologies of the fracture surfaces indicate that for the furnace-cooled material in the transition region much of the plastic deformation is associated with plastic tearing at the grain boundaries as the cleavage crack propagates from one grain to the next. The extent of this plastic tearing increases throughout the transition region from

Figure 40. X-ray back reflection photograph from a chemically polished fracture surface immediately below the notch of a furnace-cooled notch bend Armco iron specimen at the condition where fracture occurred at general yield.

the brittle to ductile range. In the quench-aged material plastic tearing is not localized at the grain boundaries and the energy transition curve is much sharper as noted previously.

The micro beam evidence indicates that the extent of plastic deformation is limited to about a grain diameter from the fracture surface. In addition, the asterism results indicate that the amount of plastic deformation decreases rapidly with temperature.

The above results suggest that the effective surface energy needed for crack propagation should be considerably larger than the true surface energy due to the plastic work performed in initiating and propagating the crack.

CHAPTER 6

DISCUSSION

The experimental results indicate that the distribution of the second phase particles is important in determining both the yield stress and fracture characteristics of low carbon steels. The results presented in Chapter 4 showed that quench ageing could increase both the yield stress and fracture resistance of the material provided the grain boundary carbides present in the furnace-cooled material were replaced by a fine dispersion of carbides within the ferrite grains.

In the preliminary results, the effect of quench ageing on the fracture behavior of a commercial 1018 steel and Armco Iron was studied. Quench ageing produced an increase in yield strength for both materials but the fracture resistance of the low carbon iron was increased whereas that of the commercial steel was decreased. This difference in fracture behavior between the commercial steel and Armco iron is associated with the differences in second-phase distribution and can best be explained by using a modified version of the Orowan fracture hypothesis (1945), which is schematically illustrated in Figure 41. The basis of this hypothesis is that yield and brittle fracture are assumed to be two separate processes, and the fracture stress is assumed to be independent of temperature. The Orowan hypothesis takes no cognisance of the detailed events relating yield and fracture. For materials which have a strong temperature dependence of the yield stress, brittle fracture becomes possible when the yield stress exceeds some critical value, for example σ_{F1} at temperature T_1 in Figure 41.

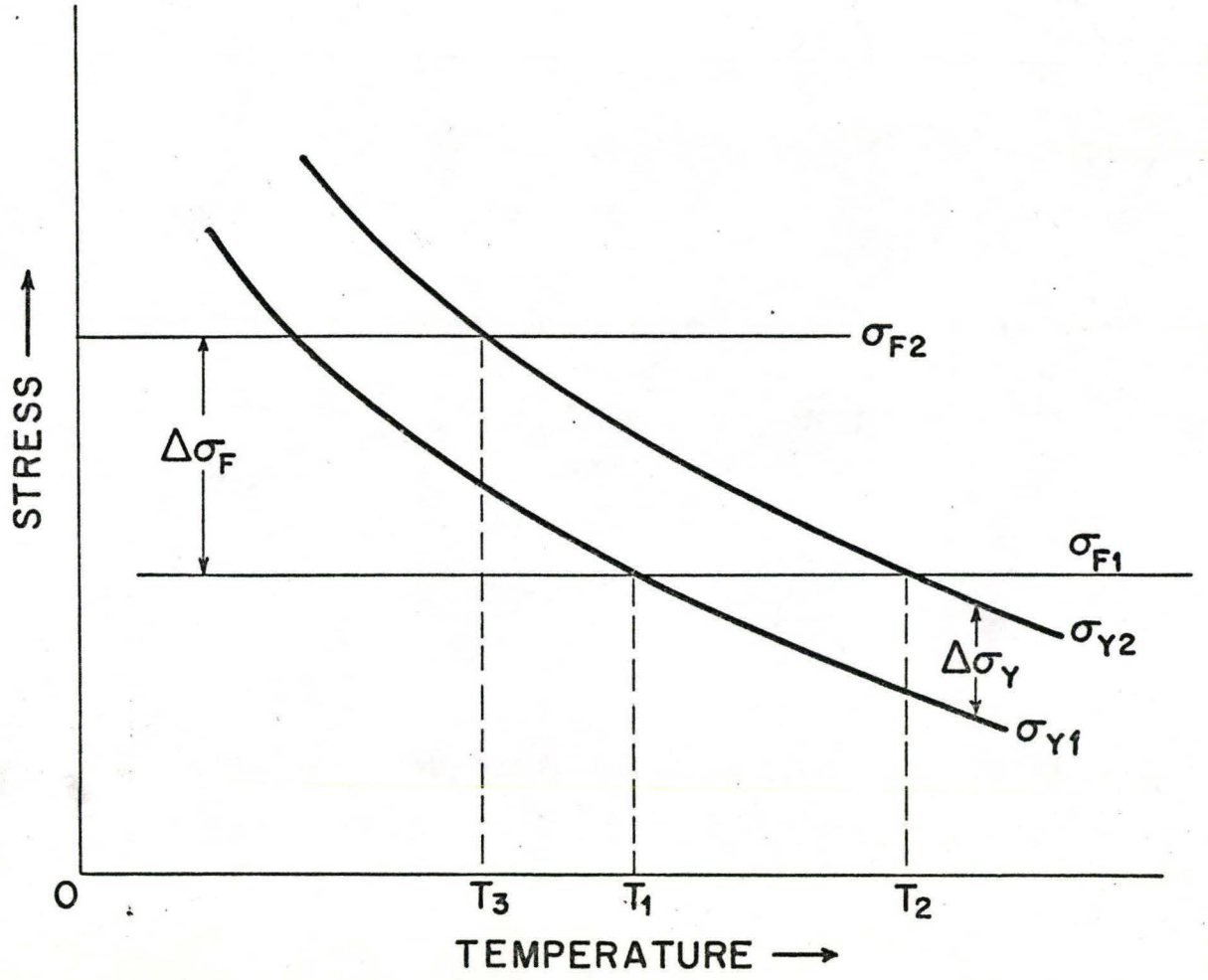

Figure 41: Schematic diagram for the interpretation of the ductile-brittle transition in low carbon steels.

Now, the yield stress of a low carbon steel can, by the Hall-Petch equation, be expressed as a function of both the grain diameter ℓ, and the friction stress σ_o where the temperature dependence of the yield stress is contained in the thermal component of the friction stress. Quench ageing produces precipitation within the matrix which also increases the lattice friction stress (athermal component of the friction stress). The fracture stress on the other hand was observed to depend not only on the grain size of the material but the distribution and size of carbides and in particular, on grain boundary carbide thickness t. With these points in mind and making the assumption that the fracture stress is independent of temperature (Knott 1966, Oates 1968, Wilshaw 1967) the variation in transition temperature between the commercial steel and the Armco iron can be readily explained with the aid of Figure 41. It was observed in the optical micrographs of the commercial steel that quench ageing did not radically alter the microstructure from that observed in the furnace-cooled material so, if the hypothesis that fracture stress is dependent on grain size and the distribution of second-phase particles is correct, the fracture stresses of the commercial steel in the furnace-cooled and quench-aged condition will not be substantially altered and may be taken to a first approximation to be equal. However, the yield stress of the quench-aged commercial steel will be increased relative to the furnace-cooled material due to the fine dispersion of carbides within the ferrite matrix, that is, the friction stress will be increased. Therefore, if the yield stress increases from σ_{y1} to σ_{y2} (Figure 41) and the fracture stress (σ_{F_1}) remains unchanged, the transition temperature will increase from T_1 to T_2 as observed in the energy absorption results. This increase in transition temperature on quench-aged commercial steel would also be predicted from the Cottrell-Petch fracture relationship, as any increase in yield or friction stress relative to the effective

shear stress will tend to make the material brittle.

For the Armco iron, on the other hand, the microstructures of the quench-aged and furnace-cooled material were quite different with respect to the distribution of the carbide phase. In this case the fracture stress, as well as the yield stress of the quench-aged material will be modified with respect to the furnace-cooled material. Thus, by increasing the yield stress by $\Delta\sigma_y$ and altering the fracture stress from σ_{F1} to σ_{F2} (Figure 41) yield and fracture become coincident at T_3 representing a decrease in transition temperature relative to the furnace-cooled material. This was observed in Figure 9 for the quench-aged Armco iron. This decrease in transition temperature for the Armco iron would not be predicted by the Cottrell-Petch fracture relationship, and thus points out one of the basic shortcomings of their model. The Cottrell-Petch model is unable to explain the behavior of quench-aged low carbon steels probably because the model does not provide for a dependence of both yield and fracture stress on microstructure. Thus, in classical derivations both the crack size and the tensile stress operating at propagation are determined by the yield stress of the material whereas in real situations there are often second phase particles present whose fracture properties can exert a marked influence on the fracture behavior of the material.

The above description of the fracture behavior of materials, by using the modified version of the Orowan fracture hypothesis, is a very qualitative one and does not indicate quantitatively the role of grain boundary carbides and dispersed carbides in the deformation process. An indication of the role played by the dispersed carbides within the grains was obtained by direct observations. In Figure 23 it was observed that localized dislocation tangling was promoted around the dispersed particles suggesting that the dispersed carbides are acting as rigid barriers and

as such are not cut by glide dislocations. Electron microscope observations by Hale and McLean (1963) and Keh et al.(1963) support this view that carbide particles in iron are strong obstacles. Now according to the Orowan mechanism (1948) the introduction of a dispersion of hard particles into a structure will increase the tensile yield stress of the matrix by an amount

$$\Delta\sigma_y \text{ (theoretical)} = \frac{Gb}{\lambda} \qquad (48)$$

where G is the shear modulus, b is the Burgers vector and λ is the mean particle spacing (the dispersed carbides were considered to a first approximation to be point sources). Values of $\Delta\sigma_y$ (theoretical) were calculated from the dispersed carbide spacings given in Table 3 using this latter formula and compared with the incremental increase in yield stress ($\Delta\sigma_y$ experimental) after quench ageing. The values of $\Delta\sigma_y$ (theoretical) and $\Delta\sigma_y$ (experimental) for Armco and NPL iron are listed in Table 7 along with the results of Almond et al.(1969) for comparison. The agreement between the experimental and theoretical values is satisfactory and suggests that to a first approximation the carbides can be regarded as rigid barriers to dislocation motion. The tangling of dislocations in the region of the particles suggests that hard particles are important in accumulating dislocations during deformation as discussed in detail by Ashby (1967).

Hahn and Rosenfield (1966) have proposed a model which predicts that a fine uniform dispersion of hard particles (particles that resist penetration by dislocations) will not only strengthen the material by inhibiting the motion of dislocations but will also raise the fracture resistance. They suggest that the enhanced fracture resistance is a

TABLE 7

Effect of quench ageing on yield stress.

Materials	Interparticle Spacing (microns)	$\Delta\sigma_y$ (expt) (Kg/mm^2)	$\Delta\sigma_y$ (theor) (Kg/mm^2)
Armco	0.3	8.5	7.6
NPL	0.4	3.5	5.7
Almond et al (1969)			
NPL (0.018 wt.%C)	0.5	4.4	5.0
Swedish Iron (0.020 wt.%C)	0.3	4.5	6.2
EN2 (0.030 wt.%C)	0.8	3.5	4.1

consequence of the hard particles limiting the effective slip distance to the interparticle spacing λ and thus reducing the effective length of the dislocation pile up responsible for fracture initiation.

Hahn and Rosenfield modified the Cottrell (1958) model of cleavage-crack initiation by re-evaluating the number of coalesced dislocations and allowing for an increase in effective shear stress due to the dispersed particles. Thus, for a single phase material the fracture stress (σ_F) can be written as:

$$\sigma_F = \frac{2\gamma}{5D} \left(\frac{G}{\tau_s'}\right)^{3/2} \tag{49}$$

where γ is the surface energy, D is the grain size, G is the shear modulus of the matrix, and τ_s' is the effective shear stress for the matrix. For a dispersion strengthened alloy the above equation must be modified to account for the increase in effective stress due to the Orowan hardening mechanism and the restriction of length of the dislocation pile-up to the interparticle spacing rather than the average grain size. Therefore, substituting λ for D and introducing the effective shear stress for the dispersion strengthened matrix,

$$\tau_m = \tau_s + \frac{Gb}{2\lambda} \tag{50}$$

The equation for the fracture stress of a dispersion strengthened matrix will be

$$\sigma_F = \frac{2\gamma}{5\lambda} \left(\frac{G}{\tau_s + \frac{Gb}{2\lambda}}\right)^{3/2} \tag{51}$$

Therefore, if the pile up length is limited to the interparticle spacing and it is assumed that the surface energy is not affected by the dispersed particles (Hahn and Rosenfield assume γ is the true surface energy of iron in the single phase and dispersion strengthened alloy), then the ratio of the fracture stress for the dispersed carbide material (quench-aged) to the fracture stress for the furnace-cooled case (taken as the single phase material) can be written as

$$\frac{\sigma_{(\text{quench-aged})}}{\sigma_{(\text{furnace-cooled})}} = \frac{D}{\lambda} \left(\frac{\gamma_s}{\gamma_s + \frac{Gb}{2\lambda}} \right)^{3/2} \qquad (52)$$

where σ(quench-aged) and σ (furnace-cooled) refer to the fracture stress in the quench-aged and furnace-cooled materials respectively. From the relative values of grain diameter and mean interparticle spacing (Table 8), and using the calculated values for $\frac{Gb}{\lambda}$ from Table 7 the ratio of the fracture stresses in the furnace-cooled and quench-aged condition should be of the order of 30 to 130 (Table 8) if the Hahn and Rosenfield model is correct. Whereas in this work and that of Almond et al.(1969) the ratio of the experimental values varies from 1.1 to 1.5 for the low carbon materials. Further, the Hahn and Rosenfield analysis predicts values much higher than could be sensibly expected since it would require the quench-aged materials to have fracture strength approaching the cohesive strength of the iron lattice. As listed in Table 3 the fracture stress of Armco iron quench-aged was 100, 000 psi (70.5 Kg/mm^2). By the Hahn and Rosenfield model this value should be about 30 times greater (2.1 x 10^3 Kg/mm^2). The cohesive strength of alpha iron <100> is 3.1 x 10^3 Kg/mm^2, Kelly 1966.

The inability of the Hahn and Rosenfield model to explain the present results arise from the assumption that because the second phase particles act as rigid barriers they restrict the lengths of dislocation

TABLE 8

Comparison of ratios of fracture stresses in quench-aged and furnace-cooled low carbon material by experiment and by the Hahn and Rosenfield model.

Material	Grain Size (mm)	Interparticle Spacing (μm)	Ratio of Fracture Stresses Experimental	Hahn and Rosenfield
Armco	0.114	0.3	1.5	120
NPL	0.146	0.4	1.4	130
		Almond et al.(1969)		
NPL	0.032	0.5	1.2	38
Swedish Iron	0.027	0.3	1.3	50
EN2	0.036	0.8	1.1	28

pile-ups involved in fracture nucleation. The metallographic evidence suggests that the dispersed carbides in the quench-aged material force turbulent flow to occur in the region of the particle rather than the formation of dislocation pile-ups. As extensive secondary slip occurs at the second-phase particles within the matrix, pile-ups can only be formed at the grain boundaries where it is difficult to transmit plastic strain to the adjacent grain. This is not accounted for in the Hahn and Rosenfield model where no account is taken of plastic relaxation at the dispersed particles. Thus, in both the furnace-cooled and quench-aged materials the only places where large stress concentrations can be developed, which are not relieved by plastic deformation, will be where the slip band meets the grain boundaries as outlined in the theories of Cottrell (1958) and Petch (1959). However, both the Cottrell and Petch theories predict that if the yield stress is increased by precipitation hardening the material would have a decreased fracture resistance.

Now Cottrell and Petch did conclude independently that for complete fracture, crack growth was the controlling event for mild steel over a wide range of testing conditions. This means in effect that the surface energy must increase as crack propagation occurs. Yet, Cottrell and Petch gave no explanation for an increase in surface energy in the development of their model. In quantitative tests the discrepancy in surface energy values has been attributed to propagation of the cleavage crack through grain boundaries as a consequence of the misorientation between adjacent regions of material. Stroh (1957) and more recently Smith (1966) have shown that crack propagation and not crack nucleation is the controlling event in fracture but only under conditions where the crack is initiated in regions with lower effective surface energy. This condition is fulfilled if cleavage is initiated by

the fracture of grain boundary carbides and the important stage is the growth of the crack from the particle into the ferrite matrix. That cracks are actually present in grain boundary carbides and propagate across ferrite grains has been observed by several workers (Allen et al.1953, Bruckner 1950, McMahon and Cohen 1965, Lindley 1969) as well as in the present work (Figure 22). Also, the observations of McMahon and Cohen (1965), Oates (1968), and Lindley (1969), along with those in this work, indicate that in the absence of pearlite, the ductile-brittle transition temperature decreases as the thickness of the grain boundary carbide decreases.

Smith (1966) has recently developed a model appropriate to the situation outlined above in which he assumes that the critical event in cleavage is the penetration of the carbide size cracks into the ferrite matrix. In this model it is assumed that cracks nucleate within the brittle carbide particles as a consequence of plastic deformation processes in the matrix and that the increase in the effective surface energy accompanying crack propagation arises because the surface energy of the brittle grain boundary particles is much less than that of the ferrite matrix. In his calculations, contributions to the critical event will depend not only on the applied stress but the effective shear stress as well.

The condition for propagation of a precipitate sized crack into the ferrite matrix has been derived by Smith from a consideration of the growth of a shear crack at the tip of a continuous distribution of infinitesimal dislocations and can be expressed as

$$\frac{t}{l}\,\sigma_F^{\,2} + \tau_s^{\,2}\left\{1 + \frac{2}{\pi}\left(\frac{4t}{l}\right)^{1/2}\frac{\tau_o}{\tau_s}\right\}^2 > \frac{8\gamma G}{\pi(1-\nu)l} \qquad (53)$$

where t is the carbide thickness, l the grain diameter, σ_F the fracture

stress, τ_s the effective shear stress, τ_o the friction stress, γ the effective surface energy of the ferrite matrix and G the shear modulus. This equation applies to the growth of a crack under the combined effect of the stress due to the pile-up and the applied tensile stress. Smith has stated that two situations arise depending on whether slip or twinning induces the carbide to crack. If the carbides fracture due to slip in the matrix the above equation can be reduced to

$$\frac{t}{l}\left\{\sigma_F^2 + \tau_o^2 \frac{16}{\pi^2}\right\} > \frac{8\gamma G}{\pi(1-\nu)l} \qquad (54)$$

which on re-arranging becomes

$$\sigma_F^2 > \left(\frac{8\gamma G}{\pi(1-\nu)t} - \tau_o^2 \frac{16}{\pi^2}\right) \qquad (55)$$

This equation indicates that the fracture stress is independent of grain size and depends solely on the carbide thickness. If values of carbide thickness t and τ_o are put in this equation and utilizing Cottrell's (1958) value for the effective surface energy, fracture stresses of the order of 145 Kg/mm^2 are obtained regardless of the grain size, which is clearly in conflict with the present results.

If the fracture is twin induced, the friction stress for twinning can be assumed to be negligible (Worthington and Smith 1966) and then the equation reduces to

$$\frac{t}{l}\sigma_F^2 + \tau_s^2 > \frac{8G\gamma}{\pi(1-\nu)l} \qquad (56)$$

Oates (1969) has used this equation to explain the temperature dependence of the fracture stress in low carbon manganese steels where

fracture results from twin induced cracking of grain boundary carbides. The model proposed by Smith is more applicable to the temperature region where twins nucleate fracture. Although Smith discusses the effects of a superimposed hydrostatic stress, and the effects of second-phase particles, the model is very restrictive and is at present limited to explaining brittle fracture at low temperatures (-196^{o}C) which is well below the temperature range of technological interest and outside the range of the experimental results reported in the present work.

As both the Hahn and Rosenfield, and Smith models are unable to explain quantitatively the experimental results in this work an attempt was made to derive a simple quantitative model for slip induced cleavage fracture (Chapter 4). The basic principles involved in the derivation of this model are similar to those of Smith's (1966) where the critical event is in propagating the carbide size crack into the ferrite matrix when it is acted upon both by the applied stress system and the stresses due to a dislocation pile-up in an unrelaxed slip band. In order to utilize the model an experimental condition must be achieved in which the processes of fracture and yielding can be equated.

The model predicts that for fine grain sized material where massive grain boundary carbides are present there will be considerable deviation from the Cottrell-Petch fracture relationship. The experimental results from the notch bend tests are in good accord with the derived curve for a grain boundary carbide thickness of 2.5 microns and utilizing Cottrell's value for the effective surface energy. As pointed out previously, altering the carbide size to 1 micron has little effect on the fracture stress at the larger grain sizes but increases the derived fracture stress value for the smaller grain sizes. Justification for the mean value of 2.5 microns can be based on the hypothesis that for fine grain sizes the presence of a crack in a large grain boundary carbide is

sufficient to propagate into the surrounding matrix due to the local tensile stress present beneath the notch at general yield. In effect then a few large grain boundary carbides situated in the region beneath the notch could be considered as a "weak" link in the material which initiates fracture.

The fracture results of other workers for furnace-cooled or normalized low carbon steel has been plotted in Figure 42 along with the present fracture results (Tresca). The solid line is the derived curve using a grain boundary carbide thickness of 2.5 microns and Cottrell's (1958) effective surface energy value. Although most of the data is at the large grain size end of the curve, the results do fit well with those from the present work and close to the derived curve. There is little evidence in the literature pertaining to the fine grain size region but the general trend of all the results appears to indicate a deviation from the Cottrell-Petch relationship at smaller grain sizes. One of the limitations of the Cottrell-Petch model was that no account was taken of the detailed microstructure in regard to the fracture process, although the role of microstructure was considered with respect to the yield stress. The results of Almond et al.(1969) were calculated from Equation 47 using the quoted grain sizes and carbide thickness reported in the paper. The fracture stresses reported in this paper were obtained from instrumented impact tests and thus the operative strain rate was about two orders of magnitude higher than for notch bend tests.

In utilizing the notch bend results it was assumed that the fracture stress was independent of temperature over the range of temperatures examined. This has been found for a number of steels (Knott 1966, Oates 1968) but in order to give some basis for this assumption in the present work specimens of constant grain size were tested with notch angles of 45° and 90°. The temperatures at which fracture was coincident with general yield was found to be $-90^{\circ}C$ and $-110^{\circ}C$ respectively

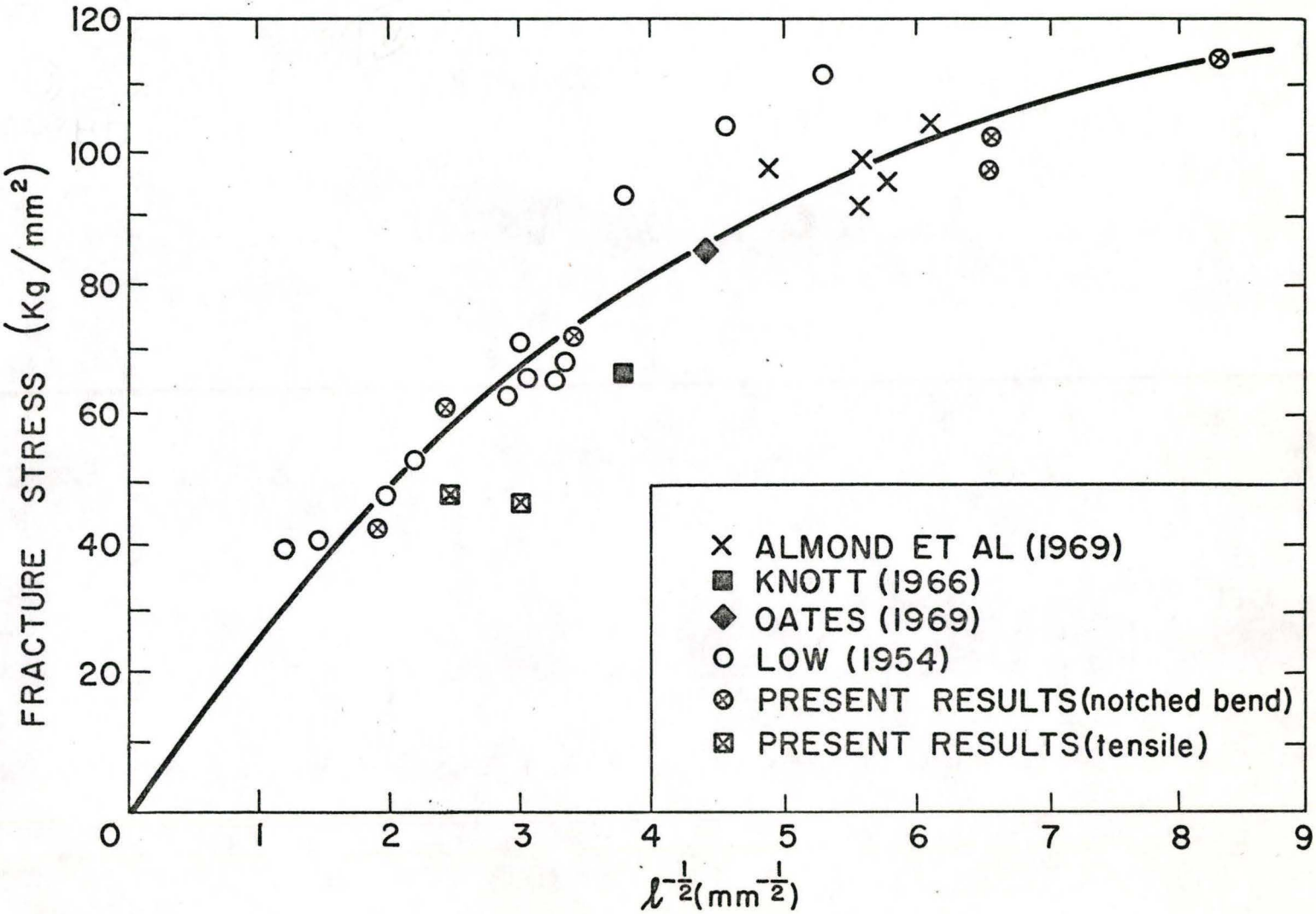

Figure 42: Summary of fracture stress results from various sources as a function of grain size.

(Figure 29). The fracture stresses were calculated from the product of the stress intensification factor and the appropriate yield stress to be 64 Kg/mm^2 (Tresca) at both temperatures. On the basis of this result the fracture stress was assumed to be insensitive to temperature over the range of temperatures utilized in the present study.

The effect of reducing the grain boundary carbide size on the fracture stress was seen in Figure 32 where the experimental results indicated that at finer grain sizes there was a slight deviation from the Cottrell-Petch relationship but not as pronounced as in the case of the furnace-cooled materials. As pointed out in Chapter 4, as the carbide thickness t tends to zero the model reduces to the Cottrell-Petch condition for crack propagation. However, the model does predict that by reducing the grain boundary carbide thickness from a mean value of 2.5 microns to 0.3 microns the fracture stress has increased from 20 to 25 Kg/mm^2 (28,000 - 35,000 psi) for grain sizes smaller than $\ell^{-1/2} = 3$. This also means that reducing the carbide size would enable quench-aged material to have a larger grain diameter yet still preserve the same fracture strength.

As Figure 32 shows, the derived curve does not fit the experimental points as well as in the case where the large grain boundary carbides were present. This deviation may be the result of a lower effective surface energy acting in the quench-aged case since the notch bend results were obtained at a much lower temperature range than the furnace-cooled specimens. However, the effective surface energy does not have to be altered significantly (from 2×10^4 to 1.5×10^4 ergs/cm^2) before the derived curve fits the experimental points (Figure 32), except at the larger grain sizes. It does not seem unreasonable, however, to assume that the effective surface energy term will be decreasing with a decrease in temperature. Oates (1969) has shown

in mild steel that the fracture stress does show a slight temperature dependence and the effective surface energy increases with increasing temperature.

It was mentioned above that for the quench-aged materials at large grain sizes ($\ell^{-1/2} = 3.4$), the experimental fracture stress values did not seem to be consistent with those obtained at the smaller grain sizes. This deviation from the derived curve also appears to be larger than can be taken as experimental error. For the notch bend specimens at this particular grain size audible twinning was encountered during the early stages of deformation, some of which were accompanied by marked load relaxations. In these specimens the general yield condition was not as well defined as in the case for the smaller grain sized material and the general yield point was taken as that point where the load-deflection curve first deviated from linearity. However, the transition temperature obtained by using this method is not consistent with the other data. It is probable that some form of twin induced fracture process is operative under these conditions of low temperature and large grain sizes and the mechanism is outside the limitation of the simple model proposed in Chapter 4. A plausible explanation for the result might be that the stress concentration factor for twin and slip induced fracture are not equivalent. In this work it is assumed that fracture occurs at general yield where the stress concentration factor reaches its maximum value (2.18 Tresca). However, Figure 3 indicates that below general yield the stress concentration factor is less than the maximum value and thus if fracture is initiated when the plastic hinge below the notch has not traversed the net cross-section of the notch bar (general yield point) the operative stress concentration factor for the crack propagation will be less than the maximum value (Wilshaw and Pratt 1965). It is, however, difficult to obtain a value of the stress concentration factor prior to general yield

without a detailed knowledge of the extent of the plastic zone below the notch.

An alternative approach is to use Smith's (1966) model for twin induced fracture propagation from the grain boundary carbides (Equation 56). If the appropriate values are substituted into this equation the calculated value of the fracture stress is 33 Kg/mm^2 which is well below the value predicted from the slip induced fracture model. The low value is not all together unreasonable however, as Hull (1961) and Hahn et al.(1962) have shown that at low temperatures twin induced fracture occurs at a lower stress than slip induced fracture. Also the low value from Smith's model is not inconsistent with the idea that the stress concentration factor could be lower for twin induced fracture.

One of the factors which has been neglected in the notch bend tests is the difference in strain rate at the base of the notch compared to the strain rate in the uniaxial tensile tests. Following the procedure of Knott and Cottrell (1963), the effective gauge length at the notch root can be approximated to the root radius which for this work is 0. 01 in ; that of the tensile specimen was 1. 0 inches. Since the cross-head speed was constant at 0. 2 in/min the effective straining speed in the root of the notch is $\frac{1}{.01} \times .2 = 20$ in/min.

Since the yield stress of low carbon materials depends on the strain rate (Almond and Embury 1968, Knott and Cottrell 1963, Hahn et al. 1964, Oates 1969) the yield stress will increase with strain rate. Therefore, the material around the notch has its yield stress raised relative to that of a smooth specimen tested at the same nominal applied strain rate. This should mean that the yield stress used in calculating the fracture stress, that is, $\sigma_y \cdot R = \sigma_F$, should be higher than that used, which has the effect of increasing all the experimental values upwards. However, the effect of strain rate on the

cleavage fracture in mild steel (0.06%C) has been studied by Oates (1969) where he varied the cross head rate for notched specimens from 0.01 in/min to 8 in/min and reports that the fracture stress for the mild steel was relatively insensitive to strain rate. This has also been observed by Knott (1966) and Hendrickson (1958). Thus the strain rate effect is not large for notched bars of the usual notch bend specimens when deformed at nominal strain rates comparable with those used for testing tensile specimens. There is an effect of strain rate, however, when tests from notch impact tests are compared with uniaxial tests where the effect of the differences in imposed strain rates are important. This was the reason for not utilizing Almond et al.(1969) quoted fracture results from instrumented impact tests in comparing the furnace-cooled results in this work and with others.

One of the uncertainties in developing any model to explain the fracture behavior of a material is in obtaining an estimate of the effective surface energy. Since the object in developing any fracture model is to relate the fracture stress to basic material properties and microstructure, it is of importance to estimate the value of the effective surface energy required for crack propagation. Some previous workers (Hahn and Rosenfield 1966) have assumed a true surface energy value and calculated the fracture stress, others (Cottrell 1958, Knott 1966, Oates 1969) calculate a surface energy from experimental values of the fracture stress.

However, in light of the evidence that plastic deformation accompanies crack propagation (direct metallographic evidence by Tetelman and Robertson 1962) as well as the work of Stroh (1957) and Smith (1966) that cleavage crack growth in mild steel will only be more difficult than crack nucleation if the effective surface energy is increased sufficiently above the true surface value, it is very unlikely the effective surface energy would have the true surface value in this

work. Although, it is possible the effective surface energy would approach the true surface value at very low temperatures. Throughout this work Cottrell's value for the effective stress has been used which is about a order of magnitude above the true surface value for pure iron.

In the results of Chapter 5 it was observed that considerable plastic deformation occurred during both the initiation and propagation of the cleavage crack. The scanning electron microscopy study showed that there were regions of plastic deformation associated with the grain boundaries in furnace-cooled material which are indicative of a higher surface energy for crack propagation across the grain boundaries in the transition region. In the tensile test this same effect may be responsible for the high incidence of non-propagating grain size microcracks near the ductile-brittle transition temperature (Hahn et al 1959, McMahon and Cohen 1965, Lindley 1969). The quench-aged material did not have the extensive plastic zone associated with grain boundaries. This may result from the fact that for the quench-aged material no non-propagating microcracks were observed so that once conditions for fracture initiation are established the specimen fractures with little tearing at the boundaries.

However, the best fit to the quench-aged results was obtained by using an effective surface energy only slightly less than that used for the furnace-cooled results so it would appear that the effective surface energy involved in the initial process of propagating the crack from the carbide into the ferrite is unaffected by the dispersion of carbides in the quench-aged material. This does not necessarily mean that the total surface energy involved in crack propagation across the specimen is not dependent on carbide dispersion nor can it be assumed that the effective surface energy will be unaffected by all carbide dispersions.

The most conclusive test that plastic deformation is taking place when a crack propagates is by observing the asterism occurring on back reflection Laue photographs. The Laue micro-beam results in this work indicate that some plastic deformation is occurring when fracture is coincident with general yield. This is in agreement with the concept of yielding in the region below the notch as shown schematically in Figure 3 , and confirmed by etching techniques (Hahn and Rosenfield, 1965; Knott and Cottrell, 1963; Wilshaw 1966; Knott 1967). Knott (1966) obtained an effective surface energy value in mild steel using the Cottrell-Petch fracture relationship ($\sigma_F \propto l^{-1/2}$) by measuring the fracture stress as a function of grain size at a constant temperature using notch bars with notches of different angles. Thus by balancing the amount of hydrostatic tension below the notch against the grain size of the material, fracture occurred at the general yield point. By plotting fracture stresses against (grain size)$^{-1/2}$ Knott obtained a surface energy value of about 10^4 ergs/cm^2. Oates (1969) using Smith's model (1966) has also obtained a surface energy value for mild steel specimens using a notch bar with a 120^o notch angle. By measuring carbide thickness, grain size, and introducing the appropriate values for effective stress and friction stress, Oates quoted an effective surface energy of 1.38×10^4 ergs/cm^2 at -150^o when fracture occurred at general yield.

Another means of assessing the surface energy of low carbon steel is by simply treating the carbide as a pre-existing Griffith crack and ignoring the effect of the pile-up. The values obtained by this method for the Armco and NPL iron can be seen in Table 9 . The values obtained by this method are always lower than those obtained by using other methods (Low 1963) which are also summarized in Table 9 .

Thus the evidence from the microbeam X-ray method and

TABLE 9

Values of surface energy obtained by applying the Griffith's equation to the present results.

Material		Temperature	γ (ergs/cm^2)
Armco	f.c.	-100°C	4.3×10^3
	q.a.	-180	3.1×10^3
NPL	f.c.	- 80°C	4.6×10^3
	q.a.	-180	2.6×10^3

Value of surface energy determined by other methods (Low 1963)

Material	Temperature	γ ergs/cm^2	Method
Mild Steel	25°C	2×10^5	X-ray line broadening at fracture surface
.05% carbon steel	-196°C	1×10^5	Fracture stress grain size relationship for brittle fracture
Mild Steel and .04%C ferrite	-140°C to -20°C	2×10^4	Cottrell theory for crack nucleation and observed fracture stresses
Mild Steel and .04%C ferrite	-160°C to -60°C	2×10^5	Griffith-Orowan theory assuming crack size equal to grain size

the scanning electron microscope indicates that the effective surface energy in the present work should be considerably higher than the true surface energy of the material. The value used in the present studies is consistent with that obtained by Oates (1969) and Knott (1966) for similar materials.

The results of the present work indicate that the precipitation of carbides within the matrix is responsible for the increased yield strength, while the fracture resistance is determined by the size of the grain boundary carbides and their modification on quench ageing. Also, the results indicate that at very fine grain sizes, of the order of a few microns, the fracture stress will be determined predominantly by the thickness of the grain boundary carbides rather than the grain sizes. This may be of considerable practical significance in the technology of low alloy fine grain structural steels. In these materials simultaneous grain refinement and precipitation hardening are achieved by the use of niobium or vandium additions. The present work suggests that in order to exploit the potential of these materials in regard to the fracture resistance inherent in fine grained materials, simultaneous refinement of both grain size and boundary carbide size is necessary. One method of accomplishing this may be by the use of thermo-mechanical treatments of materials during the transformation from the austenite range and this may provide a useful area for future study.

CHAPTER 7

INTERGRANULAR FRACTURE IN LOW CARBON IRON

7.1 Introduction

As outlined in the literature review in chapter 2 the phenomenon of intergranular fracture in low carbon ferrite is well documented. Although a number of plausible explanations of the phenomenon have been advanced which involve the segregation of oxygen in the region of the grain boundaries, the detailed mechanisms of both fracture initiation and propagation remain obscure. In part this reflects the difficulty of providing experimental proof for local segregation to the grain boundaries. However in considering the phenomena of intergranular fracture it is necessary to delineate under what conditions intergranular fracture occurs in preference to plastic yielding. To this end a study was undertaken to investigate the influence of grain size and temperature on the yielding and fracture characteristics of two types of low carbon ferrite.

The objectives of the experimental program described in this chapter are four fold: to study the influence of decarburization onthe fracture behaviour of low carbon ferrite, to examine the temperature dependence of the tensile properties, to examine the influence of grain size on intergranular fracture, and to provide detailed metallographic evidence regarding the fracture topology.

7.2 Experimental Procedure

The material used in this investigation was Armco iron and NPL iron having compositions listed previously in Table 1 . Before the

specimens were fabricated to tensile specimens (Figure 5) the material was given the heat treatments listed in Table 10 to produce a range of grain sizes. After the annealing treatments, the tensile specimens were fabricated, then electropolished in Morris' (1949) solution to remove any surface irregularities. The specimens were then reheated to 720°C in a low pressure of air (50 torr) and held at temperature in order to decarburize the samples, and then quenched into ice water (0°C). Tensile tests were performed at -196°C and the fracture surfaces were examined using a Cambridge scanning electron microscope. All the tensile specimens were tested in an Instron testing machine with the cross head driven at a rate of 0.2 in/min.

Following testing, the specimens were sectioned for metallographic observations. Grain sizes were obtained by the linear intercept method (Lement et al.1954).

The carbon contents of the specimens after various decarburization times at 720°C were determined by the gas chromatograph method. In a few of the specimens, oxygen contents were measured by the vacuum fusion method. The analyses were obtained from the broken gauge length sections of the tensile specimens. Before each section was submitted for analysis, it was first mechanically polished on Emery paper, chemically polished in a solution of 80 percent hydrogen peroxide, 15 percent distilled water, and 5 percent hydrofluoric acid and washed in acetone. The carbon results were reproducible to within $\pm$ 0.0005%. The oxygen contents showed more scatter and were only reproducible to $\pm$ 0.002 %.

It was established that sufficient decarburization occurred to give 100% intergranular fracture at -196°C for specimens held for 1000 minutes at 720°C. A number of specimens of various grain sizes were treated in this manner and quenched into ice water (0°C). These were tested in uniaxial tension at a variety of temperatures to study

TABLE 10

The heat treatments used to obtain various grain sizes.

	grain size (mm)	
	Armco	NPL
swaged 75%, annealed 725°C for 24 hours, furnace-cooled	.040	.040
swaged 75%, annealed 925°C for 4 hours, furnace-cooled	.082	.097
swaged 75%, annealed 800°C for 1 hour, strained 10%, annealed 800°C for 1 hour, furnace-cooled	.241	.250

the grain size and temperature dependence of the tensile behaviour.

7.2.1 Micro Hardness Measurements

Measurements of the hardness of a grain boundary region and of the interior of its adjacent grains were obtained with a Reichert Micro-hardness tester designed for use on the Reichert Universal Microscope.

Each of the specimens tested was first mounted in Lucite, mechanically polished, finishing on a low speed rotating lap polisher with 0.3 micron diamond. The sample was then chemically polished to remove surface defects and damage due to mechanical polishing. Time for polishing was determined by noting micro hardness changes with time.

The hardness was taken at room temperature on ten randomly selected grain boundaries and ten adjacent grains in each specimen under a constant load of 5 grams for 5 secs. The relatively short loading time was chosen to minimize errors due to incidental vibration of the hardness instrument. Because carbides might interfere with the microhardness measurement, the microhardness tests were only made on decarburized material to detect if there is a correlation between grain boundary hardening and intergranular brittle fracture as suggested by Westbrook and Wood (1961).

7.3 Results

For clarity the results are reported in five sections.

7.3.1 Effect of the Time of Decarburization on the Tensile Properties at -196°C

Examples of the load-elongation curves of NPL and Armco iron tested in uniaxial tension at -196°C after quenching from 720°C after various holding times are shown in Figures 43 and 44 . Load drops were seen and load clicks were heard during the early stages of deformation; in the NPL iron up to about 200 minutes and, in the Armco

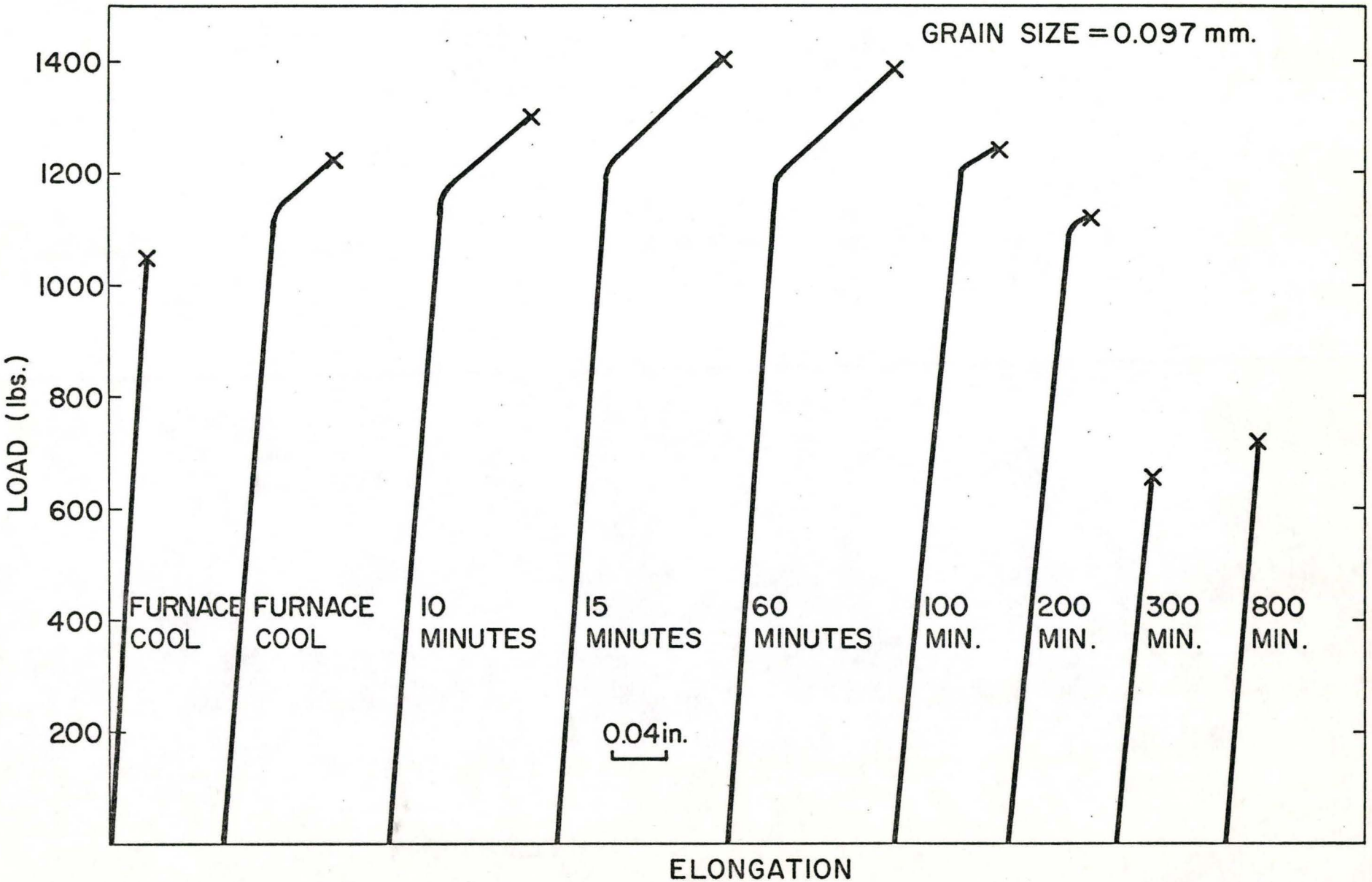

Figure 43: Typical load-elongation curves for quenched NPL iron after various holding times at 720°C.

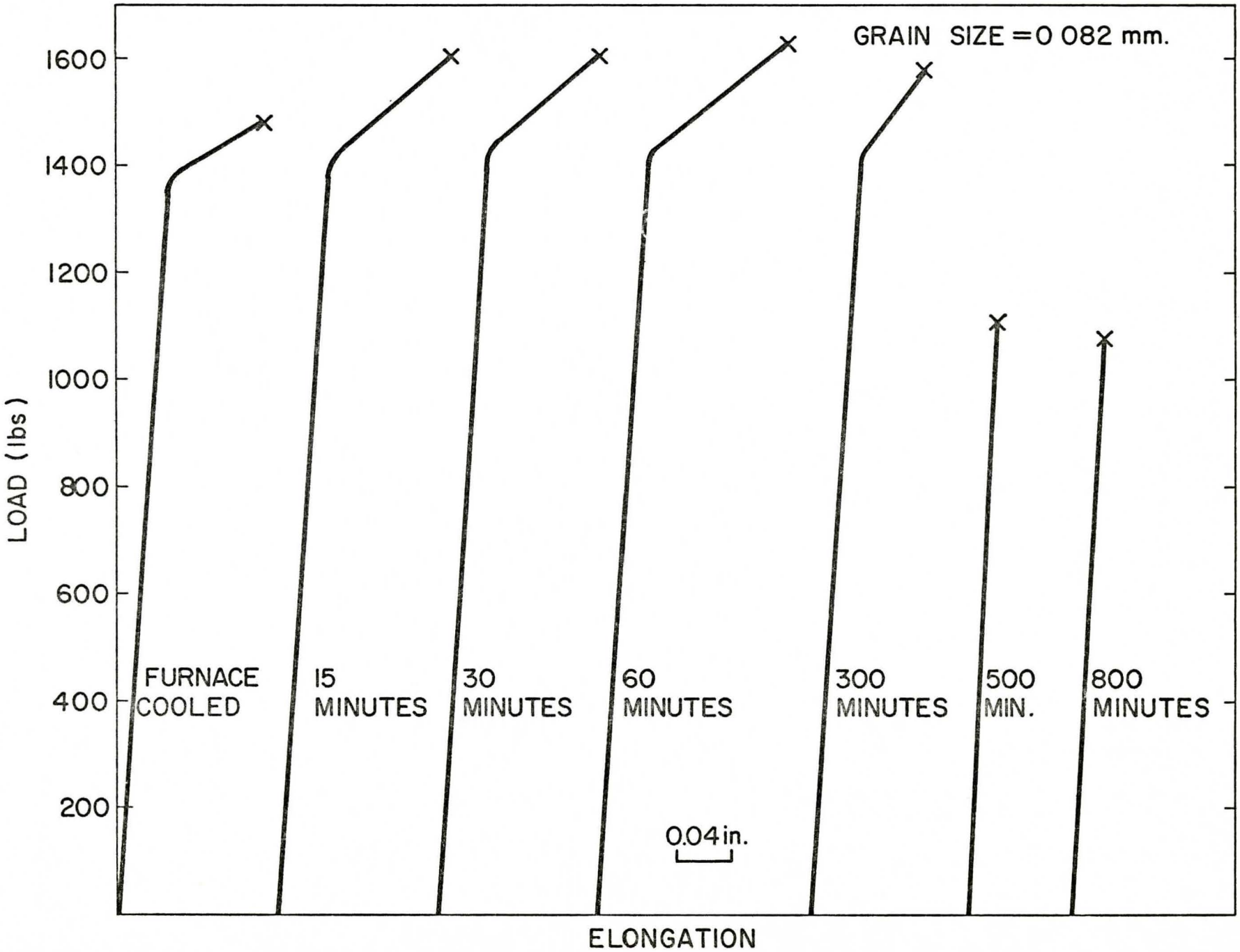

Figure 44: Typical load elongation curves for quenched Armco iron after various holding times at 720°C.

iron up to about 300 minutes indicating that extensive twinning occurs. No twinning was observed after these times, that is, below stresses of the order of 60, 000 psi for NPL and 80, 000 psi for Armco.

The tensile properties for NPL and Armco iron with holding time at 720°C are plotted in Figures 45 and 46. The fracture stress was calculated on the final cross-sectional area. The use of log holding time as an ordinate is for convenience only.

As seen by the load-elongation curves and the tensile properties versus holding time curves there is a sharp decrease in strength and ductility after about 100 minutes for NPL iron and after about 300 minutes for Armco iron. This change in properties is associated with a change in the mode of fracture from cleavage to intergranular.

Table 11 lists the carbon and oxygen contents corresponding to various holding times at 720°C. The analyses show that the carbon content is decreasing with increasing holding time and that when intergranular fracture occurs the carbon level is about 0. 003 wt. %. The oxygen content shows a tendency to increase with holding time at 720°C.

7.3.2 Metallographic Observations

The variation in the mode of fracture with holding time at 720°C can be followed very easily by using the scanning electron microscope. Figure 47 shows the fracture surfaces of NPL iron tested in tension at -196°C after various holding times. The individual pictures have been obtained at random, and no attempt was made to locate a certain section of the sample.

The first visible change in fracture mode can be seen to start around 200 minutes which corresponds closely with the first signs of a decrease in the tensile properties. At 300 minutes the fracture surface

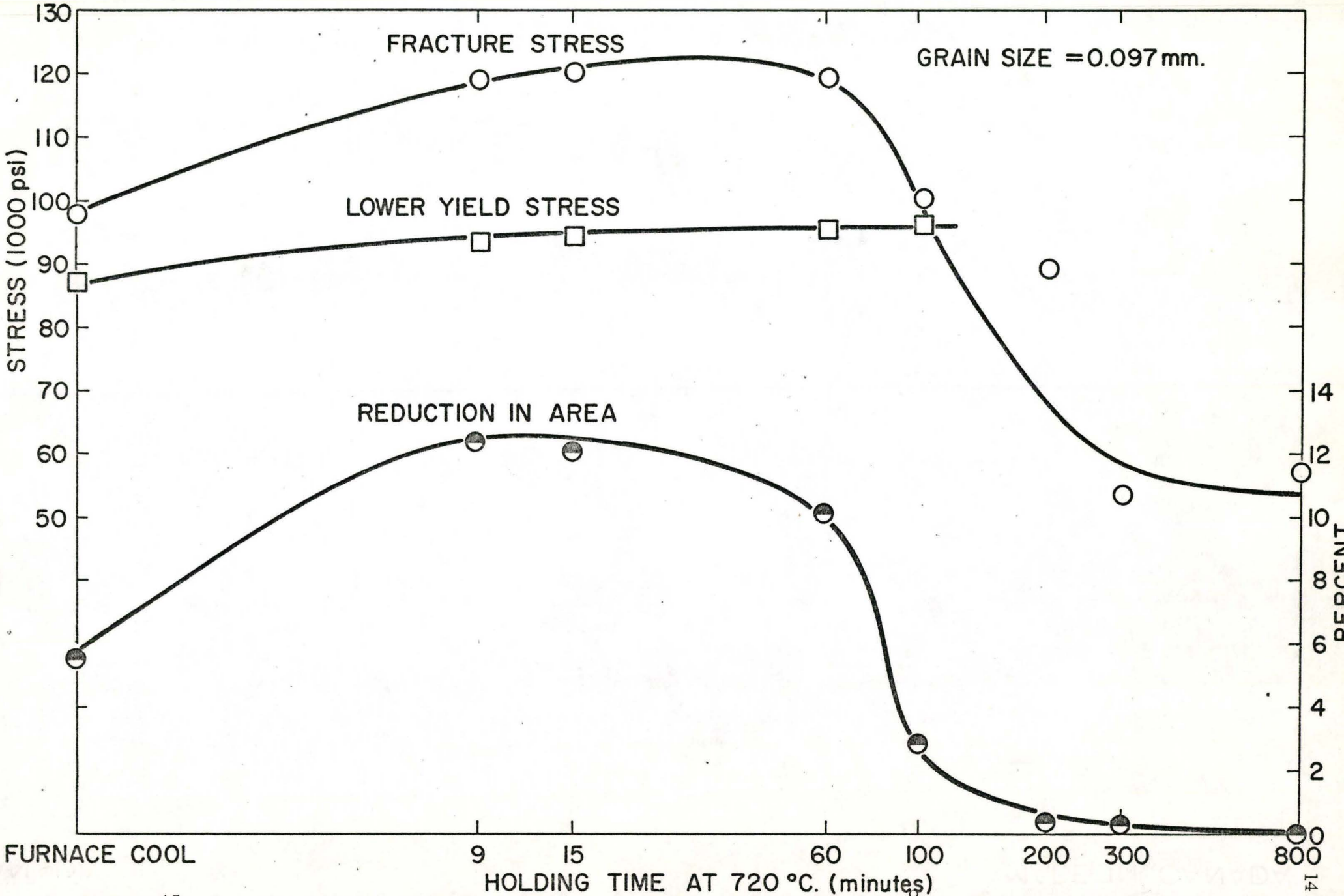

Figure 45: Tensile properties of NPL iron after various holding times at 720° C.

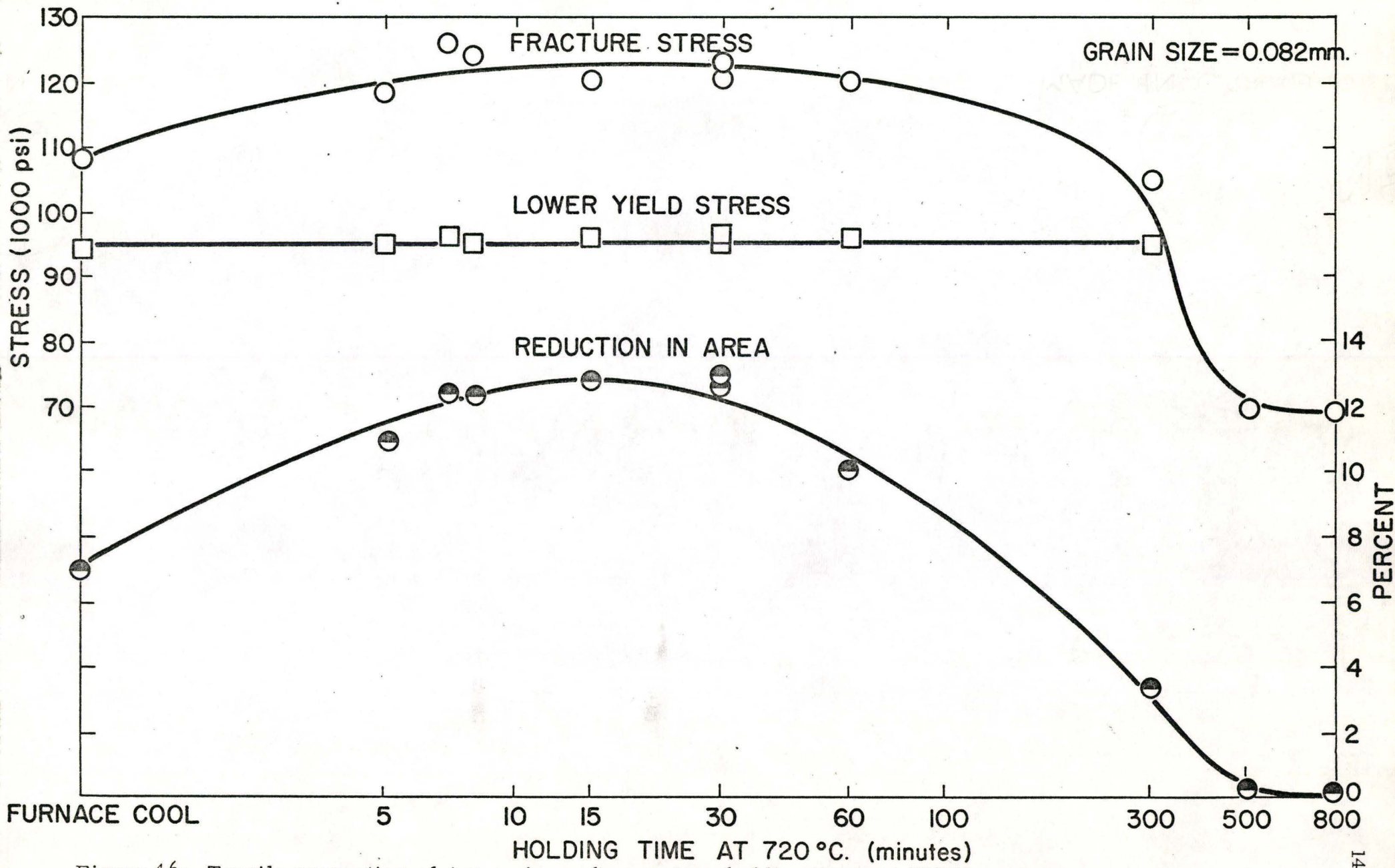

Figure 46: Tensile properties of Armco iron after various holding times at 720°C.

TABLE 11

Resultant contents (wt. %) of carbon and oxygen after various holding times (minutes) at 720°C.

NPL

Time at Holding Temperature	Carbon	Oxygen
furnace-cooled	.0180	.004
200	.0060	.005
800	.0030	.006

ARMCO

furnace-cooled	.0200	.099
300	.0040	.096
800	.0014	.093

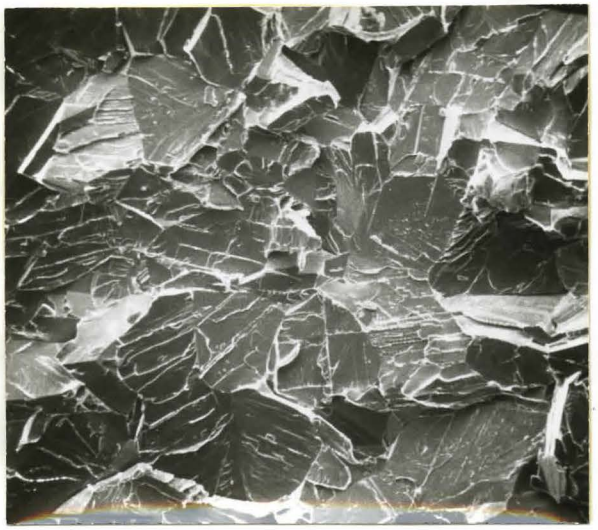

FURNACE COOLED

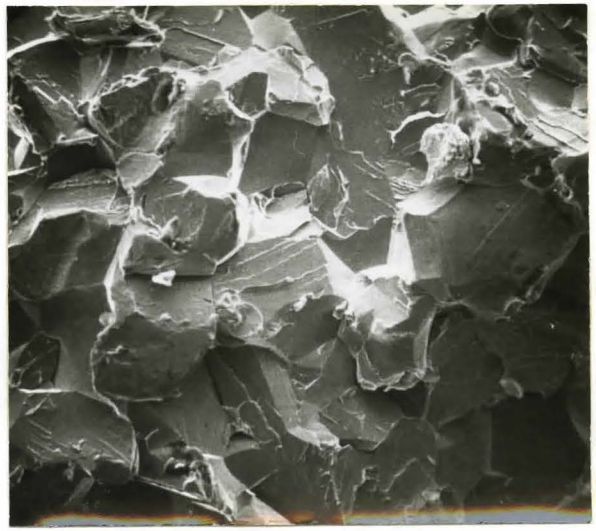

200 MINUTES

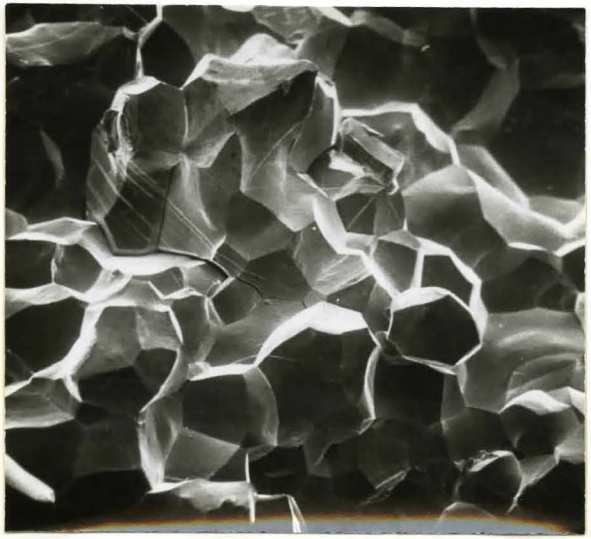

300 MINUTES

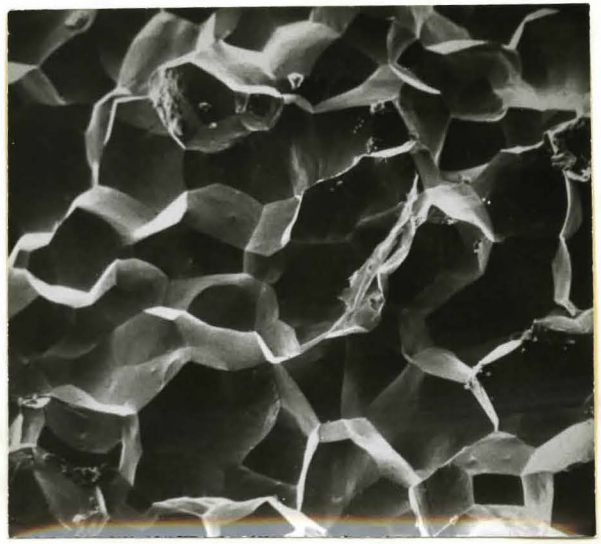

800 MINUTES

Figure 47: Comparison of fracture surfaces of NPL iron tested in tension at -196°C after various holding times at 720°C. X100

is composed of nearly 100 percent intergranular facets. Figure 48 is an optical micrograph of a nickel plated sample of NPL after 300 minutes showing where grain boundary decohesion has occurred in some boundaries adjacent to the surface. It was observed that many intergranular fracture facets showed regular parallel markings as seen in Figure 49 . In order to identify these markings a section was taken through the fracture surface and Figure 50 is a scanning electron micrograph simultaneously showing two perpendicular surfaces. The left part of the micrograph corresponds to the mechanically polished and etched section, while the right side shows the fracture surface. The parallel markings observed on the intergranular fracture surface correspond to twins intersecting the surface.

The density of twins (number of grains containing twins) was observed as a function of holding time and the results are plotted in Figure 51 . The sharp decrease in twin density coincides with the change in fracture mode observed in Figure 47 . Very little twinning was observed once the fracture mode became intergranular except for some twins in the region of the fracture surface (Figure 52).

The scanning electron micrographs obtained on Armco iron were similar to those found on NPL iron only the change in mode occurred at a later time.

7.3.3 The Effect of Temperature on the Tensile Properties of Decarburized Iron

Specimens of Armco iron were decarburized at a low atmospheric pressure of 50 torr. at 720°C for 1000 minutes. This had previously been determined to be a time for sufficient decarburization to occur at all grain sizes to give intergranular fracture at -196°C. Specimens of various grain sizes in the decarburized conditions were tested at temperatures between 22°C and -196°C. The fracture surfaces

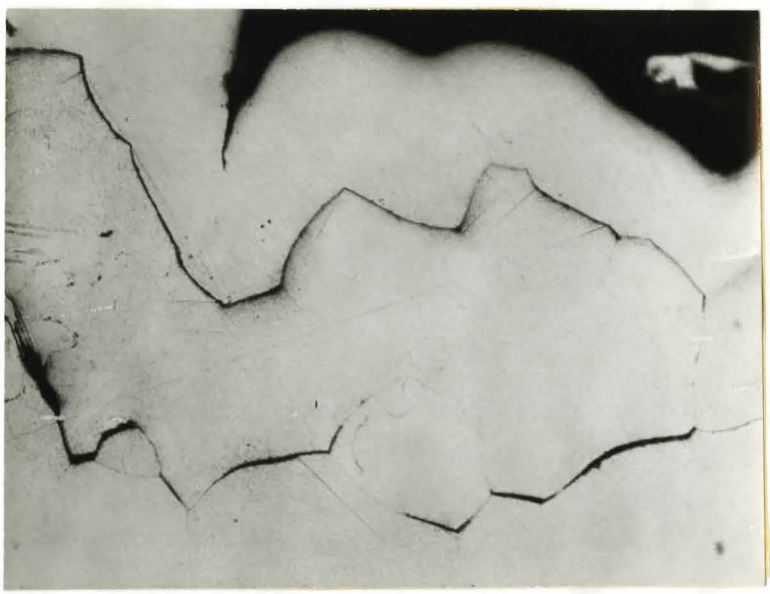

Figure 48 Optical micrograph of fracture surface of NPL iron after 300 minutes at 720°C. X400

Figure 49· Scanning Electron Micrograph of NPL iron after 300 mins. illustrating surface markings on fracture surface. X500

Figure 50 Scanning Electron Micrograph of NPL iron after 30 mins. showing correspondence of twins with markings on intergranular surface. X1000

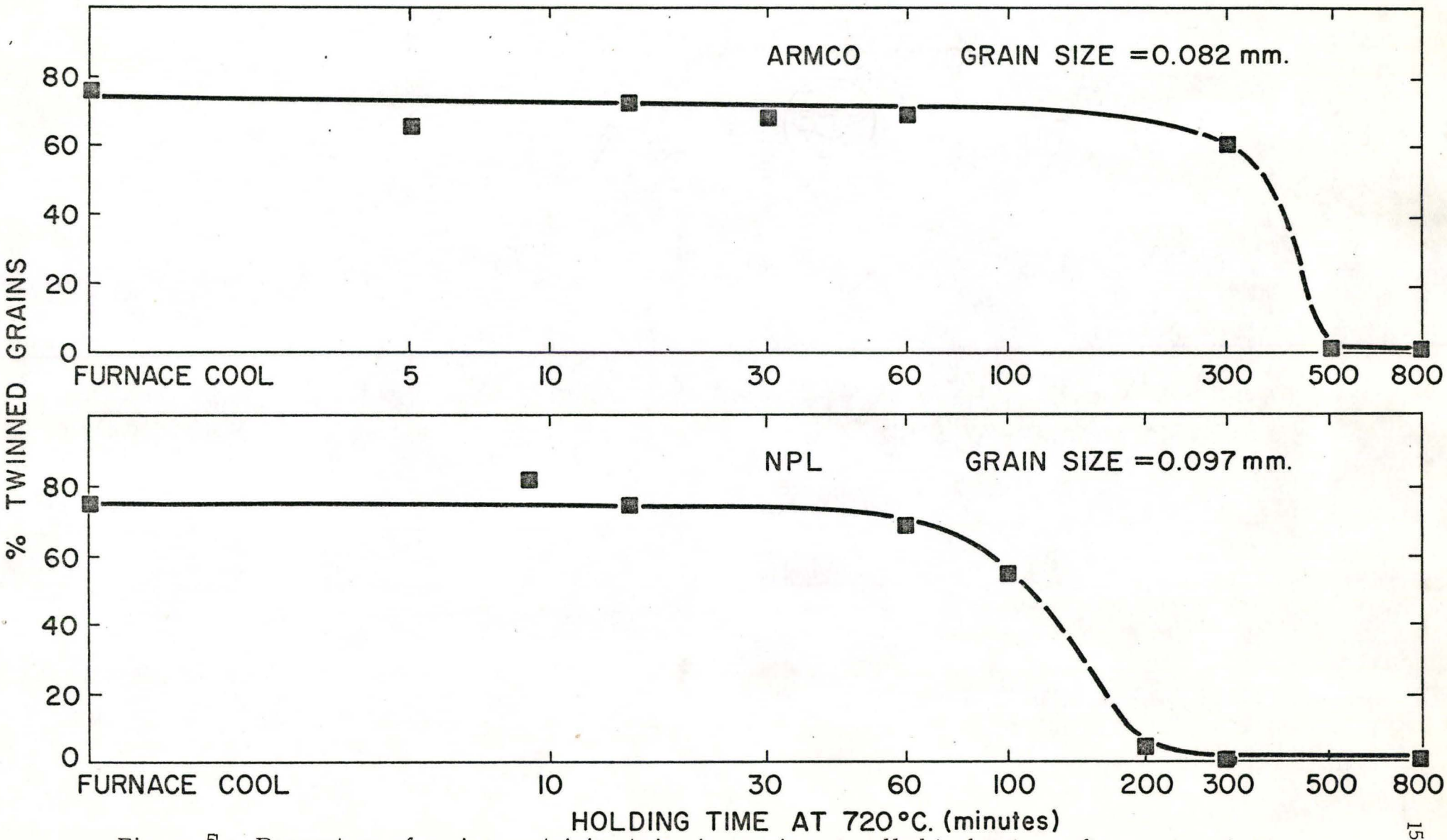

Figure 51 : Percentage of grains containing twins in specimens pulled to fracture after various holding times at 720°C.

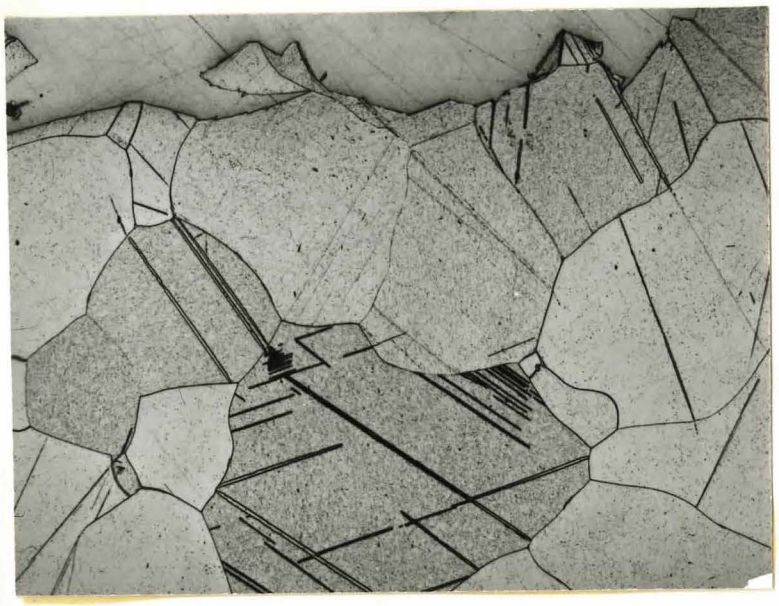

FURNACE COOLED

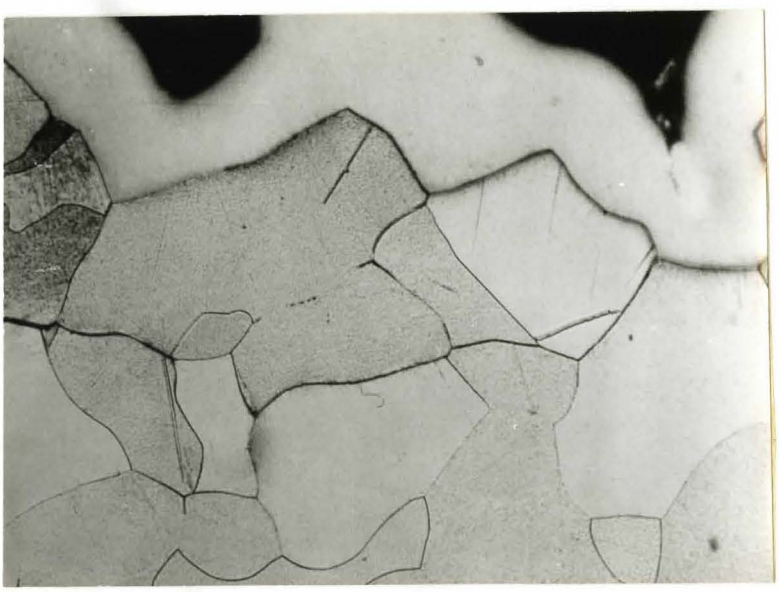

800 MINUTES

Figure 52: Optical micrographs showing extent of twinning in NPL iron furnace cooled and after 800 minutes at 720°C. X400

of the specimens were examined in the scanning electron microscope.

Figure 53 shows examples of typical load-elongation curves for decarburized specimens of average grain diameter 0.082 mm after tensile testing at various temperatures. The tensile properties of the decarburized material are shown as a function of temperature in Figure 54. For comparison, specimens of as received material of similar grain size tested over the same temperature range (see Figure 14) are also plotted on the figure. It can be seen that the temperature at which fracture occurs at the tensile yield stress is raised from -100°C to about -70°C and the critical fracture stress is decreased from 75, 000 psi (53 Kg/mm^2) to 40, 000 psi (28 Kg/mm^2).

Above -70°C the decarburized material yields prior to fracture, however for temperatures in the range -50°C to -70°C intergranular fracture occurs after some uniform elongation. Specimens tested at 22°C showed no evidence of intergranular failure and showed appreciable necking prior to fibrous fracture.

In order to try and establish the condition of the grain boundaries which led to the onset of intergranular fracture, some reheating experiments were performed. Specimens in the decarburized condition were reheated to temperatures between 720°C and 920°C under a pressure of 1×10^{-5} torr for 30 minutes and allowed to furnace cool (50 deg. C/hour). When tested at -196°C these specimens behaved identically to those quenched initially from 720°C and failed in an intergranular manner at stresses very close to that shown in Figure 53.

7.3.4 The Effect of Grain Size

For the NPL iron a range of grain sizes were obtained as outlined previously. Specimens of a range of grain sizes were decarburized and tested over a range of temperatures and the results compared with the behaviour of the as received NPL iron.

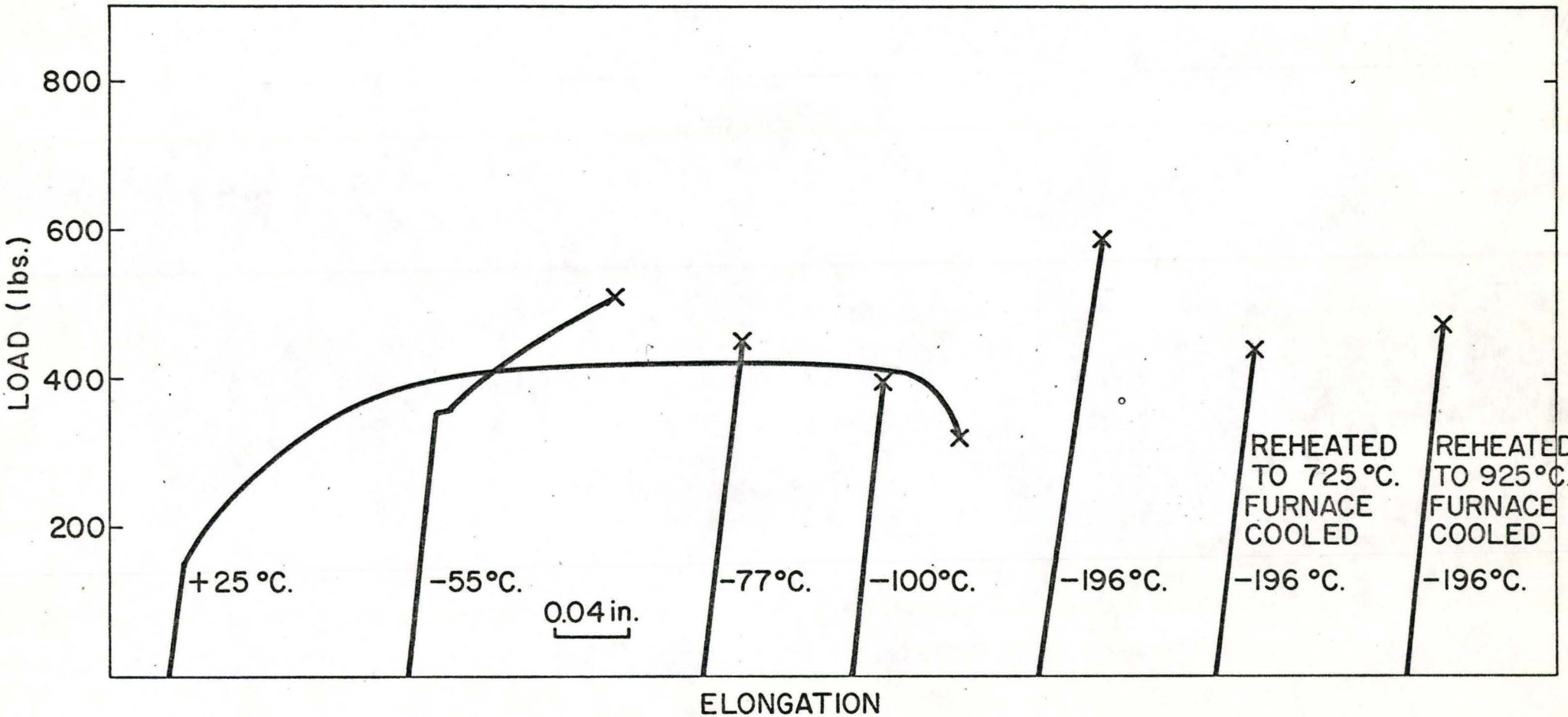

Figure 53: Typical load elongation curves for Armco iron decarburized at 720°C for 1000 minutes and tested at various temperatures.

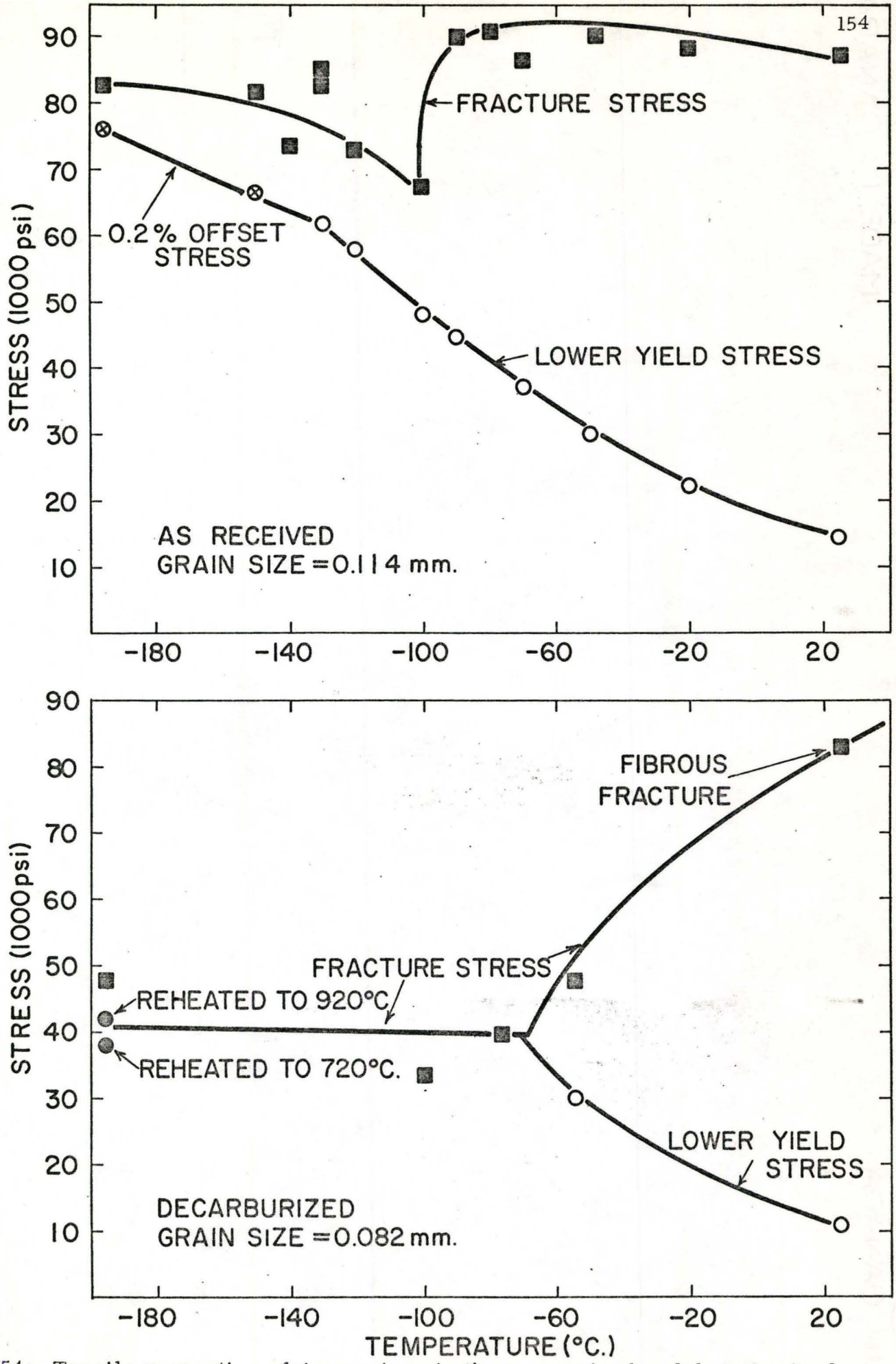

Figure 54: Tensile properties of Armco iron in the as received and decarburized condition at various temperatures.

On testing at 22°C both the decarburized and as received specimens showed yield points. When plotted according to the Hall-Petch relationship, that is stress as a function of (grain size)$^{-1/2}$, as in Figure 55 , values for the Hall-Petch slope, k_y, for both conditions is of the order of 2.2 Kg/mm$^{3/2}$.

Tensile tests of the as received NPL iron at -196°C indicate that at coarse grain sizes twinning occurred either prior to or simultaneously with transgranular fracture whereas in the fine grained material yielding occurred by slip. The results are plotted in Figure 55 and indicate that the Hall-Petch slope for twinning is of the order of 11 kg/mm$^{3/2}$. This is in good agreement with the values obtained by Hull (1961) and Hahn et al.(1962). The change in deformation mode from twinning to yield at a (grain diameter)$^{-1/2}$ of 4 is also in accord with previous results. In Figure 55 a line of slope 2.2 Kg/mm$^{3/2}$ has been drawn through the data for the fine grained material to clarify the discussion. It is recognized that the fine grained data is limited. However, it has been observed by a number of workers (Hull 1961, Hahn et al, 1962, Armstrong et al. 1962) that for yielding by slip the Hall-Petch slope is independent of testing temperature and it is this general observation which has been utilized to justify the form of the data provided in Figure 55.

On testing the decarburized material at -196°C neither lower yield point nor twinning were observed prior to intergranular failure. The data is plotted in Figure 56 and indicates that the fracture stress is a function of the inverse square root of the grain diameter with a slope of about 4.5 Kg/mm$^{3/2}$. The same slope is obtained for fracture stresses measured at -55°C as shown in Figure 56. However it should be noted that at -55°C for the fine grained material yielding and homogeneous deformation precede the onset of intergranular fracture. The results indicate that the slope of the fracture stress versus (grain diameter)$^{-1/2}$

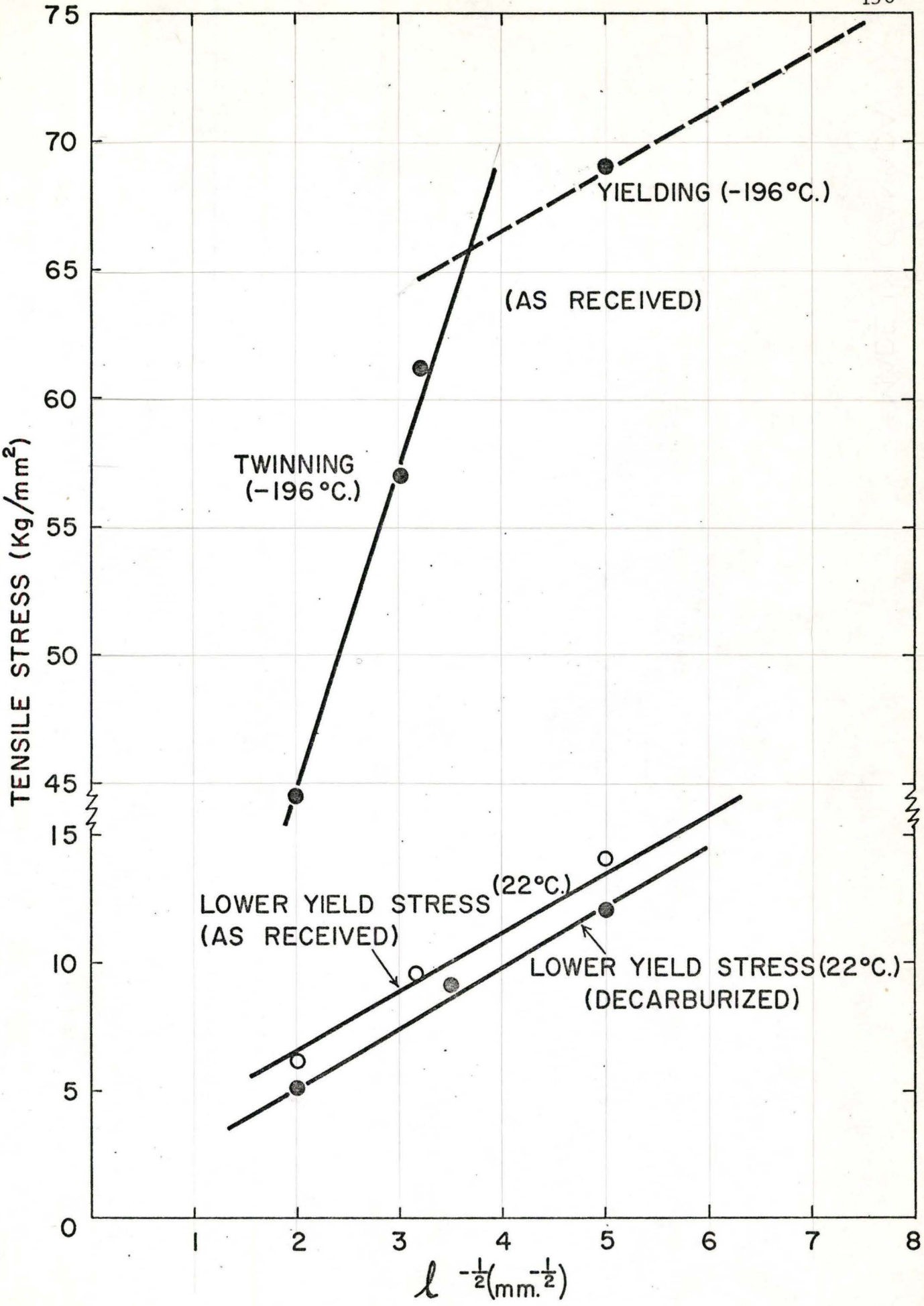

Figure 55: Grain size dependence of lower yield and twinning stress for NPL iron.

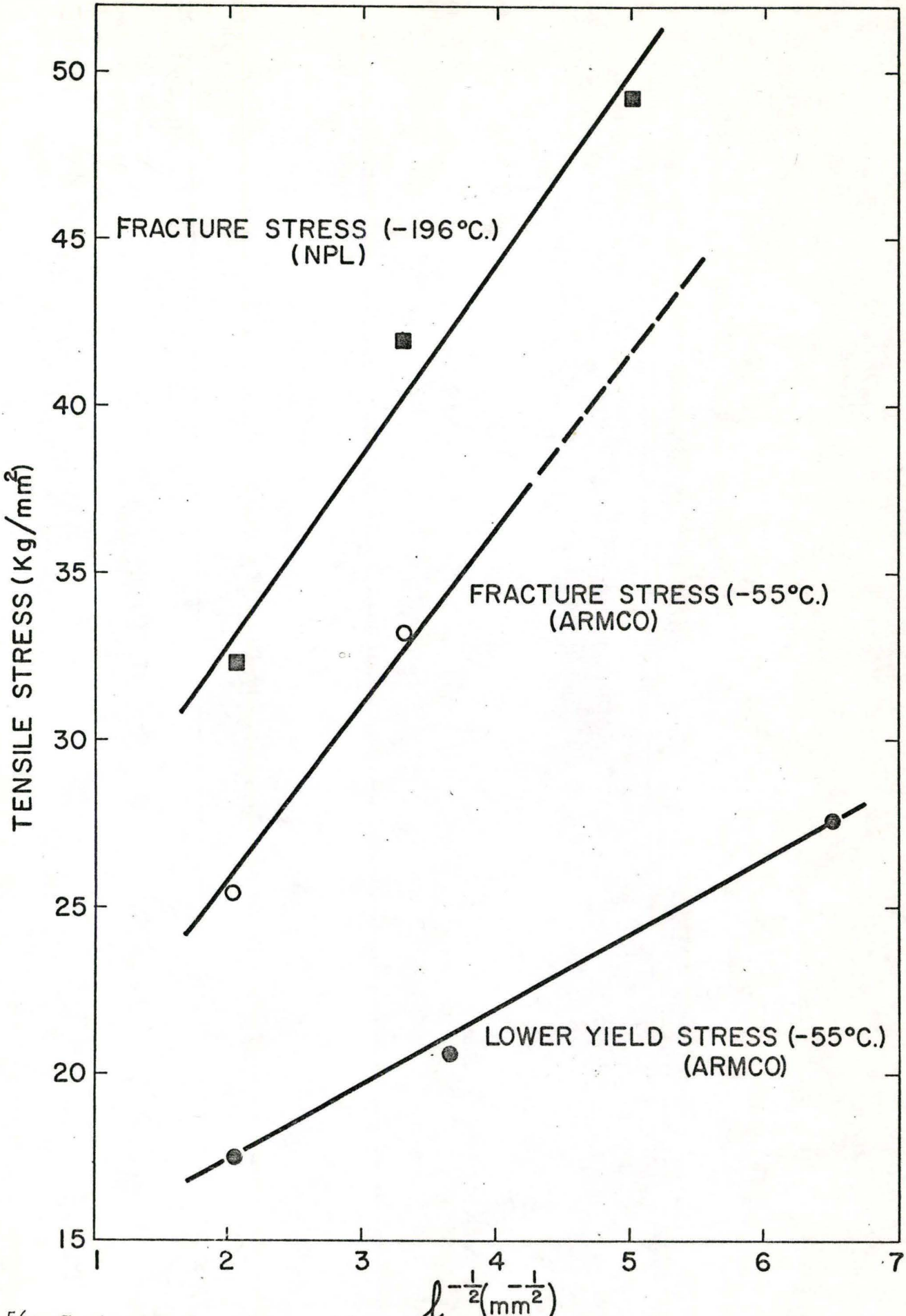

Figure 56: Grain size dependence of fracture and lower yield stress as a function of (grain size)$^{-1/2}$ for decarburized NPL and Armco iron.

plot is independent of temperature and that the intercept, that is the friction stress, is much less temperature dependent than that normally observed for the grain size dependence of the lower yield point.

7.3.5 Microhardness Tests

Microhardness measurements were made on an NPL iron sample which had been decarburized at a low atmospheric pressure of 50 torr at 720°C for 1000 minutes. The distribution of sizes of the hardness indentations were then analyzed using the "t" (Spiegel 1961) test to determine if there were significant differences between the hardness of the matrix and the grain boundary. The results from a typical test are presented in Table 12.

It is observed that the grain boundaries are detectably harder than the matrix, and analysis by the "t" test indicates that the probability that the mean values are different is greater than 99 percent. Therefore, the microhardness tests indicate that hardening at the grain boundaries occurs during the decarburization treatment suggesting a local variation in composition near the grain boundary region.

TABLE 12

Comparison of grains and grain boundary microhardness.

Diamond Pyramid Hardness

Grain Boundary	Grain
72.5	49.2
72.5	49.2
70.0	64.1
80.6	47.9
76.5	51.3
76.5	49.2
73.8	52.2
68.8	56.3
79.4	51.4
71.0	49.2
arithmetic mean 74.2	52.0
standard deviation 3.76	4.62

7.3.6 Summary of Results

The results indicate that severe grain boundary embrittlement occurs during decarburization of low carbon irons. The salient observations are:

1) for embrittlement to occur the overall carbon level must be reduced below 30 ppm. In the present investigation the oxygen levels showed considerable scatter but in all cases were in the range 70 to 990 ppm.

2) at low temperatures intergranular fracture precedes twinning or general yielding in tension and the fracture stress plotted as function of (grain diameter)$^{-1/2}$ has a slope of about 4.5 Kg/mm$^{3/2}$ which is independent of temperature.

3) for finer grain sizes at temperatures in the range -50°C to -77°C yielding and some uniform deformation precedes fracture. However at a critical stress intergranular fracture occurs regardless of whether this is attained prior to general plastic yielding or during the uniform work hardening process.

4) the fracture surfaces observed by scanning electron microscopy and optical microscopy are exceedingly smooth showing no obvious features except the traces of twins which are formed during crack propagation.

5) the increased hardness of the grain boundary region relative to its adjacent bulk material in decarburized iron suggests a local variation in composition in the region of the grain boundaries.

7.4 Discussion

The results describing the onset of intergranular fracture due to decarburization are in accord with previous workers in regard to the influence of composition. In all the cases investigated in this work when the carbon level was reduced below about 30 ppm intergranular failure occurred regardless of the oxygen level. This is in agreement with the data reported by Honda and Taga (1968) in which it was found that embrittlement occurred for carbon levels less than 21 ppm and for all oxygen levels, because oxygen was considered to be in excess of its solubility limit (Hume-Rothery 1968). As in previous work the present investigation gave no direct evidence for the segregation of oxygen to the grain boundary region except for the indirect evidence from the increase in microhardness in the grain boundary region and from the reheating experiments performed on decarburized specimens. The increase in microhardness in the grain boundary region is in agreement with the observations of Westbrook and Wood (1961) who showed that there is a correlation between grain boundary hardening and intergranular brittle fracture. In the reheating experiments on decarburized material it was observed that furnace cooling the specimens from 720°C or 920°C did not alter the fracture stress and they behaved identical to those quenched initially from 720°C. This at first appears to contradict the work of Richards et al,(1968) until the compositions of the two materials are compared. Richards et al,(1968) carbon level was near the critical level and furnace cooling would allow sufficient carbon to segregate to the boundary to restore cohesion. Whereas in this work the carbon level was below the critical level and thus there would not be sufficient carbon available to restore cohesion. Even when the specimens are recrystallized at 920°C and furnace-cooled, conditions must be such that sufficient time is available for segregation but because of the low available carbon level the new

boundaries are just as weak. It is generally believed that oxygen will lead to a reduction of surface energy and grain boundary energy although, the only direct evidence for this reduction is the work of Hondros(1968) on delta ferrite at high temperatures.

The smooth topology of the fracture surfaces observed in intergranular fracture by scanning electron microscopy indicate that much less plastic deformation occurs in conjunction with intergranular failure than with the cleavage failures discussed previously. The development of a sectioning technique to examine two faces simultaneously in the scanning electron microscope showed conclusively that the regular striations observed on the fracture facets are due to twins. However, since no twinning bursts were heard, or any load drops seen during the early stages of deformation, it is believed that these twins were produced during fracture propagation rather than as a pre-requisite to fracture. This view is in keeping with the observations of Richards et al.(1968). It is further substantiated by the distribution of twins along the fracture path as shown in Figure 48 , and by the fact that in general no twins were observed on sections remote from the fracture surface.

Let us now consider the effects of temperature and grain size on decarburized iron. The important observation is that for the decarburized material a complete range of behaviour from ductile to intergranular brittle behavior may be observed as the testing temperature is varied. Further, the critical stress for the onset of intergranular fracture can be attained either prior to general deformation in tension or by work hardening the material up to the required critical stress as shown in Figure 56. The observation that the critical stress for fracture is grain size dependent (Figure 56) gives an important indication regarding the mechanism of fracture initiation. It clearly indicates that some form of stress concentration at the grain boundary is necessary for the initia-

tion and propagation of intergranular fracture. The process of intergranular failure occurs at temperatures where no twinning is observed either prior to or in conjunction with the fracture process. Thus it can be concluded that twinning or the impingement of twins on the grain boundary is not the critical event leading to the initiation of intergranular failure.

The most likely method of attaining the stress concentration necessary for intergranular fracture is that arising from inhomogeneous yielding events such as the impingement of a slip band on the grain boundary. Such events can occur either in the pre-yield microstrain region or during the uniform deformation period since both the flow stress after plastic prestrain and the initial yield stress are grain size dependent.

From the data presented in Figure 56 it can be seen that the grain size dependence of the intergranular fracture stress is greater than that for the lower yield stress. However, under some conditions of temperature and grain size, intergranular failure may occur prior to reaching the general yield condition. Thus the situation is analogous to that occurring for twinning in the undecarburized material. This suggests that depending on the temperature, grain size, and the condition of the grain boundaries, a range of events can take place when a slip band is held up at a boundary. In order to rationalize this, consider the situation of an idealized pile-up at a grain boundary shown in Figure 57. As shown by Zener (1948) the pile-up of n dislocations may be treated as a shear crack and the stress concentration τ' at the tip can be expressed as

$$\tau' = n\,\tau \tag{57}$$

where τ is the applied shear stress. The concentrated shear stress at some point r from the end of the pile-up is given by

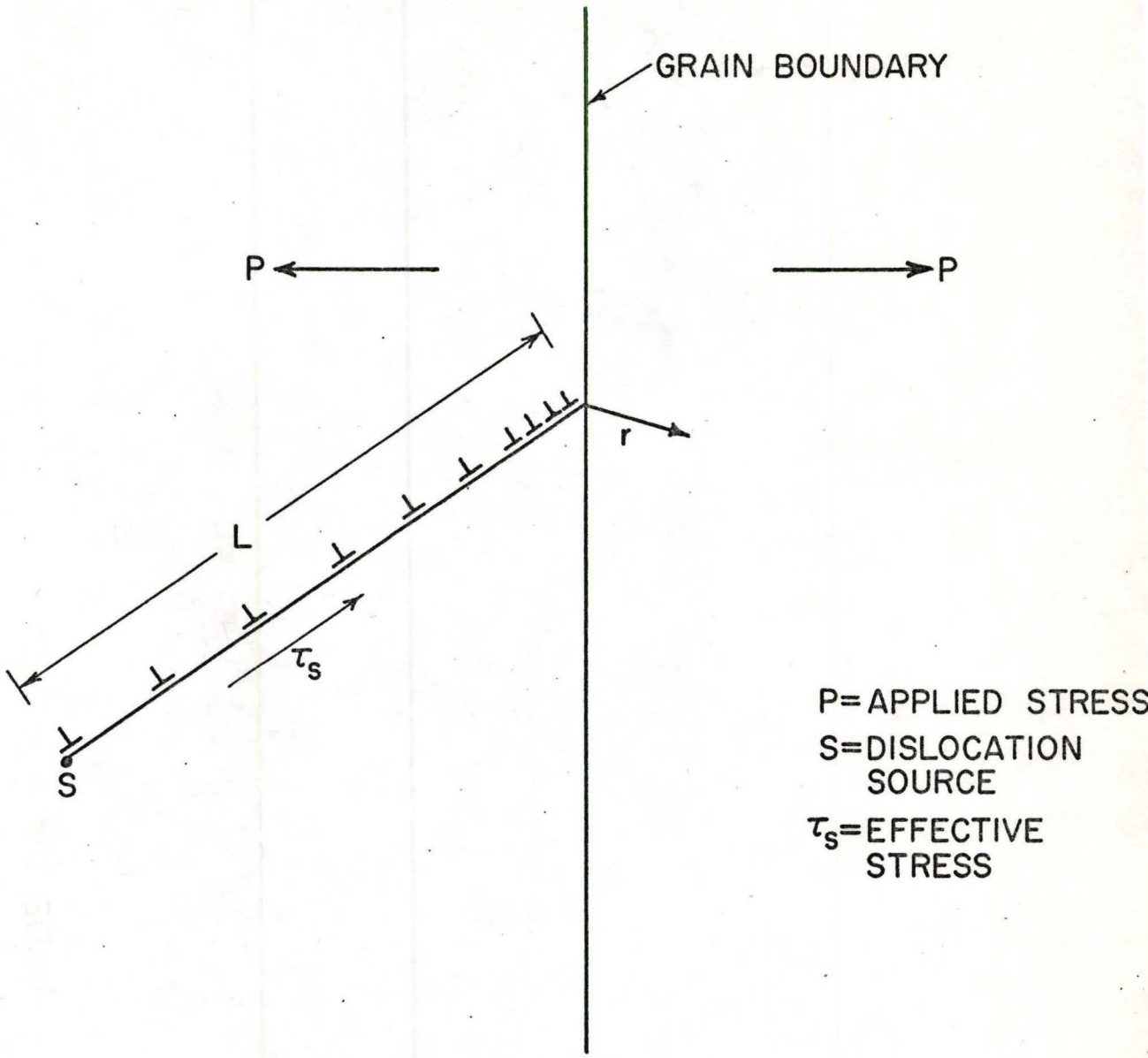

Figure 57: Schematic representation of a pile-up of dislocations at a grain boundary.

$$(\tau - \tau_i)\left(\frac{L}{r}\right)^{1/2} = \tau_s \left(\frac{L}{r}\right)^{1/2} \tag{58}$$

where τ_i is the friction stress which opposes dislocation motion and L is the length of the dislocation pile-up. Now this concentrated shear stress can trigger three possible events: yielding, twinning or fracture.

In the first case, yielding will occur in the grain adjacent to the pile up when the concentrated shear stress attains a critical value τ_{crit} to activate a dislocation source situated at a point r. Thus the criterion for yield propagation is

$$(\tau - \tau_i)\left(\frac{L}{r}\right)^{1/2} = \tau_{crit} \tag{59}$$

or when $\tau = \tau_y$ for yielding

$$\tau = \tau_y = \tau_i + \tau_{crit}(r)^{1/2} L^{-1/2} \tag{60}$$

If the slip band is assumed to make an angle of 45^o with the tensile axis the equation can be written

$$\sigma_y = \sigma_i + k_y \ell^{-1/2} \tag{61}$$

where $k_y = 2\tau_{crit}(r)^{1/2}\ell^{-1/2}$ and L is equated with the average grain size ℓ. This is known as the Hall-Petch equation for yielding.

On a simple physical picture this equation means that deformation spreads by a slip band in one grain operating a dislocation source in the next grain at a distance r ahead of the pile-up, where k_y is a measure of the difficulty in activating the dislocation source in the adjacent grain. However, once the dislocation source has been activated and a slip band starts to propagate across the grain, dislocation interactions result

due to the dislocation motion and multiplication, and the propagation of the slip band is resisted due to the internal stresses present in the second grain and the friction stress of the lattice. Thus, as the internal stress increases with increasing amounts of plastic strain, an increase in applied stress is required for further dislocation motion and multiplication. This increase in stress is reflected in a modification of τ_i due to the build up of dislocations. For small strains k_y is not affected. Therefore, yielding is likely to occur under conditions where dislocation sources are weakly pinned, and at higher temperatures where more slip systems can be activated and the friction stress due to the lattice is less.

In the case of twinning, a much higher critical stress is required to form the nucleus of a mechanical twin (Bell and Cahn 1957) but its subsequent propagation can be made under a much smaller stress, that is, the effective value of the friction stress opposing the movement of a twin dislocation will be smaller than the friction stress for a slip dislocation (Worthington and Smith 1966). Since its nucleation requires a much higher critical stress this would be reflected in a higher k value in the Hall-Petch relation. This has been observed by Hull (1961), Worthington and Smith (1966), and Hahn et al.(1962) where k for twinning is greater than k for yielding by about a factor of 5.

The nucleation of a twin can be compared with the difficulty in developing a stacking fault. Friedel (1964) suggests that the stress necessary to develop a fault is given by

$$\tau \sim \frac{f}{b} \tag{62}$$

where f is the stacking fault energy and b is the Burgers vector. Introducing the appropriate values for f and b from Friedel gives a local stress approaching the order of G/10 to nucleate a twin, where G

is the shear modulus of the material. Since such high stresses are required to nucleate twins, it would be expected that twin formation would be more prevalent in larger grain size material, since the effective pile-up length is longer, and at lower temperatures, where τ_i for yield is greater. Hull, Hahn et al, and Worthington and Smith concluded that as the temperature decreased slip bands in the preyield region caused twins to form, instead of the stress concentration being relieved by slip in the adjacent grain. The lower friction stress opposing the motion of twin traversing the grain has been attributed to the fact that twinning dislocations have smaller burgers vectors (hence a smaller Peierls-Nabarro force) than normal dislocations (Friedel 1964). For large grain sizes at low temperatures the local stress concentration due to micro-yield are sufficient to form a twin burst which subsequently leads to fracture initiation.

The case of intergranular fracture appears to be similar to the case for twinning, only in this case the cohesive strength of the boundary is much lower. At the higher temperatures and smaller grain sizes it was observed that yielding occurred in preference to intergranular fracture. As the temperature was lowered a condition at the grain boundary was reached where intergranular fracture could occur prior to general yield in tension or after some work hardening depending on the grain size. For the case where failure occurs prior to general yield, dislocation pile-ups will occur in the micro-yield region and provided no plastic relaxation occurs, the concentrated shear stress at the tip of the pile-up can be equated to the cohesive stress of the material by

$$(\tau - \tau_i)\left(\frac{L}{r}\right)^{1/2} = \left(\frac{E\gamma_s}{a}\right)^{1/2} \qquad (63)$$

where E is Young's modulus, γ_s is the true surface energy and a is the

interplanar spacing If the condition is fulfilled so that crack nucleation occurs when the applied shear stress τ equals the critical shear stress for fracture τ_F, then

$$\tau_F = \tau_i + \left(\frac{E\gamma_s r}{a}\right)^{1/2} L^{-1/2} \qquad (64)$$

Since E is approximately equal to 2G and if r is equated to a, the stress necessary for crack nucleation becomes

$$\tau_F = \tau_i + \left(2G\gamma_s\right)^{1/2} L^{-1/2} \qquad (65)$$

If $(2G\gamma_s)^{1/2}$ is now equated with the slope of the grain size dependency of the intergranular fracture stress, it is possible to obtain a value of γ_s equal about 3000 ergs/cm^2, a value very close to the true surface energy for pure iron (Price et al.1964). Since it is observed that the fracture spreads with very little plastic deformation, it would be expected that once the conditions for crack nucleation are satisfied catastrophic failure would result. Since Hondros (1968) has shown evidence for oxygen segregating to grain boundaries of delta ferrite and lowering the surface energy, it could be assumed that oxygen would have an equally deleterious effect on alpha iron.

At the higher temperatures where some deformation precedes intergranular fracture, the condition is analogous to the build up of internal stresses due to dislocation interactions. Once the internal stress builds up to a certain magnitude it becomes energetically more favorable for the material to fracture at the grain boundaries. That is, the stress necessary to nucleate a slip event at the boundary and propagate it into the adjacent grain now exceeds the stress to cause decohesion of the boundaries. Further, since the effective surface energy at the boundaries is less than that required for transgranular fracture the

fracture path will be confined to the boundary region.

For the very fine grain sizes or at higher temperatures (22°C) the decarburized material failed by a fibrous manner. This can be explained by the fact that the degree of work hardening resulting from the strain to plastic instability is not sufficient to result in a high enough stress concentration at the grain boundary to cause decohesion.

It may also mean that the events for high stress-low strain (large grain size) and low stress-high strain (small grain size) conditions are not equivalent (Worthington 1969). This is analogous to twinning where at low temperatures and large grain sizes, fracture can occur as a consequence of twinning whereas at fine grain sizes where twins are formed before fracture the condition for crack growth is not satisfied until the applied stress is raised to a sufficient level so that a crack nucleated by a twin will grow.

In conclusion, indirect evidence is available for the segregation of oxygen to grain boundaries and that the segregated oxygen results in a lowering of the effective surface energy of the boundary. Under the proper conditions of temperature, grain size and condition of the boundary region, micro-slip can result in local stress concentrations of sufficient magnitude to either propagate slip in the adjacent grain or result in failure along the boundary regions with little observable plastic deformation. The proposed model clearly delineates the range of events which can occur at the grain boundary, and does not require a large effect of solute segregation on the true surface energy. It merely requires the surface energy to be reduced so that decohesion can occur at the head of a pile-up and propagation can occur with little concomitant plastic deformation.

Summary

In the discussion in the previous sections the effect of second phase particles on the cleavage fracture resistance of low carbon steels was very important and the results indicated that refinement of grain boundary carbides would enhance the fracture behavior of the material. On the other hand however, the discussion on the decarburized iron indicates that complete removal of carbon from the boundary has a deleterious effect on the fracture behavior. Figure 58 summarizes the effect of reducing the carbon level in the furnace-cooled material to the fully decarburized material. These results indicate that initially it is advantageous to remove the carbon as far as the fracture resistance is concerned. However, further reduction of the level of carbon at the grain boundary is very deleterious due to the onset of intergranular fracture.

Conclusions

The important feature of the results is that in low carbon steels the critical fracture stress is dependent on the size of the grain boundary carbide and that refinement of the size of the grain boundary carbide by quench ageing can result in a considerable improvement in the fracture resistance of the material.

The simple energy criterion is proposed to account for the influence of both grain size and grain boundary carbide size on the fracture stress which is consistent with the experimental results obtained under conditions where fracture is coincident with general yield.

The scanning electron microscopy and micro-focus X-ray studies of the fracture surfaces indicates that considerable plastic deformation occurs during both the initiation and propagation of cracks in the furnace-cooled and quench-aged materials. Further, the dispersed carbides do not seem to affect the effective surface energy

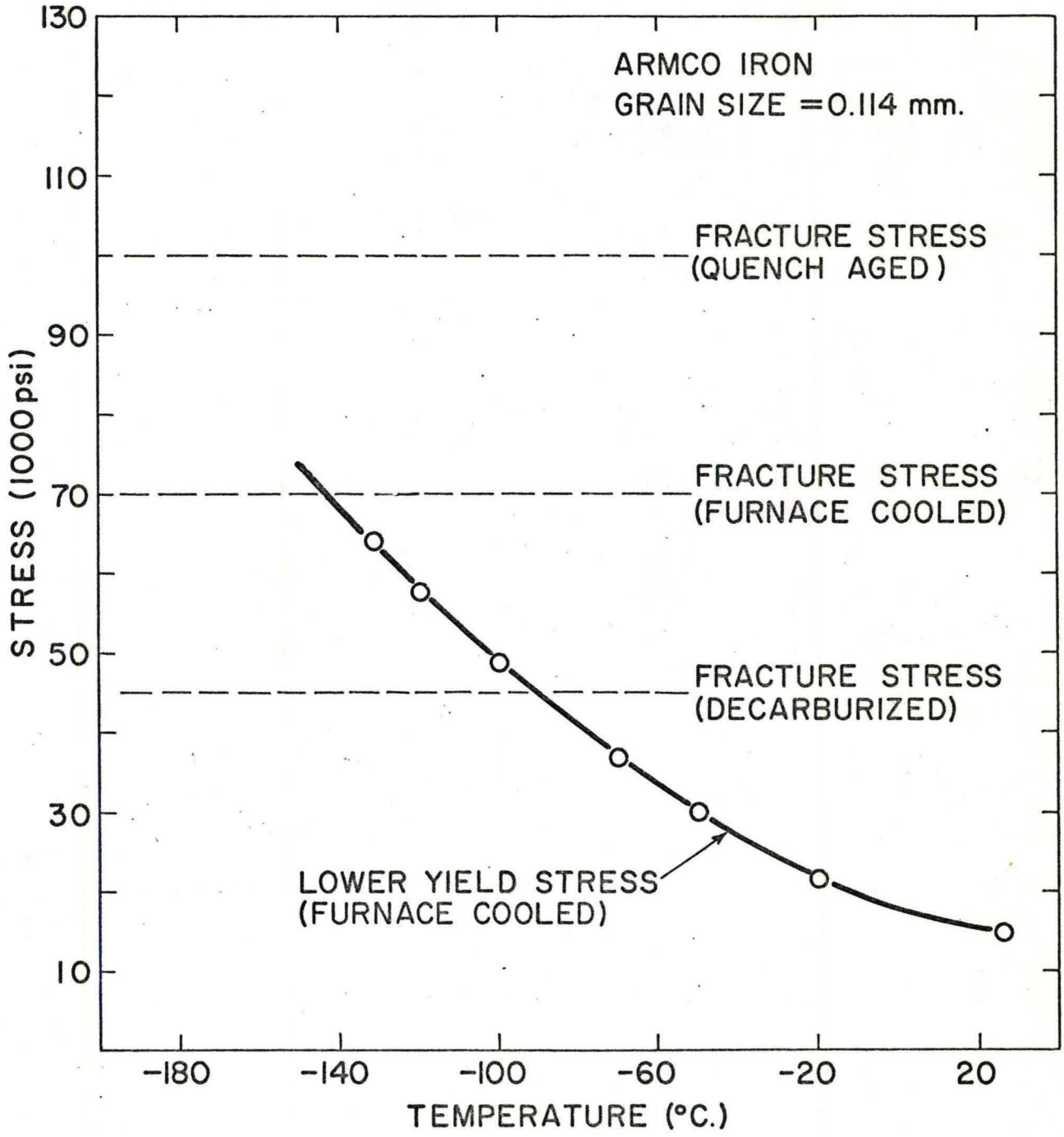

Figure 58: Effect of reducing the carbon level at the grain boundaries on the fracture stress in Armco iron.

involved in the initial process of propagating a cleavage crack.

Reducing the carbon level at the grain boundary below a critical level has a deleterious effect on the resistance of low carbon steels due to the onset of intergranular fracture. From a study of the temperature and grain size dependence of the intergranular fracture stress the incidence of grain boundary fracture relative to the competitive processes of yielding and twinning can be rationalized in terms of the initial event occurring at the head of a slip band impinging on a grain boundary.

Proposals for Future Work

The experimental results obtained in this work indicate that more information is necessary to delineate the effect of twinning on quench-aged low carbon steels particularly with regard to the larger grain sizes. A simple modification of the model for the difference in effective stress does not appear plausible and it may be necessary to re-examine the model to modify the simple relations derived in Chapter 4.

More data on fine grained furnace-cooled materials would be welcomed as this not only increases yield strength but toughness as well, provided there is refinement of the carbides. Some work is already progressing in this manner with the introduction of thermo-mechanical treatments to structural steels. Isoforming has been one such thermo-mechanical treatment which has shown much promise in obtaining good yield and excellent impact results, and can be readily incorporated into existing deformation cycles.

Another area of particular interest is in the competitive processes of yielding, twinning, and fracture. Not only could further work be performed on low carbon irons but extension to other materials such as intermetallics would also be fruitful.

BIBLIOGRAPHY

Allen, N.P., Rees, W.P., Hopkins, B.E., and Tipler, H.R., 1953, J.I.S.I., 174, 108.

Almond, E.A. and Embury, J.D., 1968, Met. Sci. Jour., 2, 194.

Almond, E.A., Timbres, D.H., and Embury J.D., 1969, Can. Met. Quart., 8, 51.

Armstrong, R.W., Codd, I., Douthwaite, R.M. and Petch, N.J., 1962, Phil. Mag. 7, 45.

Armstrong, R.W., 1968, Dislocation Dynamics, McGraw-Hill.

Ashby, M.F., 1967, Harvard Report, Cambridge, Mass.

Barrett, C. and Massalski, T.B., 1966, Structure of Metals, McGraw-Hill.

Bell, R.L. and Cahn, R.W., 1957, Proc. Roy. Soc. 239, 494.

Biggs, W.D., 1960, The Brittle Fracture of Steel, McDonald and Evans, London.

Bruckner, W.H., 1950, Weld. J. Res. Sup., 29, 476S.

Bullen, F.P., and Wain, H.L., 1965, Proc. of the First Int. Conf. on Fracture, The Japanese Society for the Strength and Fracture of Metals, Sendai, Japan.

Cahn, R.W., 1955, J. Inst. Met., 83, 493.

Chou, Y.T., Garafalo, F. and Whitmore, R.W., 1960, Acta Met., 8, 480.

Conrad, H., 1963, Iron and Its Dilute Solid Solutions, Wiley, 315.

Cottrell, A.H., and Bilby, B.A., 1951, Phil. Mag., 42, 573.

Cottrell, A.H., 1953, Dislocations and Plastic Flow in Crystals, 105.

Cottrell, A.H., 1958, Trans. A.I.M.E., 192, 1958.

Cottrell, A.H., 1963, The Relation Between the Structure and Mechanical Properties of Metals, H.M.S.O., London 2, 455.

Cullity, B.D., 1956, Elements of X-ray Diffraction, Addison-Wesley.

Ebeling R. and Ashby, M.F., 1966, Phil. Mag. 13, 805.

Eshelby, J.E., Frank, F.C., and Nabarro, F.R.N., 1951, Phil. Mag., 42, 351.

Fast, J.D., 1950, Philips Tech. Rev. 11, 303.

Fisher, J.C., Hart, E.W., and Pry, R.H., 1953, Acta Met., 1, 336.

Floreen, S., and Westbrook, J.H., 1969, Acta Met. 17, 1175.

Friedel, J., 1964, Dislocations, Pergamon Press.

Gell, M., and Worthington, P.J., 1966, Acta Met., 14, 1265.

Gell, M., and Smith, E., 1967, Acta Met., 15, 253.

Green, A.P., and Hundy, B.B., 1956, J. Mech. Phys. Solids, 4, 128.

Griffith, A.A., 1920, Phil. Trans. Roy. Soc. Lond., A221, 163.

Griffiths, J.R., and Cottrell, A.H., 1965, J. Mech. Phys. Solids, 13, 135.

Guessier, A. and Castro, A., 1949, Rev. Mét. 46, 517.

Hahn, G.T., Averbach, B.L., Owen, W.S., and Cohen, M., 1959, Fracture, Swampscott Conference, Wiley, 91.

Hahn, G.T., Cohen, M., and Averbach, B.L., 1962, J.I.S.I. 200, 634.

Hahn, G.T. and Rosenfield, A.R., 1964, Battelle Memorial Report.

Hahn, G.T., and Rosenfield, A.R., 1965, Acta Met., 13, 293.

Hahn, G. T. and Rosenfield, A.R., 1966, Acta Met., 14, 1815.

Hahn, G. T. and Rosenfield, A.R., 1967, Trans. A.I.M.E., 239, 668.

Hale, K. F. and McLean, D., 1963, J.I.S.I., 201, 337.

Hall, E.O., 1951, Proc. Phys. Soc. 64, 747.

Hall, K. F., and McLean, D., 1963, J.I.S.I., 201, 337.

Head, A.K., and Louat, N., 1955, Aust. J. Phys., 8, 1.

Hendrickson, J.A., 1958, Trans. ASM, 50, 656.

Honda, R., 1961, J. Phys. Soc. Japan 16, 1309.

Honda, R., and Taga, H., 1968, Met. Sci. J., 2, 172.

Hondros, E.O., 1968, Acta Met. 16, 1377.

Hull, D., 1960, Acta Met., 8, 11.

Hull, D., 1961, Acta Met., 9, 191.

Hull, D., 1962, Fracture of Solids, Maple Valley Conf., Gordon and Breach, 417.

Hull, D., Beardmore, P., and Valentine, A.P., 1965, Phil. Mag. 12, 1021.

Hume-Rothery, W., 1966, The Structures of Alloys of Iron, Pergamon Press.

Inman, M.C. and Tipler, H.R., 1963, Met. Rev. 8, 105.

Johnston, T.L., and Parker, E.R., 1963, Fracture of Solids, Seattle Conference, Wiley, 267.

Keh, A.S., and Leslie, W.C., 1962, Structure and Properties of Engineering Materials, Interscience.

Keh, A.S., Leslie, W.C., and Sponseller, D.L., 1963, Symposium on Precipitates in Iron Base Alloys, AIME.

Keh, A.S., 1968, Dislocation Dynamics, McGraw-Hill.

Kelly, A., 1966, Strong Solids, Clarendon Press, Oxford.

Kelly, A., and Nicholson, R.B., 1963, Prog. Mat. Sci., 10, 149.

Knott, J.F. and Cottrell, A.H., 1963, J.I.S.I., 201, 249.

Knott, J.F., 1965, Proc. Roy. Soc., A285, 150.

Knott, J.F., 1966, J.I.S.I., 204, 104.

Knott, J.F., 1967, J.I.S.I., 205, 285.

Lement, B.S., Averbach, B.L., Cohen, M., 1954, Trans. ASM, 46, 851.

Leslie, W.C. and Fisher, R.M. and Sen, N., 1959, Acta Met., 7, 632.

Leslie, W.C., 1961, Acta Met., 9, 1004.

Lindley, T.C., 1965, Acta Met., 13, 681.

Lindley, T.C., 1966, Acta Met., 14, 1835.

Lindley, T.C., 1969, J.I.S.I., 207, 984.

Low, J.R. and Feustel, R.G., 1953, Acta Met. 1, 185.

Low, J.R., 1954, Relation of Properties to Microstructure ASM, Cleveland, Ohio.

Low, J.R., 1956, Deformation and Flow of Solids, Springer-Verlag, Berlin, 60.

Low, J.R., 1963, Prog. Mat. Sci. 12, 1.

McMahon, C.J. and Cohen, M., 1965, Acta Met. 13, 591.

McMahon, C.J., 1966, Acta Met., 14, 839.

McMahon, C.J., Rellick, J.R., and Schultz, B., 1969, Second Int. Conf. on Fracture, Brighton, England, p23/1.

Morris, G. E., 1949, Metal Progress, 56, 696.

Nicholson, R. B., Thomas, G., Nutting J., 1958, Brit. J. Appl. Phys. 9, 25.

Oates, G., 1966, J. I. S. I., 204, 991.

Oates, G., 1967, J. I. S. I., 205, 41.

Oates, G., 1968, J. I. S. I., 206, 930.

Oates, G., 1969, J. I. S. I., 207, 353.

Orowan, E., 1945, Trans. Inst. Eng. and Shipbuild. 89, 165.

Orowan, E., 1948, Sym. on Internal Stresses in Metals and Alloys, Institute of Metals, 451.

Orowan, E., 1949, Rep. Prog. Phys. 12, 185.

Orowan, E., 1955, Welding J. Res. Suppl., 570S.

Parker, E. R., 1957, Brittle Behavior of Engineering Structures, Wiley.

Parker, E. R., 1959, Fracture, Swampscott Conference, Wiley.

Petch, N. J., 1953, J. I. S. I., 174, 25.

Petch, N. J., 1954, Progress Met. Phys. 5, 1.

Petch, N. J., 1959, Fracture, Swampscott Conference, Wiley, 54.

Phillips, V. A., 1963, Acta Met. 11, 1139.

Price, A. T., Hall, M. A. and Greenough, A. P., 1964, Acta Met. 12, 49.

Rees, W. P., Hopkins, E. B., and Tipler, H. R., 1951, J. I. S. I., 169, 157.

Rees, W. P. and Hopkins, B. E., 1952, J. I. S. I., 172, 403.

Richards, C. E., Reid, C. N., and Smallman, R. E., 1968, Proceeding of the International Conference on the Strength of Metals and Alloys, 9, 961.

Sleeswyk, A. W. and Helle, J. N., 1963, Acta Met. 11, 187.

Sleeswyk, A. W., 1968, Dislocation Dynamics, McGraw-Hill, 507.

Smith, R. L. and Rutherford, J. L., 1957, Trans. A. I. M. E., 209, 857.

Smith, R. P., 1962, Trans. A. I. M. E., 224, 105.

Smith, G. V., Kranzlein, P. M., Burton, M. S., 1963, Trans. ASM, 56, 701.

Smith, E., 1966, Acta. Met., 14, 985.

Smith, E., 1966, Proc. Conf. on Physical Basis of Yield and Fracture, Oxford, 36.

Smith, E., and Barnby, J. T., 1967, Met. Sci. Journ. 1, 56.

Spiegel, M. R., 1961, Statics, Schaum's Outline Series.

Stein, D. F. and Low, J. R., 1966, Acta Met. 14, 1183.

Stokes, R. J., Johnstone, T. L., and Li, C. H., 1959, Phil. Mag., 4, 920.

Stroh, A. N., 1954, Proc. Roy. Soc. A223, 404.

Stroh, A. N., 1955, Proc. Roy. Soc. A232, 548.

Stroh, A. N., 1957, Adv. Phys. 6, 418.

Tetelman, A. S., 1962, Proc. A. I. M. E., Intern. Conf. on Fracture, Seattle.

Tetelman, A. S., and Robertson, W. D., 1962, Acta Met. 11, 415.

Tetelman, A. S. and McEvily, A. J., 1967, Fracture of Structural Materials, Wiley.

Tomalin, D. S., and Stein, D. F., 1965, Trans. A. I. M. E., 233, 2056.

Wells, M. G. H. and Butler, J. F., 1966, Trans. ASM, Quart. 59, 427.

Westbrook, J. H. and Wood, D. L., 1961, Nature 192, 1280.

Wilshaw, T. R. and Pratt, P. L., 1965, J. Mech. Phy. Solids, 13, 7.

Wilshaw, T.R., 1966, J.I.S.I., 204, 936.

Wilshaw, T.R., 1967, Nat. Symp. on Fracture, Mech. Lehigh University.

Wood, D.S., and Clark, D.S., 1952, Trans. ASM, 43, 930.

Worthington, P.J. and Smith, E., 1966, Acta Met. 14, 35.

Worthington, P.J., 1969, Private Communication.

Zener, C., 1948, Fracturing of Metals ASM, 3.